ABSTRACT

Title of Dissertation: QUANTUM INFORMATION SCRAMBLING AND PROTECTION IN MANY-BODY SYSTEM

Gong Cheng
Doctor of Philosophy, 2023

Dissertation Directed by: Professor Brian Swingle
Department of Physics

This work is focused on two main topics in quantum information theory: the scrambling of quantum information and the preservation of quantum information in many-body system. In terms of information scrambling, the main focus of this work is on the Out-of-time-order correlator (OTOC), which is used to probe the dynamics of quantum information as it spreads from localized degrees of freedom to those that are distributed throughout the system. On the other hand, the aim of the study of quantum information protection is to construct a system that can preserve quantum information for a sufficiently long time when coupled to a finite-temperature environment.

The many-body systems analyzed in this work belong or are related to a class of strongly interacting systems known as holographic quantum models. The standard examples in this class are believed to be equivalent to gravitational theory in spacetime that is one-dimensional higher than that the quantum model lives in. Therefore, the results may also provide insights into topics

in quantum gravity.

The first part of the thesis explores the scrambling dynamics close to a critical point where conformal symmetry emerges. The second case deals with the scrambling dynamics with conservation law constraints in holographic quantum field theory. The result also clarifies how conserved charges influence the dynamics in the bulk dual.

The third part of the thesis presents a matrix model with a large matrix rank N that belongs to the class of approximate quantum error correction codes. We investigate its thermal stability by coupling it to a thermal bath and demonstrate that it behaves as a self-correcting quantum memory at finite temperature. The coherent memory time scales polynomially with the system size N.

QUANTUM INFORMATION SCRAMBLING AND PROTECTION IN MANY-BODY SYSTEM

by

Gong Cheng

Dissertation submitted to the Faculty of the Graduate School of the
University of Maryland, College Park in partial fulfillment
of the requirements for the degree of
Doctor of Philosophy
2023

Advisory Committee:
Professor Maissam Barkeshli, Chair
Professor Brian Swingle, Co-Chair/Advisor
Professor Paulo F. Bedaque
Professor Victor V. Albert
Professor Xiaodi Wu

Dedication

Dedicated to my parents, whose unwavering and unconditional support has always been my beacon of strength and inspiration.

Acknowledgments

I owe my gratitude to all the people who have made this thesis possible and because of whom my graduate experience has been one that I will cherish forever.

First and foremost, I would like to express my deepest gratitude to my advisor, Professor Brian Swingle, for his invaluable guidance throughout my graduate journey. From the very beginning of my graduate studies, his patience in answering my questions and engaging in stimulating discussions on various topics has been instrumental to my growth. We have spent countless hours in his office discussing intriguing physics concepts and exchanging emails to refine our research plans.

Professor Swingle has not only been an exceptional academic mentor but also a compassionate supporter in my personal life. During the pandemic, I faced numerous challenges and found myself feeling disheartened and directionless. However, Brian's unwavering support and encouragement helped me navigate those difficult times and ultimately emerge stronger.

I extend my heartfelt gratitude to Professors Maissam Barkeshli, Paulo Bedaque, Victor Albert, and Xiaodi Wu for graciously agreeing to serve on my thesis committee and for dedicating their invaluable time to review my manuscript.

I would also like to acknowledge the assistance and support I received from Professor Shabnam Jabeen, with whom I had the pleasure of working as a teaching assistant. Additionally, I would like to express my thanks to all the professors at the University of Maryland who

have imparted their knowledge to me, with special thanks to Professors Ted Jacobson, Raman Sundrum, Victor Galitski, and Zackaria Chacko for their invaluable instruction and guidance.

Moreover, I would like to express my appreciation to former postdoc Charles Cao, who provided invaluable assistance in discussing physics concepts and offered guidance on scientific writing for research papers.

My time at the University of Maryland has been greatly enriched by my colleagues, including Rodrigo Andrade e Silva, Yixu Wang, Wance Wang, Stefano Antonini, Batoul Banihashemi, and Subhayan Sahu. Our academic discussions have been invaluable, and I am grateful for their camaraderie both in and out of the academic sphere. I would also like to convey my gratitude to staff members Josiland Chambers and Melanie Dolores for their help in managing school affairs.

I owe my deepest gratitude to my family - my mother and father, who have steadfastly supported and guided me throughout my career. Their unwavering belief in me has enabled me to overcome seemingly insurmountable challenges. Words cannot express how much their love and support mean to me.

I would also like to acknowledge the financial support provided by the U.S. Department of Energy, Office of Science, Office of Advanced Scientific Computing Research.

I apologize to anyone I may have inadvertently omitted, as it is impossible to recall everyone who has contributed to my journey.

In conclusion, I would like to express my sincere appreciation to all those mentioned and extend my gratitude to the University of Maryland for providing a nurturing environment during my time as a graduate student.

Table of Contents

Chapter 1: Introduction

1.1 Overview

Quantum systems process and transmit information in ways that are vastly different from classical systems. One special feature that plays a central role in different disciplines of physics, including topological order, thermalization of quantum systems, quantum computing, and even quantum gravity, is quantum entanglement.

In topological phases of matter, for example, the ground state of the system can have long-range entanglement that cannot be removed by local unitary operators [1, 2]. Entanglement is also useful for characterizing quantum phase transitions in many-body systems. The behavior of entanglement entropy and correlation functions can provide insight into the nature of the transition and the critical behavior of the system [3, 4].

Entanglement is a crucial resource for quantum computing. One of the key advantages of quantum computers over classical computers is their ability to exploit quantum entanglement to perform certain tasks exponentially faster than classical computers [5]. Additionally, entanglement is important in designing quantum memory, which typically stores quantum information in a collection of entangled quantum systems, such as an ensemble of atoms or solid-state qubits.

In recent developments in quantum gravity, entanglement entropy and other quantum information tools have proven to be fruitful in deriving important results, such as the tensor network

representation of AdS space-time [6], the Page curve of black hole radiation [7, 8], and the emergence of Einstein's equations from the thermodynamics of entanglement [9, 10, 11].

With these exciting developments, a better understanding of quantum information and quantum entanglement is essential to modern physics. In this thesis, I focus mainly on two aspects of quantum information: spreading and storing in many-body systems.

In the remainder of the introduction, I will review some basic concepts and tools related to quantum information scrambling and protection, along with a brief introduction to AdS/CFT duality. Then, I will give an overview of my contributions to this field.

1.2 Quantum information scrambling

1.2.1 Basic concept

Quantum information scrambling pertains to the growth of complexity within a quantum state [12, 13, 14]. As unitary time evolution progresses, this complexity accumulates. An initially prepared tensor product state can evolve into a highly entangled state over time. In particular, the entanglement entropy of a subregion tends to increase as time passes [15, 16, 17].

At later stages, once the state has become fully thermalized, any subsystem appears to be in local thermal equilibrium. Specifically, any observable with local support measures its thermal expectation value. Consequently, from the perspective of local probes, the initial state's information appears to be lost. However, due to unitarity, the information is conserved and must be concealed within non-local degrees of freedom. This transfer of information from local to non-local degrees of freedom is referred to as quantum scrambling [18, 19, 20, 21].

Scrambling can alternatively be viewed as a process in which local entanglement propa-

gates throughout the system [22, 23]. Consider a spin chain where a small section is initially entangled with reference spins. As time evolves, this entanglement disperses across the entire system, necessitating access to an increasing number of spins to recover the entanglement with the reference. When the state reaches full thermalization, more than half of the system's degrees of freedom are required to retrieve the entanglement.

Quantum information scrambling plays a vital role in understanding the thermalization process [24, 25, 26]. For instance, it differentiates between systems that rapidly thermalize and localized systems that never reach thermal equilibrium [27, 28]. Scrambling provides a quantitative approach to examine the mechanics of thermalization and the rate at which the process occurs.

Quantum information scrambling has been found to be related to other fundamental concepts in quantum physics, such as the black hole information paradox [29, 30, 31]. The paradox arises from the observation that quantum information that falls into a black hole appears to be lost forever, even though quantum mechanics suggests that information cannot be destroyed. Some researchers have proposed that the information may be scrambled in a way that is analogous to the process of quantum information scrambling [19, 32], and that understanding this relationship could lead to new insights into the nature of quantum gravity.

1.2.2 OTOC and probes of scrambling

There are various ways to probe scrambling. For instance, the time-dependent behavior of the entanglement entropy of a subregion A, as mentioned in the previous section, can be calculated [22]. Other probes include the spectrum form factor (SSF) [33], tripartite mutual

information (TMI) [18], and quantum teleportation protocols [34].

One particular probe that has been extensively studied in the literature is the out-of-time-order correlator (OTOC) [35, 36, 37, 38, 39]. Given an initial state $|\psi\rangle$, the OTOC can be defined as the overlap between two states. The first state is obtained by applying a local operator V at time $t = 0$, followed by evolving the state forward by a time t, then acting with another local operator W and evolving the state back to the original time. This gives $e^{iHt}We^{-iHt}V|\psi\rangle$. The other state is obtained by first evolving forward by t, applying W and evolve backward by $-t$ and finially act by V, which produces $Ve^{iHt}We^{-iHt}|\psi\rangle$. The OTOC is the overlap of the two states:

$$OTOC := \langle\psi|W(t)VW(t)V|\psi\rangle. \tag{1.1}$$

The OTOC can also be viewed as a means of probing the growth of the Heisenberg operator $W(t) = e^{iHt}W(0)e^{-iHt}$. In general, we anticipate that this operator will increase in size as time progresses, which can be expressed by the following expansion:

$$\begin{aligned} W(t) =& W(0) + it[H, W(0)] + \frac{(it)^2}{2}[H, [H, W(0)]] + \cdots \\ =& \sum_{n=0} \frac{(it)^n}{n!}[H, \cdots, [H, W(0)]]. \end{aligned} \tag{1.2}$$

.

For models defined on a lattice, the Hamiltonian generally comprises a sum of local terms,

$$H = \sum_l h_l, \tag{1.3}$$

where each h_l involves a product of a finite number of operators. Suppose each product contains

k operators, then repeatedly applying the commutator n times can generate a large operator that generally involves nk number of local operators. Consequently, we expect the size of the operator to grow exponentially with time.

We can examine the operator size of $W(t)$ by measuring its commutator with another operator V that is initially far away from W. Therefore, the commutator $[W(t), V(0)]$ is of particular interest. The magnitude of this commutator is constrained by an exponential function of time.

$$\frac{||[W(r,t), V(r',0)]||}{||W|| \cdot ||V||} \leq a e^{\lambda(t - \frac{|r-r'|}{v_{LR}})}. \tag{1.4}$$

This is established by the Lieb-Robinson theorem [40]. The Lieb-Robinson speed, denoted as v_{LR}, bounds the velocity of information propagation for a given Hamiltonian. Suppose both W and V are Hermitian local operators separated by a distance at $t = 0$. Initially, the commutator vanishes and becomes finite only when $W(r,t)$ expands to reach the region where $V(r',0)$ is situated. The state-dependent version of this commutator is defined as the expectation value of the squared commutator.

$$\langle [W(r,t), V(r',0)]^2 \rangle \tag{1.5}$$

We square the commutator because the expectation value of the commutator alone decays rapidly with time, within the dephasing time scale. The squared commutator is related to the OTOC through the following equation:

$$\begin{aligned} \langle [W(r,t), V(r',0)]^2 \rangle \sim & \langle W(r,t)V(r',0)W(r,t)V(r',0) \rangle - \langle W(r,t)W(r,t) \rangle \langle V(r',0)V(r',0) \rangle \\ & + (W \leftrightarrow V). \end{aligned} \tag{1.6}$$

The squared commutator attains its maximum value when the local excitation created by $W(r,0)$ propagates to the region where $V(r',0)$ is located. Consequently, it is conceptually aligned with scrambling, as defined in the previous section, which concerns the velocity at which local inforamtion propagate [41].

For systems with a large number of local degrees of freedom or unbounded local operators, the early time growth of the squared commutator can be expressed as [42]:

$$\langle [W(r,t), V(r',0)]^2 \rangle \sim \epsilon e^{\lambda_L t}, \tag{1.7}$$

where ϵ is a small parameter. In systems with a large N number of local degrees of freedom, ϵ is proportional to $\frac{1}{N}$. In models with a classical limit, such as single particle quantum mechanics, this small parameter is equal to the Planck constant $\epsilon = h$. The exponential growth of this correlator can be interpreted as chaos, with λ_L representing the Lyapunov exponent.

1.3 Quantum information protection

Information stored in a quantum state is vulnerable to environmental noise. These states are typically continuous, unlike classical computers that exclusively store digital information [43]. As a result, even minor changes to the state can cause significant errors. In a quantum circuit, such errors can propagate and accumulate, leading to significant mistakes. Hence, the use of quantum error correction is critical for quantum information processing.

We can conceive of scrambling as a natural mechanism that safeguards quantum information [44]. It is a powerful method of hiding information from a few degrees of freedom to many non-local degrees of freedom. In a fully scrambled pure state, the density matrix of any small

region appears to be in a thermal state, as long as the region's size is smaller than half of the system. This implies that through scrambling, any small region cannot contain any information about the entire state. Consequently, errors that only affect that small region and do not affect the stored information of the global state. Therefore we learn from scrambling the effectiveness of concealing a small amount of qubits information into a larger number of qubits. Typically, we can store quantum information in a subspace of the Hilbert space of a large quantum many-body system, referred to as the code subspace.

1.3.1 General property of Quantum error correction code

A quantum error correction code is generally defined by a code subspace $\mathcal{C}$. If any state ρ is inside the code subspace $\mathcal{C}$, it is referred to as a logical state. Our objective is to ensure that all logical states are protected under the influence of a noise channel $\mathcal{E}$, which is characterized by a set of error operators E_a. The noise channel acts on any state via the following expression:

$$\mathcal{E}(\rho) = \sum_a E_a \rho E_a^\dagger. \tag{1.8}$$

Here, these error operators must satisfy the condition $\sum_a E_a^\dagger E_a = 1$. In order for these errors to be correctable, a fundamental requirement is that they cannot convert a logical state $|i\rangle$ into another logical state $|j\rangle$. Specifically, if these logical states are orthogonal, then we must satisfy the following relation:

$$\langle j|E_b^\dagger E_a|i\rangle = 0, \quad \text{for } \langle i|j\rangle = 0. \tag{1.9}$$

This is a necessary condition for a quantum error correction code. Another requirement is that the expectation value of these error operators on any logical state must be identical. In other

words, we must have the following relation:

$$\langle i|E_b^\dagger E_a|i\rangle = \langle j|E_b^\dagger E_a|j\rangle \tag{1.10}$$

Thus, we cannot differentiate between the logical states $|i\rangle$ and $|j\rangle$ using these error operators. We can understand this necessity by considering an error operator E that only modifies the amplitude of the logical states, i.e., $E|i\rangle = c_i|i\rangle$ and $E|j\rangle = c_j|j\rangle$. If $c_i \neq c_j$, then a state that is a superposition of $|i\rangle$ and $|j\rangle$ will be transformed into a different state,

$$E(|i\rangle + |j\rangle) = c_i(|i\rangle + \frac{c_j}{c_i}|j\rangle). \tag{1.11}$$

The ratio $\frac{c_j}{c_i}$ corresponds exactly to the ratio between the two expectation values in Eq. (1.10). it is proved that Eq. (1.9), together with Eq. (1.10), are also sufficient conditions for quantum error correction. When combined, they can be summarized as the Knill-Laflamme condition [45]:

$$\langle j|E_b^\dagger E_a|i\rangle = C_{ab}\delta_{ij}. \tag{1.12}$$

The matrix C_{ab} is independent of the logical state. Diagonalizing this matrix results in an orthogonal set of bases for the error operators such that the states generated by different operators are orthogonal to each other inside any logical state. We denote this new basis as F_a, and these operators are orthogonal to each other within any logical state.

$$\langle i|F_b^\dagger F_a|i\rangle = 0, \quad \text{for } a \neq b\ . \tag{1.13}$$

Therefore, if the matrix C_{ab} is non-degenerate (i.e., it has the maximum rank), then $F_a|i\rangle \neq 0$ for all F_a. Consequently, we can determine which error operator was acted upon the logical state. In contrast, if the matrix C_{ab} is degenerate, it is not possible to ascertain which error operator was used on the logical state.

The Knill-Laflamme condition establishes an upper bound on the number K of logical states given the size of the physical Hilbert space N and the number of independent error operators $|\mathcal{E}|$ that constitutes the noise channel $\mathcal{E}$. This bound is given by the inequality,

$$K|\mathcal{E}| \leq N \tag{1.14}$$

In the qubit model, suppose we have n physical qubits and k logical qubits. If we wish to correct all errors that are composed of Pauli operators X, Y, Z that act on less than l number of qubits, then the number of correctable errors is given by $|\mathcal{E}| = \sum_{j=1}^{l} 3^j \binom{n}{j}$. So the bound becomes,

$$2^k[\sum_{j=1}^{l} 3^j \binom{n}{j}] \leq 2^n \tag{1.15}$$

This inequility is refered as quantum Hamming bound [46].

1.3.2 Bosonic Code

In Chapter 4 of our construction, we utilize a special class of quantum codes known as Bosonic codes, which play a crucial role. A comprehensive review of these codes can be found in [47]. Bosonic codes are particularly relevant because they operate on physical degrees of freedom that are bosonic in nature, typically represented by harmonic oscillators.

One noteworthy characteristic of bosonic codes is that the Hilbert space dimension of a single oscillator is infinite. Consequently, the total Hilbert space dimension of a bosonic code is also infinite. This infinite-dimensional nature provides unique opportunities for information storage and processing.

Several examples of bosonic codes have been developed, each with its distinctive features and applications. Notable among them are:

GKP code [48]: The Gottesman-Kitaev-Preskill (GKP) code is a prominent bosonic code that encodes quantum information in the continuous-variable regime. It has been extensively studied and finds applications in fault-tolerant quantum computing.

Cat code [49]: The cat code is another notable bosonic code that relies on superposition states of coherent states. It has been investigated for quantum error correction and quantum teleportation.

Binomial code [50]: The binomial code is a bosonic code constructed using binomial states. It exhibits intriguing properties and has potential applications in quantum communication and cryptography.

These examples highlight the diversity and versatility of bosonic codes in the field of quantum information processing. By leveraging the infinite-dimensional Hilbert space of bosonic systems, these codes offer promising avenues for advancing quantum computing, communication, and related technologies.

Among the various bosonic codes, we specifically highlight the Gottesman-Kitaev-Preskill code (GKP code) [48] as a notable example. In this code model, logical information is encoded in the position space state. For instance, a one-qubit state can be encoded as follows:

$$
\begin{aligned}
|0_L\rangle &= \sum n \in \mathbb{Z} | q = 2n\sqrt{\pi}\rangle \\
|1_L\rangle &= \sum m \in \mathbb{Z} | q = (2m+1)\sqrt{\pi}\rangle
\end{aligned}
\tag{1.16}
$$

The error operators in the GKP code are displacement operators, given by $E_p(\alpha) := e^{i\alpha\hat{p}}$ and $E_q(\beta) := e^{-i\beta\hat{q}}$. The displacement in position space is correctable as long as $\alpha \in (-\sqrt{\pi}, \sqrt{\pi})$. Similarly, small displacements in momentum space are also protected for $\beta \in (-\sqrt{\pi}, \sqrt{\pi})$. This is because the logical states can be expressed in terms of the momentum eigen-basis as:

$$
\begin{aligned}
|+\rangle_L := |0\rangle + |1\rangle &= \sum_{n\in\mathbb{Z}} |p = 2n\sqrt{\pi}\rangle \\
|-\rangle_L := |0\rangle - |1\rangle &= \sum_{m\in\mathbb{Z}} |p = (2m+1)\sqrt{\pi}\rangle
\end{aligned}
\tag{1.17}
$$

Therefore, the code distance can be defined in terms of the shift magnitude $\delta = \sqrt{\pi}$. To increase the code distance, one can concatenate this continuous code with other qubit codes. This involves utilizing multiple harmonic oscillators. In Chapter 4, we delve into constructing a quantum code that harnesses a large number of oscillators, denoted by N. We employ different encoding methods to protect information even in finite temperature environments.

1.3.3 Passive Quantum Memory

Systems that satisfy the aforementioned criteria are guaranteed to detect local errors and recover information. However, there always exists a bound on the weight of correctable local

error operators, referred to as the code distance. If the system is coupled to an environment at a finite temperature and left without interference for a long time, any perturbation will generally accumulate or propagate from a local supported error to a large non-local error, which could exceed the code distance and invalidate the code's protection ability.

While it would be ideal to find a many-body quantum system that could preserve quantum information coherently for an indefinitely long time, such systems are not known to exist. In practice, we can aim to construct quantum memories that can store quantum states for a time that can be tuned for arbitrary long as a function of physical parameters, such as system size. This would enable us to implement arbitrarily long quantum algorithms given sufficient quantum resources. To distinguish such systems from general quantum error correction codes, which require actively applying detection and recovery, they are called *self-correcting quantum memories* or *passive quantum memories*.

A conjectured property of passive quantum memories is that their coherent time τ scales exponentially with the energy cost ϵ of introducing a logical error to the system. This exponential scaling can be expressed in terms of the inverse temperature β, which is related to the temperature T by $\beta = \frac{2\pi}{T}$. Specifically, the conjecture is that

$$\tau \sim e^{\beta\epsilon} \tag{1.18}$$

An example of a two-dimensional model that satisfies this exponential scaling rule is the toric code model [51], which is a passive quantum memory at zero temperature. However, the energy barrier for logical errors is a constant that is independent of the system size. As a consequence, it is not a desired passive memory at finite temperature, since the coherent time τ does

not scale with system size.

There are established no-go theorems [52][53] which state that the energy barrier for logical errors cannot scale with system size for any two-dimensional local Hamiltonian with Pauli-commuting property. This means that such systems cannot be finite-temperature passive quantum memories according to the conjectured scaling rule (1.18). It should be noted that the restriction to Pauli-commuting terms is not necessarily physically justified, but rather a means of connecting the construction to the well-developed stabilizer code formalism, which will not be elaborated on in this review.

In contrast to the two-dimensional case, the no-go theorems for passive quantum memories in three dimensions are less restrictive. It has been proven that for three-dimensional Hamiltonians that satisfy translational symmetry, Pauli-commuting, and constant ground state degeneracy, the energy barrier must be constant and independent of system size [54]. However, this restriction on ground state degeneracy can be relaxed to surpass the no-go theorem, as explicitly shown in [55][56], leading to a coherent time that scales polynomially with system size according to the rule (1.18) at finite temperature.

In dimensions higher than three, quantum codes with polynomially scaled energy barrier of logical operators have been constructed. An example is the four-dimensional toric code [57]. It has been rigorously proven that the coherent time scales exponentially with system size [58].

The aforementioned models are examples of passive quantum memories that belong to the class of commuting Hamiltonians and are based on the guiding principle of finding macroscopic scaling energy barriers. However, there are other models that go beyond these restrictions. For a comprehensive review on these topics, we refer the interested reader to the article [59].

1.4 Holographic Duality

The holographic principle posits a relationship between $(D+1)$-dimensional semi-classical gravity and a D-dimensional quantum system without gravity. The non-gravitational quantum theory is considered to exist on the boundary of the spacetime where the semi-classical gravity resides. The two systems are believed to be equivalent. Two key hints led to the development of this principle. The first was from black hole thermodynamics [60, 61], which established a bound on the entropy of a region based on the area of its boundary. The second hint came from string theory, which provided a concrete example of this equivalence, known as AdS/CFT duality [62, 63]. Unfortunately, it is currently impossible to construct the holographic dual of an arbitrary gravitational or quantum system. Only a few examples, including AdS/CFT, are believed to exhibit this holographic or bulk/boundary duality in a spectacular manner.

1.4.1 Basics of AdS/CFT

The AdS/CFT correspondence is the observation that a gravity theory living in an asymptotic anti-de Sitter (AdS) spacetime can be described by a conformal field theory (CFT) living on the boundary of that spacetime. The gravity theory can be any theory that can be approximated by general relativity, weakly coupled to matter. The duality asserts that the Hilbert space of the gravity theory and the CFT are equivalent. In other words, the states and observables in the gravity theory can be mapped to states and observables in the CFT, and vice versa. This duality has provided a powerful tool for understanding strongly-coupled quantum field theories, which are difficult to study using traditional perturbative techniques.

1.4.2 Gravity and quantum information scrambling

The operator growth picture that we discussed in the information scrambling section has an interesting bulk dual in the context of the AdS/CFT correspondence. In this duality, the finite temperature CFT state is dual to a black hole in the asymptotic AdS bulk. When a local operator is acted on the boundary, it creates a single particle state close to the boundary. As time progresses, the particle flies towards the black hole deep inside the bulk. Its momentum grows exponentially with time,

$$p \sim e^{\frac{t}{\beta}}. \tag{1.19}$$

which is analogous to the growth of operator size in the CFT. One van further calculate OTOC on the CFT which is also exponentially growing in the form of Eq. (1.7) with the same exponent. In the black hole background $\frac{1}{\beta}$ is the corresponding Lyapunov exponent. In fact it was proved that for general many body system, there is a bound for this exponent [64], $\lambda_L \leq 2\pi T$. Therefore the CFT with a holographic dual saturate this bound and is one of models that scrambles the fastest. [20]. We will review the detail of this calculation in section 3.

1.4.3 Brief review of SYK model

A toy model in quantum mechanics that has a conjectured holographic dual is the Sachdev-Ye-Kitaev (SYK) model [42, 65, 66]. This model describes random interactions of a large number (N) of Majorana fermions in 0+1 dimensions. Its gravitational dual is believed to be the 1+1 dimensional Jackiw-Teitelboim (JT) gravity [67, 68].

Hamiltonian of SYK model is in the following form:

$$H_{SYK} = \sum_{ijkl} J_{ijkl}\psi_i\psi_j\psi_k\psi_l. \tag{1.20}$$

The indices i, j, k, l run over all the fermions, making this interaction highly non-local. The coupling constants J_{ijkl} are random real numbers with a vanishing mean value and a large variance,

$$\begin{aligned} \overline{J_{ijkl}} &= 0 \\ \overline{J_{ijkl}^2} &= \frac{3!J^2}{N^3} \end{aligned} \tag{1.21}$$

The power of N in this variance is chosen in a way that the model has a well-defined large N limit. In this limit, we send N to infinity while keeping the magnitude J fixed. By integrating out the fundamental fermions in the path integral, we can obtain an effective action for this model.

$$\begin{aligned} I_{eff} &= N[-\frac{1}{2}\log\det\left(\partial_t - \Sigma\right) + \frac{1}{2}\int_0^\beta d\tau \int_0^\beta d\tau' \left(-\frac{J^2}{4}G(\tau,\tau')^4 + G(\tau,\tau')\Sigma(\tau,\tau')\right)]. \\ Z &= \int D\Sigma DG e^{-I_{eff}} \end{aligned} \tag{1.22}$$

In the large N limit, the path integral is dominated by the saddle point of the action, where the bi-local fields Σ and G enter as Lagrange multipliers. At the saddle point, Σ scales as J^2. Therefore, at strong coupling where $\beta J \gg 1$, the kinetic term can be neglected. Without the kinetic term, The action is invariant under the following conformal symmetry (time reparametrization

symmetry) transformation:

$$\begin{aligned} G(\tau,\tau') &\to f'(\tau)^{\Delta} f'(\tau')^{\Delta} G(f(\tau), f(\tau')) \\ \Sigma(\tau,\tau') &\to f'(\tau)^{1-\Delta} f'(\tau')^{1-\Delta} \Sigma(f(\tau), f(\tau')) \end{aligned} \tag{1.23}$$

At saddle point the bi-local fields are solution of the following equations,

$$\begin{aligned} &\Sigma(\tau,\tau') = J^2 G(\tau,\tau')^3 \\ &\int d\tau'' \Sigma(\tau,\tau'') G(\tau'',\tau') = -\delta(\tau-\tau'). \end{aligned} \tag{1.24}$$

However, the only non-trivial solution that preserves the maximal symmetry is the conformal two-point function with dimension Δ, which is given by $G(\tau_1,\tau_2) \propto \frac{\text{sgn}(\tau_{12})}{|\beta \sinh(\frac{\tau_{12}}{\beta})|^{2\Delta}}$. Although this solution preserves a subgroup of the conformal symmetry, it spontaneously breaks other parts of it. Additionally, since the symmetry only holds exactly in the limit where βJ approaches infinity, it is explicitly broken by a magnitude of $\frac{1}{\beta J}$ at finite coupling. Given this spontaneous as well as explicit symmetry breaking pattern, we expect the existence of a pseudo-Goldstone boson, whose action is suppressed by $\frac{1}{\beta J}$ and has the following form:

$$I_{Sch}(f) = \frac{c}{J} \int d\tau \text{Sch}(f(\tau),\tau). \tag{1.25}$$

It has been shown that the JT gravity in AdS_2 has the same action as this one obtained from SYK model [69, 70].

1.5 Structure of the thesis

The thesis comprises of three published works which are presented as separate sections. A brief summary of the results is given below:

Chapter 2 is based on the publication *'Chaos in quantum rotor model' by Gong Cheng and Brian Swingle, published as arxiv 1901.10446*. In this chapter we investigate a model of quantum rotors, with each of them being constrained on a sphere. This model bears striking similarities to the well-known SYK model, as both possess strong all-to-all interactions and disorder. Additionally, analysis of the dynamics reveals the presence of a reparametrization symmetry at the phase transition point. However, we demonstrate that the critical point of this model does not possess holographic duality by calculating the OTOC and comparing it with the chaos bound. We further explain this by analyzing the difference in the pattern of reparametrization symmetry breaking between this model and the SYK model.

Chapter 3 is based on the publication *'scrambling with conservation laws' by Gong Cheng and Brian Swingle, published as JHEP11(2021)174*. In this chapter we analyze scrambling in a holographic CFT with a conserved charge. Our result demonstrates that the conservation law constraint slows down the scrambling in the late time regime. We establish this by calculating the OTOC in the gravity dual, and provide a bulk picture that involves a different way in which the gauged particle is accelerated towards the black hole. We also extend our results to include energy conservation, which is present in most physical systems.

Chapter 4 is based on the publication *'Large N Matrix Model as Quantum Memory' by ChunJun Cao, Gong Cheng and Brian Swingle, published as arxiv: 2211.08448* . In this chapter we construct a passive quantum memory using a gauged matrix quantum mechanics model. The

system size N in this model is rank of the matrix. Through an open system analysis, we show that the memory time of this model is polynomial in N when coupled to a thermal bath at finite temperature. Inspired by this construction, we further propose another model consisting of large N number of qubits, with strong all-to-all interactions. The qubit model also gives a similar result for the memory time. This qubit model has the potential to be realized in the laboratory.

1.6 Outlook and future directions

Moving forward, one of my primary focus will be the continued exploration of quantum memory models.

There are numerous open questions within the domain of gauge theory models for quantum memory. For instance, the possibility to employ models with finite rank gauge groups, which also exhibit confinement-deconfinement transitions. It's also worth investigating scenarios with Abelian or large N discrete gauge groups. Furthermore, a detailed analysis on the practical implementation of the recovery channel for our gauge theory memory is both challenging and crucial.

Beyond the realm of gauge theory models, I'm intrigued by other many-body systems, that possess long-range entanglement within their finite temperature phases. Examples include certain models of good quantum low-density parity-check codes. It would be compelling to apply the techniques we've utilized in this thesis to study the thermal stability of these models and assess their potential as passive memory systems.

All my research thus far has been tied to the concept of holography, which forms a link between quantum information problems and gravitational physics. In line with this, I plan to further

delve into their intersections. One area of interest is to understand how holography could enhance our processing of quantum information, such as through the use of holographic quantum error correction codes. Conversely, I also aim to address quantum information problems that might shed light on our understanding of gravity and holography, specifically focusing on overlapping qubits and holographic tensor networks.

Chapter 2: Chaos in a quantum rotor model

This chapter is based on the publication 'Chaos in a quantum rotor model' by Gong Cheng and Brian Swingle, published as arxiv 1901.10446.

2.1 Overview

We study scrambling in a model consisting of a number N of M-component quantum rotors coupled by random infinite-range interactions. This model is known to have both a paramagnetic phase and a spin glass phase separated by second order phase transition. We calculate in perturbation theory the squared commutator of rotor fields at different sites in the paramagnetic phase, to leading non-trivial order at large N and large M. This quantity diagnoses the onset of quantum chaos in this system, and we show that the squared commutator grows exponentially with time, with a Lyapunov exponent proportional to $\frac{1}{M}$. At high temperature, the Lyapunov exponent limits to a value set by the microscopic couplings, while at low temperature, the exponent exhibits a T^4 dependence on temperature T.

2.2 Introduction

2.2.1 Motivation

There have been a number of recent developments in the field of many-body quantum chaos driven in part by newly found relations to other areas of physics. Connections to quantum information scrambling and to the black hole information problem via holographic duality have been particularly fruitful [18, 19, 20, 36, 42]. On the theoretical side, this has led to an intense effort to compute so-called out-of-time-order correlators (OTOCs) in many-body systems [21, 30, 35, 71, 72, 73, 74, 75, 76, 77, 78, 79, 80, 81, 82, 83, 84, 85, 86, 87, 88, 89, 90, 91, 92]. On the experimental side, following a number of proposals [**? ? ? ? ? ? ?**], at least six early experiments have already been carried out [38, 93, 94, 95, 96, 97]. The study of a special fermionic system with infinite-range random interactions, the Sachdev-Ye-Kitaev (SYK) model [42, 65, 66], has revealed interesting features about scrambling, conformal symmetry and holography.

Here we study many-body quantum chaos in another infinite-range model consisting of a large N number of interacting M-component quantum rotors [98]. Our motivations for this study are as follows. We are interested to understand if the maximal chaos of the SYK model can be replicated in other physical systems, particularly in spin models of a type amenable to experimental realization. Since maximal chaos in SYK and two-dimensional gravity have to do with a certain pattern of conformal symmetry breaking, it is natural to study other infinite-range models with quantum critical points to attempt to extract a minimal set of ingredients for maximal chaos. This is particularly relevant given the recent experimental developments, since it would be desirable to physically instantiate and experimentally study models with maximal chaos, but

the SYK model is quite elaborate from an experimental perspective [99, 100]. Finally, the model we study has both paramagnetic and spin glass phases, and it would be interesting to understand the interplay between chaos and glassiness. Although we do not address the spin glass phase, our work represents a necessary first step to doing so.

The system is analyzed in the limit of large M and N, where it is known to be solvable. One interesting features is the presence of both a disordered paramagnetic phase and a spin glass phase separated by second order phase transition. We study the paramagnetic phase with a particular focus on the region of the phase diagram near the transition. The physical observables of interest are related to scrambling and diagnose how quantum information stored in a local part of a system spread to the whole system through interactions. Quantitatively, this process can be measured by the growth of certain local operator in the Heisenberg picture, which is characterized by the thermal average of squared commutator of two operators at different locations. Focusing on the rotor variables, we study the following quantity,

$$\mathcal{C}_{i,j}(t) = -\text{Tr}\left(\rho[n_i(t), n_j(0)]^2\right), \tag{2.1}$$

where n_i is the rotor at site i and $n_i(t) = e^{iHt} n_i e^{-iHt}$ is the corresponding Heisenberg operator for Hamiltonian H. We specify the index structure of the M-component rotors more carefully below.

This is essentially a four-point function of rotor variables and can be calculated using perturbation theory. For some systems, this quantity grows exponentially with time t for a period of time between the local relaxation time and the scrambling time where the commutator begins to saturate to its late-time value. This growth diagnoses chaos, and it shows how an initial local

perturbation causes an influence that grows exponentially with time [35, 36, 42]. Accordingly, the growth exponent is called a quantum Lyapunov exponent. This notion has recently been generalized to define a whole spectrum of quantum Lyapunov exponents [101]. In quantum systems satisfying a set of conditions related to thermalization, the exponent has an upper bound given by $\frac{2\pi T}{\hbar}$ [64].

2.2.2 Model and results

The model consists of a large N number of M-component rotor fields, labeled by $\vec{n}_i$, with non-local and random interaction. The classical part of the Hamiltonian is

$$H_c = \sum_{(ij)} J_{ij} \vec{n}_i \cdot \vec{n}_j = \sum_{(ij)} \sum_{\mu=1}^{M} J_{ij} n_i^\mu n_j^\mu, \tag{2.2}$$

where the J_{ij} couplings Gaussian random variables with mean zero and variance $\frac{J^2}{N}$. The interaction is non-local in the sense that the summation over (ij) runs over all pairs of rotors. In the quantum version of this model, a kinetic term is added for each rotor which is proportional to the conjugate angular momentum squared. The full quantum Hamiltonian is

$$H = \frac{g}{2} \sum_{i=1}^{N} \vec{L_i}^2 + \sum_{(ij)} J_{ij} \vec{n}_i \cdot \vec{n}_j. \tag{2.3}$$

This model is exactly solvable in the large N and large M limit [98], defined by the fol-

lowing conditions:

$$\begin{aligned} \langle J_{ij}^2 \rangle &= \frac{J^2}{N} \\ \vec{n}_i \cdot \vec{n}_i &= \sum_{\mu=1}^{M} (n_i^\mu)^2 = M, \quad \text{for each } i. \end{aligned} \tag{2.4}$$

Here the angular brackets denotes disorder average, and more generally they denote a combination of disorder and quantum average. As shown in the previous work, in this limit a factor of N can be factorized from the Euclidean Lagrangian. Therefore the path integral is dominated by its leading saddle point contribution. We briefly review this background material in the following.

The Euclidean path integral is

$$\begin{aligned} Z &= \int \prod_i Dn_i(\tau)\delta(n_i(\tau)^2 - 1) e^{-\int_0^\beta d\tau [\frac{1}{2g}\sum_{i=1}^N (\partial_\tau n_i)^2 + \sum_{(ij)} J_{ij} n_i \cdot n_j]} \\ &\to \int \prod_{i,a} Dn_i^a(\tau) D\lambda_i^a(\tau) \{ e^{-\frac{1}{2g}\int_0^\beta d\tau \sum_i \sum_{a=1}^q (\partial_\tau n_i^a)^2 + \frac{J^2}{2N}\int_0^\beta d\tau \int_0^\beta d\tau' \sum_{(ij)} \sum_{a,b} n_i^a(\tau)\cdot n_j^a(\tau) n_i^b(\tau')\cdot n_j^b(\tau')} \\ &\qquad \times e^{-\frac{1}{2}\int_0^\beta d\tau \sum_{i,a} \lambda_i^a n_i^a \cdot n_i^a} \} \\ &= \int \prod_{i,a} Dn_i^a(\tau) D\lambda^a(\tau) \prod_{cd\mu\nu} DQ_{\mu\nu}^{cd}(\tau,\tau') e^{-N I_E(n_i^a, \lambda^a, Q_{\mu\nu}^{cd})} \end{aligned} \tag{2.5}$$

where the final normalized Euclidean action is

$$\begin{aligned} I_E =& \frac{1}{2g}\int_0^\beta d\tau \frac{1}{N}\sum_{i=1}^N \sum_{a=1}^q [\partial_\tau n_i^a(\tau)]^2 + \frac{J^2}{2}\int_0^\beta d\tau \int_0^\beta d\tau' \sum_{ab\mu\nu} [\frac{1}{2} Q_{\mu\nu}^{ab}(\tau,\tau')^2 - \\ & \frac{1}{N}\sum_{i=1}^N n_i^{a\mu}(\tau) n_i^{b\nu}(\tau') Q_{\mu\nu}^{ab}(\tau,\tau')] + \frac{1}{2}\int_0^\beta d\tau \frac{1}{N}\sum_{i=1}^N \sum_{a=1}^q \lambda^a(\tau) n_i^a(\tau)\cdot n_i^a(\tau). \end{aligned} \tag{2.6}$$

In the second equality, the ensemble average of J_{ij} has been taken using the replica trick. The

upper index of n^a represents the replica index ranging from 1 to q, which is ultimately taken to be $q \to 0$. The delta functions enforcing the normalization are represented using auxiliary fields λ_i^a. Their dynamics is generated by quantum corrections which are suppressed by $\frac{1}{M}$. In the large M limit, they are just numbers serving as a chemical potential. A factor of N was extracted in the third step, so that the auxiliary field Q is coupled to the site average of rotor pairs.

One can show that the saddle point is determined by

$$Q^{ab}_{\mu\nu}(\tau,\tau') = \frac{1}{N}\sum_{i=1}^{N}\langle n_i^{a\mu}(\tau) n_i^{b\nu}(\tau')\rangle. \tag{2.7}$$

Treating Q as a non-dynamical field, the action of the rotor fields is that of a free theory. Therefore the two-point correlator of rotor variables can be obtained exactly. It is known that this model has a paramagnetic phase (replica symmetric) and a spin glass phase (replica symmetry breaking) separated by a second order phase transition. Our main focus in this article is the chaotic behavior within the paramagnetic phase, especially near the critical point.

To analyze scrambling in the model, we deviate slightly from the strict large N and large M limit to account for the fluctuations of the two auxiliary fields Q and λ which are suppressed by $\frac{1}{N}$ and $\frac{1}{M}$, respectively. The squared commutator is obtained by taking N much larger than M and summing over all the terms that are proportional to $\left(\frac{t}{M}\right)^n$ at long time in the ladder diagrams, while only keeping the leading $\frac{1}{N}$ contribution. In this limit we will show that the squared commutator, Eq. (3.10), is proportional to $\frac{1}{NM}$ and the Lyapunov exponent is suppressed by $\frac{1}{M}$:

$$\frac{1}{M^2}\sum_{\mu\nu}\langle [n_i^\mu(t), n_j^\nu(0)]^2\rangle_\beta \;\sim\; \frac{1}{MN} e^{\frac{1}{M}f(T)t}. \tag{2.8}$$

The chaos exponent is

$$\lambda_c = \frac{f(T)}{M}. \tag{2.9}$$

In the above formula, $f(T)$ is a increasing function of temperature. It is proportional to T^4 for low temperature near the critical point, and it saturates to a value proportional to $\sqrt{Jg}$ at large T. Although the calculation is performed for leading $\frac{1}{M}$ expansion. The T^4 behavior at small T is still true for finite value of M.

2.3 Two-point function

The analysis begins with the two-point function of rotor fields. At leading order of large N and M limit, the correlator can be obtained either from the previously mentioned method or by solving the Schwinger-Dyson (SD) equation. In the paramagnetic phase, one can use the time translation symmetry to write the SD equation diagrammatically as

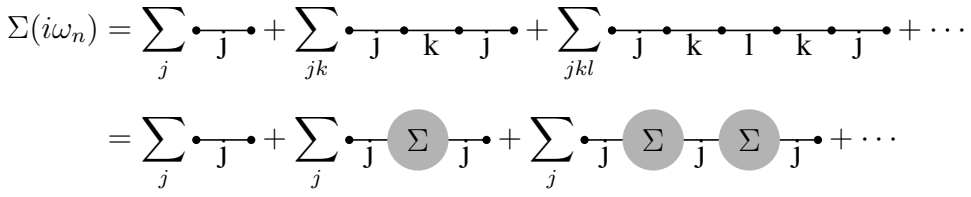

$$\begin{aligned} \Sigma(i\omega_n) &= \frac{J^2}{N}\sum_{j=1}^{N} G_j(i\omega_n) = J^2 G(i\omega_n) \\ G^{-1}(i\omega_n) &= \frac{\omega_n^2}{g} + \lambda - \Sigma(i\omega_n). \end{aligned} \tag{2.10}$$

The two-point function is diagonal, $\langle n_i^\mu(\tau) n_j^\nu(\tau')\rangle = G(\tau,\tau')\delta_{ij}\delta_{\mu\nu}$, due to the $O(M)$ rotational symmetry and local Z_2 symmetry of the model. The solution of these equations is

$$G(i\omega_n) = \frac{2}{J}\left(\frac{\lambda}{4J} + \tilde{\omega}_n^2 - \sqrt{\left(\tilde{\omega}_n^2 + \frac{\lambda}{4J}\right)^2 - \frac{1}{4}}\right). \tag{2.11}$$

Note that the solution depends on frequency only through the dimensionless combination $\tilde{\omega}_n = \frac{\omega_n}{2\sqrt{gJ}}$. The chemical potential λ is determined by the normalization condition

$$G(\tau = 0) = T\sum_n G(i\omega_n) = 1. \tag{2.12}$$

Now define the spectral function

$$\begin{aligned} A(\omega) &= \frac{1}{\pi}\Im G(\omega + i0^+) \\ &= \mathrm{sgn}(\omega)\frac{2}{\pi J}\sqrt{\frac{1}{4} - (\tilde{\omega}^2 - \lambda')^2}, \quad \lambda' = \frac{\lambda}{4J}. \end{aligned} \tag{2.13}$$

It is non-zero only when $-\frac{1}{2} + \lambda' < \tilde{\omega}^2 < \frac{1}{2} + \lambda'$. The paramagnetic phase corresponds to $\lambda' > \frac{1}{2}$. The phase transition from paramagnetic phase to spin glass phase occurs at temperature T_c when λ' reaches $\frac{1}{2}$ and the system becomes gapless. From condition Eq. (2.12) and $\lambda' = \frac{1}{2}$, T_c can be solved as a function of J and g. In particular, near $T_c = 0$, one obtains

$$g = \frac{9\pi^2}{16}J - \frac{\pi^2}{2}\frac{T_c^2}{J} + \cdots \tag{2.14}$$

Sitting at the critical point, the two point function is proportional to

$$\sqrt{\frac{g}{J}}\frac{1}{\sin^2(\frac{\pi\tau}{\beta})} + \cdots \tag{2.15}$$

at strong coupling, $\beta\sqrt{gJ} \gg 1$, and $\tau > 0$.

We define the retarded Green's function as $G_R(\omega) = G(i\omega_n \to \omega + i0^+)$. It can be expressed using the spectral function

$$G_R(\omega) = -\int d\nu \frac{A(\nu)}{\omega - \nu + i0^+}. \tag{2.16}$$

At the critical point, this expression allows us to obtain the real time dynamics by Fourier transformation,

$$\begin{aligned} \langle [n_i^\mu(t), n_i^\mu(0)] \rangle \theta(t) :=& (-i) G_R(t) \\ =& \frac{2}{J} \frac{J_2(\tilde{t})}{\tilde{t}}, \end{aligned} \tag{2.17}$$

where $J_2(z)$ is the Bessel function of the first class and $\tilde{t}$ denotes the normalized time $2t\sqrt{gJ}$. At large $\tilde{t}$ it has the asymptotic behavior

$$(-i) G_R(\tilde{t}) \sim \tilde{t}^{-\frac{3}{2}} \cos\left(\tilde{t} - \frac{\pi}{4}\right). \tag{2.18}$$

This is polynomially decaying at large t, and we will see in the next section that the four-point function constructed solely from it has no exponential growing behavior.

Chaos is obtained only after deviating slightly from the large M limit. Since the kinetic term for the λ field generated by quantum corrections is of order $\frac{1}{M}$, we need to take into consideration the λ fluctuations to this order. Its correlation function is denoted $\langle \lambda(\tau)\lambda(0) \rangle$ and is given by

$$G_\lambda(\omega_n) = -\frac{1}{M} \frac{1}{\Pi(i\omega_n)} \tag{2.19}$$

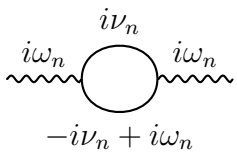

Figure 2.1: Diagram corresponding to the polarization function $\Pi(\omega_n)$.

in frequency space. Here $\Pi(i\omega_n)$ is the polarization function given by

$$\Pi(i\omega_n) = T\sum_n G(i\nu_n)G(i\omega_n - i\nu_n) \tag{2.20}$$

Since there is a summation over M rotor components in the loop, the propagator $G_\lambda(i\omega_n)$ is proportional to $\frac{1}{M}$. This justifies treating λ as a non-dynamical field at large M limit.

The polarization function is calculated in Appendix A.1. Generally, there is no analytical expression for Π, but at the critical point and in the strong coupling limit it has a simple form,

$$G_\lambda(\tau) = \frac{1}{M}\frac{cJ^2}{\sin^4\frac{\pi\tau}{\beta}}. \tag{2.21}$$

It is also useful to define the spectral function of λ as

$$\frac{1}{M}A_\lambda(\omega) = \frac{1}{\pi}\Im G_\lambda(\omega + i0^+) = -\frac{1}{\pi M}\Im\frac{1}{\Pi(\omega + i0^+)}. \tag{2.22}$$

There is another two-point function, known as the Wightman function, that will be useful later. It can be obtained as via analytic continuation of the imaginary time correlation function,

$$G_W(t) := G\left(-\frac{\beta}{2} + it\right) \tag{2.23}$$

One can derive a spectral function representation for $G_W(\omega)$ which reads

$$\begin{aligned} G_W(t) &= T\sum_n \int dx \frac{-A(x)}{i\omega_n - x} e^{-i\omega_n(-\beta/2+it)} \\ &= \frac{1}{2\pi i}\int dx \oint dz \frac{A(x)}{z-x} n_B(z) e^{-z(-\beta/2+it)} \\ &= \frac{1}{2\pi}\int d\omega \frac{2\pi A(\omega)}{2\sinh\frac{\beta\omega}{2}} e^{-i\omega t}. \end{aligned} \tag{2.24}$$

Therefore, in the frequency domain the Wightman function is

$$G_W(\omega) = \frac{\pi A(\omega)}{\sinh\frac{\beta\omega}{2}}. \tag{2.25}$$

Below we use these various correlators for both rotor n fields and auxiliary λ fields. We can associate to each a Euclidean correlator, a retarded correlator, and a Wightman function. They will be distinguished by adding a superscript or subscript to indicate the relevant field.

2.4 Four point function

2.4.1 General prescription

This section contains the main analysis of the four-point function of n fields which yields the squared commutator. The squared commutator is

$$\mathcal{C}(t) = -\frac{1}{M^2}\sum_{\mu\nu}\langle [n_i^\mu(t), n_j^\nu(0)]^2\rangle_\beta, \tag{2.26}$$

where we have suppressed the position labels i, j on $\mathcal{C}$. To avoid short-time divergences, it's more convenient to consider the regulated version [102]:

$$\tilde{\mathcal{C}}(t) = -\frac{1}{M^2}\sum_{\mu\nu}\mathrm{Tr}\left(\rho^{\frac{1}{2}}[n_i^\mu(t), n_j^\nu(0)]\rho^{\frac{1}{2}}[n_{i\mu}(t), n_{j\nu}(0)]\right), \tag{2.27}$$

This can be interpreted as a combination of contour ordered four point functions living on a complex time contour as in Figure 2.2.

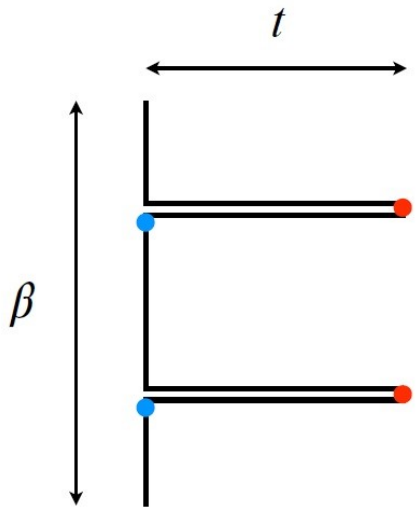

Figure 2.2: Complex time contour defining $\tilde{\mathcal{C}}$. The horizontal direction represents real time while the vertical line is the periodic thermal circle.

At large real time t, the dominant contribution to $\tilde{\mathcal{C}}(t)$ comes from the propagators stretching between the two horizontal contours. The ones that stretch between the imaginary time line and one of the real time lines cannot affect the large time behavior due to the damping of propagator with respect to the real time separation of the two inserting points. Following this intuition, we will neglect the latter type of dressings to focus on the ladder diagrams shown below.

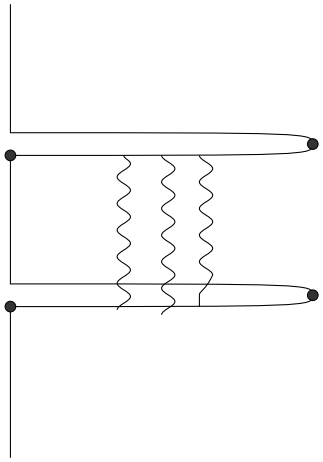

Figure 2.3: Schematic of the ladder diagrams that sum up to give exponential growth of $\tilde{\mathcal{C}}$.

For each vertical rung, the real time separation of the two ending points cannot be too large in order for it to remain a finite value. Therefore by integrating their ending points in the real time contour, each vertical rung roughly contributes a factor of t. Finally, we also need to sum over all the diagrams with different number of rung insertions. This suggests writing $\tilde{\mathcal{C}}(t)$ in the following form at large t,

$$\tilde{\mathcal{C}}(t) \propto \sum_n \frac{1}{n!}(at)^n = e^{at}. \tag{2.28}$$

The factor of $n!$ comes from the permutation of different rungs and a is related to the contribution of the individual rung insertions. In this model, a is a positive number of order $\frac{1}{M}$, which will be clear as we proceed. We will see that a ladder diagram won't damp too fast when two individual rungs are separated by a large real time interval, which justifies the approximation of summing each rung's contribution independently in Eq. (3.15). Similar to the treatment in Ref. [102], we distinguish two types of rungs as shown below.

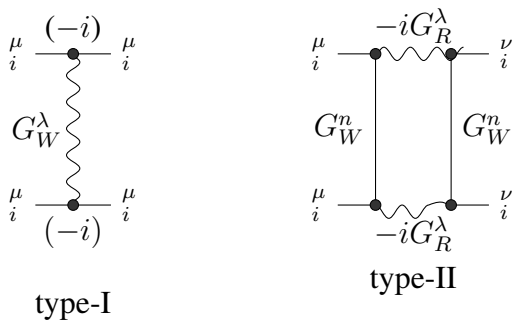

Figure 2.4: The two types of rungs that enter the ladder summation.

The type-I rung is composed of a single Wightman function of the auxiliary field λ stretching between the two real time contours, while the type-II rung is composed of two Wightman functions of rotor fields and two retarded Green's functions of the λ field.

Each interaction vertex inserted in the real time contour, which in our case is $(-i)J_{kj}n_k(t)n_j(t)$, has a partner in the other half of the same real time contour (see fig 2.5 below) but with a minus sign in front. Therefore, adding them together after wick contractions produces a retarded Green's function.

$$\left[\langle n_j(t_2)n_i(t_1)\rangle - \langle n_i(t_1)n_j(t_2)\rangle\right]\theta(t_2-t_1) = (-i)G_R(t_2-t_1)\delta_{ij} \tag{2.29}$$

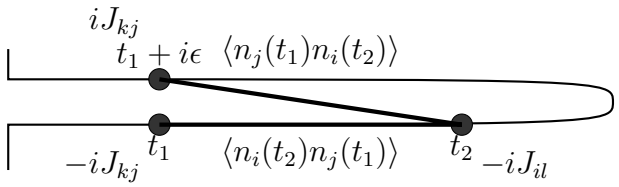

Figure 2.5: An example of interaction vertex insertion. If $n_i(t_2)$ is contracted with $n_j(t_1)$, n_i should at the left of n_j in the correlator. If $n_i(t_2)$ is contracted with $n_j(t_1 + i\epsilon)$, they should be reversed due to the contour ordering. When we add all the possible contractions, these two correlators are combined together to produce a retarded function.

Therefore, in our following calculations all the propagators that stretch within the same real

time contour will be the taken as the retarded Green's function and the ones stretch between two different real time contours are identified as the Wightman function defined in the last section.

2.4.2 Leading order

To leading order at large N and M, the diagrammatic expansion of the four-point function is shown in Figure 2.6. Each disorder average of J_{ij} contains a factor of $\frac{1}{N}$. Each summation over the site indices contains a factor of N. So all of these diagrams are of the same order in $\frac{1}{N}$. Since this is just a geometric series, it's easy to obtain that in the leading behavior,

$$\begin{aligned}&\langle n_i^\mu(\tau_1)n_i^\mu(\tau_2)n_j^\mu(\tau_3)n_j^\mu(\tau_4)\rangle - \langle n_i^\mu(\tau_1)n_i^\mu(\tau_2)\rangle\langle n_j^\mu(\tau_3)n_j^\mu(\tau_4)\rangle \\ =&\frac{J^2}{N}T^2\sum_{\omega_n\nu_m}\frac{G(i\omega_n)^2G(i\nu_m)^2}{1-J^2G(i\omega_n)G(i\nu_m)}e^{-i\omega_n\tau_{13}}e^{-i\nu_m\tau_{24}} + (\tau_3 \leftrightarrow \tau_4)\end{aligned} \tag{2.30}$$

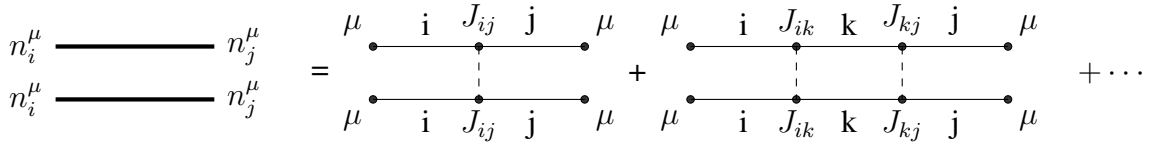

Figure 2.6: Leading order of four point function. The dashed line means the ensemble average of J_{ij}.

Then we analytically continue it to the real time contour. To do this, just replace $G(i\omega_n)$ by the retarded Green's function $G_R(\omega)$. This is equivalent to summing the diagrams in Figure 2.6 directly on the real time contour. Either way, the lowest order contribution to $\tilde{\mathcal{C}}(t)$ is

$$-\tilde{\mathcal{C}}_0(t) = \frac{(-iJ)^2}{MN}\int\frac{d\nu}{2\pi}\int\frac{d\omega}{2\pi}\frac{[(-i)G_R(\omega)]^2[(-i)G_R(\nu-\omega)]^2}{1-J^2G_R(\omega)G_R(\nu-\omega)}e^{-i\nu t}. \tag{2.31}$$

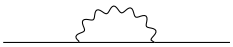

Figure 2.7: Diagram corresponding to the rotor self-energy.

After substituting the expression of G_R, we find a pole at $\nu = 0$,

$$J^2 \frac{G_R(\omega)^2 G_R(\nu-\omega)^2}{1 - J^2 G_R(\omega) G_R(\nu-\omega)} \xrightarrow{\nu \to 0} \frac{1}{J^2} \frac{\pi}{4} \frac{1}{-i\tilde{\nu}} \frac{JA(\omega)}{\omega}. \tag{2.32}$$

This pole is important for chaos, although it doesn't give the exponential growth by itself. In order to have exponential growth, we must deviate from the strict large M limit and include the rung contributions which are suppressed by $\frac{1}{M}$. Nevertheless, the presence of the pole in the lowest order four-point function allows the rungs to be separated by a large time interval, so that each rung can traverse the whole real time contour independently. Note that the right hand side of Eq. (2.31) is negative at small ν, but its multiplication with the rungs (Figure 3.3) is always positive. So the coefficient a in Eq. (3.15) is positive.

Now we see that $\frac{1}{M}$ order corrections must be included in the calculation, and therefore we also have to include the self-energy correction to the rotor two point function to that order. This amounts to evaluating the diagram in Figure 2.7, which is computed in the Appendix A.2. Write $G_R(\omega)$ as $G_R^{(0)}(\omega) + \frac{1}{M} G_R^{(1)}(\omega)$. Substituting into Eq. (2.32), we find that the correction shifts the pole by an amount proportional to $\frac{1}{M} \Re[G_R^{(0)}(\omega) G_R^{(1)}(-\omega)]$, suppressed by a factor of $\frac{1}{M}$.

2.4.3 Summing ladder diagrams

Now we have all the ingredients to calculate the four-point function $\tilde{\mathcal{C}}(t)$ by summing all the ladder diagrams with rungs composed of λ propagators. The summation of these diagrams can be done by solving a self-consistent equation. Following the method in Ref. [102], we write

down the Bethe-Saltpeter equation for $\tilde{\mathcal{C}}(t)$ as shown in Figure 2.8.

Figure 2.8: Bethe-Saltpeter equation. The wavy line contains both type-I and type-II rungs.

The diagram without any rung insertion is just $\tilde{\mathcal{C}}_0(t)$. Define $f(\nu,\omega)$ by

$$\tilde{\mathcal{C}}(\nu) = \frac{1}{MN}\int \frac{d\omega}{2\pi} f(\nu,\omega). \tag{2.33}$$

Then following Figure 2.8, we can write

$$f(\nu,\omega) = f_0(\nu,\omega)\left[1 + \frac{1}{M}\int \frac{d\omega'}{2\pi} G_{\text{rung}}(\omega,\omega') f(\nu,\omega')\right]. \tag{2.34}$$

Keeping the corrections up to order $\frac{1}{M}$ in $f_0(\nu,\omega)$ and restricting to small ν comparable to $\frac{1}{M}$, we approximate $f_0(\nu,\omega)$ by

$$f_0(\nu,\omega) \xrightarrow{\nu\to 0} \frac{1}{J^2}\frac{\pi}{4}\frac{1}{(-i\tilde{\nu})\frac{\omega}{JA(\omega)} - \frac{1}{M}\frac{\pi}{2}J^2\Re[G_R^{(0)}(\omega)G_R^{(1)}(-\omega)]}. \tag{2.35}$$

In Eq. (2.34), $G_{\text{rung}}(\omega,\omega')$ contains the contributions of both type-I and type-II rung. More specifically, it can be written as (see Figure 3.3)

$$\frac{1}{M}G_{\text{rung}}(\omega,\omega') = \frac{1}{M}\left[\tilde{G}_W^{\lambda}(\omega-\omega') + \int \frac{d\omega''}{2\pi}\tilde{G}_W^{n}(\omega-\omega'')G_R^{\lambda}(\omega'')\tilde{G}_W^{n}(\omega''-\omega')G_R^{\lambda}(\nu-\omega'')\right]. \tag{2.36}$$

In Eq. (2.36) the wavy line on top of Σ and G means that we have extracted the factor $\frac{1}{M}$ from them. Note that the second term of Eq. (2.36) contains two G_R^{λ}'s, but only one $\frac{1}{M}$ is in front.

This is because the $O(M)$ indices on the two sides of type-II rung can be different (see fig 3.3) and one of the indices must be summed over when attached to a ladder diagram, which gives a factor of M. In summary, in the small ν limit we rewrite Eq. (2.34) as

$$(-i\tilde{\nu})f(\nu,\omega) = \frac{1}{J^2}\frac{\pi}{4}\frac{JA(\omega)}{\omega}\left[1+\frac{1}{M}\int\frac{d\omega'}{2\pi}G_{\text{rung}}(\omega,\omega')f(\nu,\omega')+\frac{J^4}{M}2\Re[G_R^{(0)}(-\omega)G_R^{(1)}(\omega)]f(\nu,\omega)\right]. \tag{2.37}$$

Since $A(\omega)$ is non-zero only in a region $|\tilde{\omega}| \in \mathcal{I} = \left[\sqrt{\lambda'-\frac{1}{2}}, \sqrt{\lambda'+\frac{1}{2}}\right]$, we can approximately set $f(\nu,\omega)$ to be zero outside this region. As a result, the integral in terms of ω' is only over a finite interval, which allows us to discretize the integral and treat it as a matrix multiplication. Note also that by multiplying the both sides by J^2 the equation becomes dimensionless. Moreover, we can drop the coupling constant J in the equation and in all the Green's functions appearing in the equation, while replacing all the frequencies and temperature by normalized versions, i.e. $\omega \to \tilde{\omega} = \frac{\omega}{2\sqrt{gJ}}$. Then the equation is in terms of normalized quantities and all dimensionful couplings are gone (including factors of $2\sqrt{Jg}$). We solve the corresponding eigenvalue problem numerically and restore the physical dimensions of the chaos exponent at the final step, by multiplying it by $2\sqrt{gJ}$. The details are given in Appendix A.3.

2.5 Discussion and conclusion

In this section, we discuss the relation between chaos exponent and temperature in some special cases. Of particular interest is the situation near the phase transition between paramagnetic phase and spin glass phase. For simplicity, we only discuss the chaos behavior within the paramagnetic phase and leave the discussion of spin glass phase to the future. We also discuss

the pattern of conformal symmetry breaking as compared to the SYK model.

In the future, it would be interesting to study the spin glass phase itself, to understand the interplay between glassiness and quantum information dynamics. It would also be interesting to study the experimental realization of the model, perhaps in a cavity QED or trapped ion setting. The model is experimentally interesting because its relatively analytical tractability makes it a useful benchmark, but it also displays the physics of many-body chaos in the right limit. Another direction building on our work here is to attempt to develop other models with the needed pattern of conformal symmetry breaking to achieve maximal chaos.

2.5.1 On the critical line

There are three parameters in the model, T, J and g. By tuning J and g we can reach the phase transition where the parameters obey

$$2\sqrt{\frac{g}{J}}\int_0^1 d\tilde{\omega} JA(\tilde{\omega}) \coth\frac{\tilde{\beta}\tilde{\omega}}{2} = 1 \tag{2.38}$$

with

$$JA(\tilde{\omega}) = \frac{2}{\pi}\tilde{\omega}\sqrt{1-\tilde{\omega}^2} \tag{2.39}$$

and $\tilde{\omega} = \frac{\omega}{2\sqrt{gJ}}$. We plot the transition line relating T and g, J in Figure 2.9.

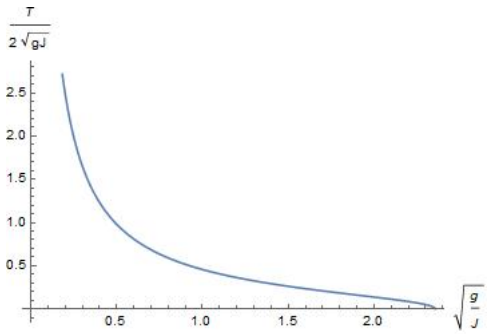

Figure 2.9: Phase transition line as a function of $\sqrt{g/J}$ and $T/2\sqrt{gJ}$.

Along the critical line the system is gapless and the spectral function of rotor field takes the simple form Eq. (2.39). So it's easier to first discuss the chaos behavior along this critical line. Using the numerical method we can only obtain the chaos exponent for temperatures bigger than the step size of the discretized frequency interval $\mathcal{I}$. Fortunately, for extremely low temperature, we can obtain a more precise relation between the chaos exponent and temperature using some approximations. When T is small, the main equation Eq. (2.37) simplifies. First, the type-I rung contribution is

$$\begin{aligned} &\int \frac{d\tilde{\omega}'}{2\pi} G_W(\tilde{\omega}-\tilde{\omega}')f(\tilde{\omega}',\tilde{\nu}) \\ &= \frac{1}{M}\int d\tilde{\omega}' \frac{A_\lambda(\tilde{\omega}-\tilde{\omega}')}{2\sinh[\frac{1}{2}\tilde{\beta}(\tilde{\omega}-\tilde{\omega}')]} f(\tilde{\omega}',\tilde{\nu}) \\ &= \frac{1}{M}\int \frac{d\bar{\omega}'}{\tilde{\beta}} \frac{A_\lambda(\frac{\bar{\omega}-\bar{\omega}'}{\tilde{\beta}})}{2\sinh[\frac{1}{2}(\bar{\omega}-\bar{\omega}')]} f(\tilde{\omega}',\tilde{\nu}), \quad \bar{\omega}=\tilde{\beta}\tilde{\omega}. \end{aligned} \tag{2.40}$$

At the limit $\tilde{\beta} \to \infty$, this integral is dominated by $(\bar{\omega}-\bar{\omega}') \sim O(1)$ due to the function $\sinh(\frac{1}{2}(\bar{\omega}-\bar{\omega}'))$ in the denominator. Thus we keep only the leading terms of the expansion

of A_λ in Appendix A.1,

$$A_\lambda\left(\frac{x}{\beta}\right)=\frac{1}{\Pi(0)^2}\frac{1}{\pi^2}\left[\frac{1}{3}\left(\frac{x}{\tilde{\beta}}\right)^3+\frac{4}{3}\pi^2\tilde{T}^2\left(\frac{x}{\tilde{\beta}}\right)+\cdots\right]. \tag{2.41}$$

Note that we have dropped all the dimensionful parameters in the calculation.

To estimate the maximal eigenvalue of this integral kernal, we approximate $f(\tilde{\omega'})$ by $f(\tilde{\omega})$ and perform the integration, which gives

$$\frac{1}{M}\frac{2\pi^2\tilde{T}^4}{\Pi(0)^2}f(\tilde{\omega},\tilde{\nu}). \tag{2.42}$$

Similarly, the type-II rung contribution can be written as

$$\begin{aligned}&M\int\frac{d\tilde{\omega}'}{2\pi}\frac{d\tilde{\omega}''}{2\pi}G_R^\lambda(\tilde{\omega}'')G_R^\lambda(-\tilde{\omega}'')G_W^n(\tilde{\omega}-\tilde{\omega}'')G_W^n(\tilde{\omega}''-\tilde{\omega}')f(\tilde{\omega}',\tilde{\nu})\\ =&\frac{1}{\tilde{\beta}^2}M\int dx\int dyG_R^\lambda\left(\tilde{\omega}+\frac{x}{\tilde{\beta}}\right)G_R^\lambda\left(-\tilde{\omega}-\frac{x}{\tilde{\beta}}\right)\frac{A(\frac{x}{\tilde{\beta}})}{2\sinh(\frac{1}{2}x)}\frac{A(\frac{y}{\tilde{\beta}})}{2\sinh(\frac{1}{2}y)}f\left(\tilde{\omega}+\frac{x}{\tilde{\beta}}+\frac{y}{\tilde{\beta}},\tilde{\nu}\right).\end{aligned} \tag{2.43}$$

We approximate $G_R(\tilde{\omega}+\frac{x}{\tilde{\beta}})$ by $G_R(\tilde{\omega})$, but still keep the x and y dependence of $f(\tilde{\omega}+\frac{x}{\tilde{\beta}}+\frac{y}{\tilde{\beta}},\tilde{\nu})$ because later we will see that the eigenfunction of interest has to change rapidly near $\tilde{\omega}$. By extracting the temperature factors, we can see the T^4 dependence of type-II rung contribution:

$$\tilde{T}^4(\frac{2}{\pi})^2MG_R^\lambda(\tilde{\omega})G_R^\lambda(-\tilde{\omega})\int d\tilde{\omega}'\int_{-\infty}^{\infty}dx\frac{x(\bar{\omega}-\bar{\omega'}-x)}{2\sinh(\frac{1}{2}x)2\sinh(\frac{1}{2}(\bar{\omega}-\bar{\omega'}-x))}f(\tilde{\omega}',\tilde{\nu}) \tag{2.44}$$

Finally, we analyze the self-energy contribution. By taking imaginary part of Eq. (A.14),

we obtain

$$\frac{1}{\pi}\Im\Sigma_R(\omega) = \int dx A_\lambda(x) A(\omega - x)(n_B(x) - n_B(x-\omega)) \tag{2.45}$$

This function is non-negative for positive frequency. By the results in Appendix A.2, we know that the self-energy contribution in Eq. (2.37) is

$$2\Re(G_R^{(0)}(\omega)G_R^{(1)}(-\omega)) = -\frac{\Im\Sigma_R(\omega)}{\Im G_R^{(0)}(\omega)}, \quad \text{for } |\omega| \in \mathcal{I}, \tag{2.46}$$

so it is always non-positive.

At small frequency and low temperature, Eq. (2.45) has the expansion

$$\frac{1}{\pi}\Im\Sigma_R(\tilde{\omega}) = \frac{1}{\Pi(0)^2}\left(\frac{1}{30\pi^3}\tilde{\omega}^5 + \frac{2}{3\pi}\tilde{\omega}^3\tilde{T}^2 + \frac{32}{15}\pi\tilde{T}^4\tilde{\omega} + ...\right). \tag{2.47}$$

The $\tilde{T}^4$ term dominates at small frequency. Since the positive contributions to chaos exponent are all proportional to $\tilde{T}^4$ at low temperature, we require the eigenfunction to center around $\tilde{\omega} = 0$ and decay rapidly within $O(\frac{1}{\tilde{\beta}})$.

Combining the type-I and type-II rung contributions, we obtain the chaos exponent at very low temperature:

$$\tilde{\lambda}_c = \frac{1.1 \times 10^3}{M}\tilde{T}^4 \tag{2.48}$$

and

$$\lambda_c = 2\sqrt{gJ}\tilde{\lambda}_c = \frac{138}{M}\frac{T^4}{(gJ)^{\frac{3}{2}}}. \tag{2.49}$$

Here we comment that the T^4 dependence of chaos exponent for low temperature still hold for finite value of M, while the proportional constant in front of T^4 does depend on M. As

commented in [98], the higher order of $\frac{1}{M}$ corrections don't modify the scaling dimension of rotor field, so the leading non-analytic part of $G(i\omega_n)$ is always proportional to $|\omega_n|$. Then further check shows that, for λ field two point function (Eq. (2.21)), these corrections only modify the constant c, while leave the scaling dimension unchanged. Therefore, $G_\lambda(i\omega_n)$ still have it's leading non-analytic part proportional to $|\omega_n|^3$ at critical point. This guarantees the form of Eq. (2.41) and Eq. (2.44) up to a proportional constant. Then by a similar analysis of this section, one can show that the chaos exponent must be proportional to T^4 at low temperature for any value of M.

At higher temperature, numerical results show that the chaos exponent always increases with T. It saturates at some fixed number when T goes to infinity.

$$\lim_{T\to\infty} \lambda_c = \frac{5.5\sqrt{gJ}}{M} \tag{2.50}$$

The following table shows the results for finite temperature.

Inverse $\tilde{T}$ $\tilde{\beta}$	**Chaos exponent** $M\tilde{\lambda}_c$
0.01	2.75
0.5	2.72
1	2.63
10	0.14
30	0.0014
60	0.000073

Table 2.1: Numerical data: along the phase transition line. In the table, $\tilde{\beta} = \frac{2\sqrt{gJ}}{T}$, and $\tilde{\lambda_c} = \frac{\lambda_c}{2\sqrt{gJ}}$.

2.5.2 At fixed ratio of $\frac{g}{J}$

Another case we studied is when $\frac{g}{J}$ is fixed and temperature changes. In this case, Eq. (2.38) is solved by the following ansatz,

$$JA(\tilde{\omega}) = \frac{2}{\pi}\text{sgn}(\omega)\sqrt{(\tilde{\omega}^2 - \lambda' + \frac{1}{2})(\lambda' + \frac{1}{2} - \tilde{\omega}^2)}. \tag{2.51}$$

At low temperature, we obtain the following condition by working with leading order approximation.

$$\delta\lambda \ln \tilde{T} + \frac{2\pi^2}{3}\tilde{T}^2 = 0 \tag{2.52}$$

where $\delta\lambda = \lambda' - \frac{1}{2}$. The thermal gap as a function of T is determined by it since $\Delta(T) = 2\sqrt{gJ\delta\lambda}$. Unlike the previous case, the small frequency and low temperature expansion for spectral functions are more complicated, depending on the relative order of ω and T.

$$\begin{aligned} A_\lambda(\tilde{\omega}) &= \left(\frac{1}{\Pi(0)}\right)^2 \frac{1}{\pi^2}\left[\frac{1}{3}\tilde{\omega}^3 + 2\tilde{\omega}\delta\lambda \ln \tilde{T} + \frac{4\pi^2}{3}\tilde{T}^2\tilde{\omega}\right] + \cdots, \quad \text{for } \omega \gg T \\ &= \left(\frac{1}{\Pi(0)}\right)^2 \frac{1}{\pi^2}\left[\frac{1}{3}\tilde{\omega}^3 + \frac{4\pi^2}{3}\tilde{T}^2\tilde{\omega}\right] + \cdots, \qquad \text{for } \omega \ll T. \end{aligned} \tag{2.53}$$

We can see from this expression that the chaos exponent is still proportional to T^4 at low temperature. Then we present some results for general T.

Inverse $\tilde{T}$ $\tilde{\beta}$	**Chaos exponent** $M\tilde{\lambda}_c$
0.1	121.97
1	4.27
5	0.20
10	0.037
30	0.00058
60	0.000037

Table 2.2: Relation between chaos exponent and inverse temperature, with J and g fixed. In the table, $\tilde{\beta} = \frac{2\sqrt{gJ}}{T}$, and $\tilde{\lambda_c} = \frac{\lambda_c}{2\sqrt{gJ}}$.

2.5.3 Dependence on coupling constant J

We investigated the low temperature limit of the chaos exponent in the previous two sections. From the results, it seems that λ_c is negatively related to J. However, this is not true since in both two cases we required the ratio $\frac{g}{J}$ to be a constant which may depends on T, thus forcing g to increase with J. From the Lagrangian we know that g represents the relative importance of quantum effect and it's increase tends to negatively affects the chaos exponent. So in this section we examine numerically the effect of increasing J with g fixed.

The chaos exponent as a function of T, $\sqrt{Jg}$ and $\sqrt{\frac{g}{J}}$ is represented by $2\sqrt{gJ}\tilde{\lambda}_c\left(\frac{T}{\sqrt{Jg}}, \sqrt{\frac{g}{J}}\right)$. It changes to $2\sqrt{k}\sqrt{gJ}\tilde{\lambda}_c\left(\frac{1}{\sqrt{k}}\frac{T}{\sqrt{Jg}}, \frac{1}{\sqrt{k}}\sqrt{\frac{g}{J}}\right)$ as J changes to kJ. The numerical results show that the new exponent is always smaller than the old one if k is smaller than one, within paramagnetic phase. This matches with the intuition that chaos exponent increases with the magnitude of the random interaction.

Inverse $\tilde{T}$ $\tilde{\beta}$	**factor** k	**Chaos exponent** $\sqrt{k}\tilde{\lambda}_c$
1	1	2.63
	0.8	2.17
	0.6	1.68
10	1	0.14
	0.8	0.055
	0.6	0.025
30	1	0.0014
	0.8	0.000018
	0.6	1.3×10^{-6}

Table 2.3: Relation between chaos exponent and coupling constant J, with g and T fixed. Decreasing k denotes the decreasing of coupling J.

2.5.4 Pattern of conformal symmetry breaking

The crucial feature of the SYK model that produces maximal chaos is the explicit as well as spontaneous breaking of reparameterization symmetry. According to Ref. [66], this symmetry breaking pattern implies the existence of a pseudo-Goldstone mode with a low energy effective action suppressed by the large coupling constant βJ. It is these pseudo-Goldstone modes that give an enhanced contribution proportional to βJ in the four point function, which saturates the chaos bound.

In the model that we study, by taking large $\beta\sqrt{Jg}$ limit, one also see invariance of Eq. (2.10) under reparameterization transformations of form

$$\begin{aligned} G(\tau_1,\tau_2) &\to \left[\frac{df(\tau_1)}{d\tau_1}\frac{df(\tau_2)}{d\tau_2}\right]^{\frac{1}{2}} G(f(\tau_1),f(\tau_2)), \\ \Sigma(\tau_1,\tau_2) &\to \left[\frac{df(\tau_1)}{d\tau_1}\frac{df(\tau_2)}{d\tau_2}\right]^{\frac{1}{2}} \Sigma(f(\tau_1),f(\tau_2)) \end{aligned} \tag{2.54}$$

However, there exists a function, namely $\delta(\tau_1-\tau_2)$, that is invariant under such transforma-

tion. We can see that by taking $\tilde{\omega}_n$ to 0, the solution Eq. (2.11) in frequency space indeed reduces to a constant. Therefore, in this model, although the reparametrization symmetry is explicitly broken by the parameter $(\beta\sqrt{gJ})^{-1}$, it is not spontaneously broken to $SL(2,R)$ when $\beta\sqrt{gJ}$ goes to infinity. So it's not surprising that the chaos exponent is not maximal in this model. On the other hand, the subleading contribution of order $(\beta\sqrt{gJ})^{-1}$ to the two point function is invariant under $SL(2,R)$ as shown in Eq. (2.15). This is required by the conformal symmetry of the fixed point. Note that the conformal dimension is not the same as appeared in Eq. (2.54).

Acknowledgements: This work is supported by the Simons Foundation via the It From Qubit collaboration and the National Science Foundation via the Physics Frontier Center at the Joint Quantum Institute. We thank J. Steinberg, S. Xu, and D. Chowdhury for discussions. A related independent work by D. Mao, D. Chowdhury, and T. Senthil will appear at a later date.

Chapter 3: Scrambling with conservation laws

This chapter is based on the publication 'Scrambling with conservation laws' by Gong Cheng and Brian Swingle, published as J. High Energ. Phys. 2021, 174 (2021).

3.1 Overview

In this article we discuss the impact of conservation laws, specifically $U(1)$ charge conservation and energy conservation, on scrambling dynamics, especially on the approach to the late time fully scrambled state. As a model, we consider a $d+1$ dimensional ($d \geq 2$) holographic conformal field theory with Einstein gravity dual. Using the holographic dictionary, we calculate out-of-time-order-correlators (OTOCs) that involve the conserved $U(1)$ current operator or energy-momentum tensor. We show that these OTOCs approach their late time value as a power law in time, with a universal exponent $\frac{d}{2}$. We also generalize the result to compute OTOCs between general operators which have overlap with the conserved charges.

3.2 Introduction

3.2.1 Motivation

Quantum information scrambling [13, 19, 20] is a fundamental phenomenon in chaotic many-body systems that has been under wide discussion in recent years. On the theoretical side, this activity focused on the study of out-of-time-order correlators (OTOCs) [18, 35, 36, 71, 72, 75, 76, 84, 85, 88, 103, 104, 105]. For a chaotic system with large N number of degrees of freedom per unit volume, the OTOC displays an exponentially increasing deviation from its initial value which is characterized by a quantum Lyapunov exponent. This period of growth occurs after local equilibrium is achieved but before the scrambling time, when the system approaches global equilibrium. Schematically, given simple Hermitian operators W and V, one has

$$\text{OTOC} = \langle W(t)V(0)W(t)V(0)\rangle \sim f_0 - \frac{f_1}{N}e^{\lambda_L t} + \cdots . \tag{3.1}$$

For a large N conformal field theory (CFT) holographically described by Einstein gravity, earlier works [36][84][106][107][106] calculated OTOCs through geometric methods, by studying shockwave geometries. The Lyapunov exponent in such a theory is equal to $\frac{2\pi}{\beta}$, saturating the conjectured chaos bound [37]. For times much larger than scrambling time (the late time regime), the OTOC decays to zero exponentially fast, with a different but related exponent. By contrast, it was shown in [108] that in a random circuit model with local charge conservation law, the OTOC between the charge density operator and a non-conserved operator displays a power law tail at late time. While such power law tails are expected to be generic, they have not yet been seen in holographic systems. This missing piece of physics motivated the present study.

Other studies of the interplay between conservation laws, hydrodynamics, and OTOCs include [19, 77, 81, 109, 110, 111, 112, 113, 114, 115, 116, 117, 118, 119].

The bulk of this work focuses on the $U(1)$ case: we compute OTOCs between the conserved charge density and a (non-conserved) scalar operator and show that holographic systems also exhibit power law tails consistent with the random circuit result. We also argue that power law tails will be induced by energy conservation. This has not been shown before, but it is important since Hamiltonian systems generically have energy conservation but not charge conservation. In the remainder of the introduction, we review existing holographic calculations, focusing on the scattering approach. Then, in the rest of the article, we show how these calculations are modified due to $U(1)$ charge conservation and we interpret the result physically. We also discuss the extension to energy conservation. Overall, we view this work as a study of the interplay between slow modes, as in hydrodynamics, and the fast dynamics of scrambling.

3.2.2 Review of the holographic calculation

The holographic calculation of OTOCs for scalar operators is discussed in many works. The approach that we follow here is based on the scattering approach discussed in [84]. In this approach, the boundary OTOC is written as an inner product of in and out asymptotic states.

$$\begin{aligned} \langle W(t_1,x_1)V(t_2,x_2)W(t_1,x_1)V(t_2,x_2)\rangle &= \langle out|in\rangle \\ |in\rangle &= W(t_1,x_1)V(t_2,x_2)|TFD\rangle \\ |out\rangle &= V^\dagger(t_2,x_2)W^\dagger(t_1,x_1)|TFD\rangle. \end{aligned} \tag{3.2}$$

From the bulk perspective, these in and out states may be written in terms of bulk wave-

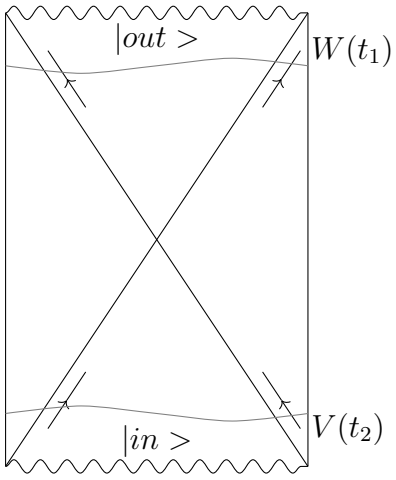

Figure 3.1: in and out sates in the Penrose diagram. The data on the in and out slices are given by Eq. (3.3).

functions as

$$\begin{aligned} |in\rangle &= \int dp^u dx \int dp^v dx' \phi_W(p^v, x)\phi_V(p^u, x')|p^u, x, p^v, x'\rangle_{in} \\ |out\rangle &= \int dp^u dx \int dp^v dx' \phi_{W^\dagger}(p^v, x)\phi_{V^\dagger}(p^u, x')|p^u, x, p^v, x'\rangle_{out}. \end{aligned} \tag{3.3}$$

Here u and v are null coordinates in the black hole geometry dual to the thermofield double state $|TFD\rangle$.

Note that the momentum states are only well-defined near the black hole horizon. We think of the scattering as taking place in the approximately flat near horizon region as described by Kruskal coordinates. This corresponds to the case of large time separation between t_1 and t_2, as

shown in Fig 3.1. The wave functions are given by bulk-to-boundary propagators. So

$$\begin{aligned}
\phi_W(p_1^v, x) &= \int dv e^{ip_1^u v} \langle \phi_W(u, v, x) W(t_2, x_2) \rangle|_{u=-\epsilon} \\
\phi_V(p_2^u, x') &= \int du e^{ip_2^v u} \langle \phi_V(u, v, x) V(t_1, x_1) \rangle|_{v=\epsilon} \\
\phi_{W^\dagger}(p_1^v, x) &= \int dv e^{ip_1^u v} \langle \phi_W(u, v, x) W^\dagger(t_2, x_2) \rangle|_{u=-\epsilon} \\
\phi_{V^\dagger}(p_2^u, x') &= \int du e^{ip_2^v u} \langle \phi_V(u, v, x) V^\dagger(t_1, x_1) \rangle|_{v=\epsilon}
\end{aligned} \tag{3.4}$$

These formulae have a direct interpretation as bulk scattering states sourced by boundary operators. The relevant energy scale is determined by the boundary time separation through the Mandelstam variable $s := 2p_1^v p_2^u \sim e^{\frac{2\pi}{\beta} t_{12}}$. For scrambling physics, we are interested in time scales that are larger than the relaxation time. The dominate contribution in this regime comes from summing ladder diagrams with graviton exchanges [120]. To leading order in s, the S-matrix approaches a pure phase, obtained from the eikonal approximation,

$$|p_1^u, x, p_2^v, x'\rangle_{out} \sim e^{i\delta(s,b)} |p_1^u, x, p_2^v, x'\rangle_{in} + \cdots \tag{3.5}$$

The physical interpretation of this phase factor is interaction of particle 1 with a gravitational shockwave sourced by particle 2 [121][122]. The shockwave metric is

$$ds^2 = A(uv) du[dv - \delta(u) h(x) du] + B(uv) d^d x. \tag{3.6}$$

While passing through the shockwave located near $u \sim 0$, the scalar wave function receives a

jump in the v coordinate,

$$\int dp_1^u \phi(p_1^u, x) e^{ip_1^u h(x)} e^{-ip_1^u v} = \phi(v - h(x), x). \tag{3.7}$$

The phase $\delta(s, b)$ is then identified with the displacement factor $h(x) = G_N p_2^v \frac{e^{-\mu|x|}}{|x|^{\frac{d-1}{2}}}$.

For scalar operators, the OTOC is evaluated in earlier works. In the limit $\Delta_W \gg \Delta_V \gg 1$, the heavy particle's wavefunction is not much affected by the shockwave sourced by the light particle. So the amplitude is simply an inner product between V particle wavefunctions with and without the shockwave,

$$\begin{aligned} \text{OTOC} &\sim \int dv dx \phi_V(v, x) \partial_v \phi_V(v - h(x), x) \\ &\sim \left[\frac{1}{1 + \frac{G_N \Delta_W}{\Gamma} e^{\frac{2\pi}{\beta} t - \mu|x|}} \right]^{\Delta_V} . \end{aligned} \tag{3.8}$$

Γ is a constant depending on the regularization of the correlator.

At early time, when the second term in denominator is much smaller than the first term, the OTOC is decreasing as shown in Eq. (3.1). Note that $e^{\frac{2\pi}{\beta} t}$ is roughly the colliding energy, and it enters through p dependence of $h(x)$. The exponent is $\frac{2\pi}{\beta}$, independent of the operator. The correlator has decayed significantly when the second term in the denominator is $O(1)$. After this time, the correlator experiences an expontial decay with an operator-dependent exponent. We refer to this as the late time regime of OTOC.

3.2.3 Results and outline

The situation is changed when we consider an OTOC that involves conserved charges. For example, the R-charge in $\mathcal{N} = 4$ SYM theory, and more generally the energy-momentum tensor. We will see that due to the hydrodynamical property of the conserved current, the particle sourced by these operators in the bulk spreads over a large region of space-time. As a result, the collision responsible for scrambling happens at a wide range of space-time points in the classical picture (see Fig 3.2). When the collision occurs near the horizon, the center of mass energy is large, but when the collision occurs further away from the horizon, the center of mass energy is smaller. This leads to a smearing of the exponential factor in Eq. (3.8), effectively replacing the OTOC formula with

$$\text{OTOC} \sim \int_0^{+\infty} ds \frac{1}{s^{\frac{d}{2}+1}} \left[\frac{1}{1 + \frac{c}{N} e^{\frac{2\pi}{\beta}(t-s)-\mu|x|}} \right]^{\alpha} \tag{3.9}$$

where c and α are some constants. One can then show that at late time, the OTOC becomes $\sim t^{-\frac{d}{2}}$.

The article is organized as follows. For simplicity, we start with the conserved charge density of a $U(1)$ symmetry. In section 3.3 we give an expression for the dual photon's wave function, to lowest order in transverse momentum and frequency. Then we analyze the inner product and equation of motion for the photon field. Using these ingredients and some additional approximations, we calculate the OTOC. In section 3.4 we interpret these calculations in terms of the classical picture in Fig. 3.2. In section 3.5 we discuss the case of the energy-momentum tensor. Finally, we generalize the result in section 3.6 to the case of generic operators with overlap with the conserved currents.

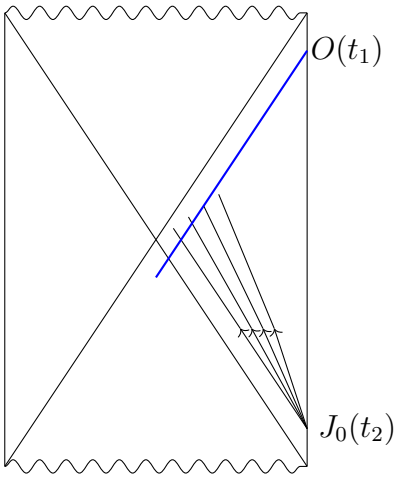

Figure 3.2: Photon scatters with shockwave. The blue line denotes the shockwave sourced by scalar operator. The photon sourced by charge operator spreads in space-time. Classically, we can view it as a bunch of photons, with different longitudinal energy.

3.3 Correlator with U(1) charge

3.3.1 Solution to equation of motion

In an AdS-Schwarzschild black hole background, the metric is

$$ds^2 = L^2 \left[-\frac{f(R)}{R^2} dt^2 + \frac{1}{R^2 f(R)} dR^2 + \frac{1}{R^2} d^d \vec{x} \right] \tag{3.10}$$

where $R = R_+$ is the horizon and boundary is at $R = 0$. The inverse temperature is $\beta = \frac{4\pi R_+}{d+1}$ and $f(R) = 1 - (\frac{R}{R_+})^{d+1}$. It's more convenient to use the tortoise coordinate, r, defined by

$$dr = -\frac{1}{f(R)} dR. \tag{3.11}$$

The domain of r is $r \in (-\infty, 0]$ with $-\infty$ corresponding to the horizon and 0 corresponding to the boundary. In this coordinate, the metric components are $g_{rr} = -g_{tt} = L^2 \frac{f(R)}{R^2}$. Here we

use $\vec{x}$ to denote the coordinates of the transverse directions. We also consider a Maxwell field propagating in this geometry whose dynamics determines the behavior of a $U(1)$ current operator J_0 on the boundary. In this note, we will focus on the four-point correlation function with two insertions of J_0 and two insertions of a scalar operator O.

The Maxwell-Einstein equation is

$$\partial_\mu(\sqrt{-g}F^{\mu\nu}) = \partial_\mu(\sqrt{-g}g^{\mu\rho}g^{\nu\sigma}F_{\rho\sigma}) = 0. \tag{3.12}$$

Consider the ansatz $A_i = 0$ for all the transverse directions. The Fourier mode decomposition is

$$A_\mu(r,t,\vec{x}) = \int d\omega d\vec{k} A_\mu(r,\omega,k)e^{-i\omega t}e^{i\vec{k}\cdot\vec{x}} \tag{3.13}$$

Using the trick in [123], we pick a transverse coordinate frame for each $\vec{k}$, such that the x-axis is parallel to $\vec{k}$ direction, with the other axes perpendicular to it. Then ∂_x can be replaced by ik when acting on that mode, and derivatives in other transverse direction are replaced by 0. We also assume that the A field is spherically symmetric and excited by a point source sitting at $\vec{x'} = 0$, so the momentum space A only depends on norm of $\vec{k}$.

Written in component form, the equations are

$$\begin{cases} \partial_r(\sqrt{-g}g^{rr}g^{tt}(\partial_r A_t - \partial_t A_r)) + \partial_x(\sqrt{-g}g^{xx}g^{tt}\partial_x A_t) = 0 \\ \partial_t(\sqrt{-g}g^{tt}g^{rr}(\partial_t A_r - \partial_r A_t)) + \partial_x(\sqrt{-g}g^{xx}g^{rr}\partial_x A_r) = 0 \\ \partial_r(\sqrt{-g}g^{rr}g^{xx}(-\partial_x A_r)) + \partial_t(\sqrt{-g}g^{tt}g^{xx}(-\partial_x A_t)) = 0. \end{cases} \tag{3.14}$$

From the second equation, one can deduce

$$\begin{aligned} -\omega^2 g^{tt} A_r + i\omega g^{tt}\partial_r A_t - k^2 g^{xx} A_r = 0 \\ \implies A_r = \frac{i\omega g^{tt}\partial_r A_t}{\omega^2 g^{tt} + k^2 g^{xx}} \end{aligned} \tag{3.15}$$

Then one can use the first equation to find a second order differential equation for A_t,

$$\partial_r(\sqrt{-g}g^{rr}g^{tt}\frac{k^2 g^{xx}\partial_r A_t}{\omega^2 g^{tt} + k^2 g^{xx}}) - k^2\sqrt{-g}g^{xx}g^{tt}A_t = 0. \tag{3.16}$$

This equation has two independent solutions. As $r \to \infty$, they behave like $e^{\pm i\omega r}$, corresponding to out-going and in-falling boundary condition at the horizon. We focus on one of them, since the other one is obtained by complex conjugation. The solution can be found explicitly in the small frequency and small momentum limit by setting $\omega \to \lambda\omega$, $k \to \lambda k$, and taking $\lambda \ll 1$. Up to first order in λ, we have

$$A_t(r,\omega,k) = e^{-i\omega r}C(\omega,k)[1 + i\omega\int_{-\infty}^{r} dr(1 - (\frac{R}{R_+})^{d-2}) + \frac{ik^2}{\omega}\int_{-\infty}^{r} dr(\frac{R}{R_+})^{d-2} f + O(\lambda^2)]. \tag{3.17}$$

The normalization constant C is fixed by requiring $\lim_{r\to 0} A_t(r,\omega,k) \to 1$. Then we find that

$$A_t(r,\omega,k) = e^{-i\omega r}\left[\frac{1 + i\omega H(r) + i\frac{k^2}{\omega}R_+\frac{1-(\frac{R}{R_+})^{d-1}}{d-1}}{1 + i\omega H(0) + i\frac{k^2}{\omega}R_+\frac{1}{d-1}} + O(\lambda^2)\right] \tag{3.18}$$

The factor $\frac{1}{d-1}R_+$ is identified as the diffusion constant D. $H(r)$ is the indeterminate integral of the second term in Eq. (3.18). If we ignore the $\omega H(0)$ term in the denominator, then this function has a pole at $\omega = -iDk^2$. With this $\omega \sim k^2$ scaling, the $\omega H(0)$ is indeed subleading

compared to the ik^2D/ω term at small ω and k. Moreover, we can anticipate that ω^2 is of order k^4 after using the residue theorem. Hence, to the leading order in small k and ω, we can neglect ω^2 and higher order terms. Another approximation is to set $(\frac{R}{R_+}) \sim 1$, corresponding to the near horizon region. Since the scrambling time is large, the relevant physics indeed happens within this region. In summary, we have

$$A_t(r,\omega,k) \sim e^{-i\omega r}\frac{\omega}{\omega + iDk^2}. \tag{3.19}$$

The real space form is

$$A_t(r,t,\vec{x}) \sim \partial_t \left[\frac{1}{(t-t'+r)^{\frac{d}{2}}} e^{-\frac{|\vec{x}-\vec{x}'|^2}{4D(t-t'+r)}}\theta(t-t'+r)\right] \tag{3.20}$$

where t' and $\vec{x}'$ label the position of the boundary source. We expect this expression to hold near the horizon when the transverse separation from the source is large. Now we use Eq. (3.15) to obtain the other components,

$$\begin{aligned} A_r &\sim \frac{i}{\omega}\partial_r A_t = A_t, \\ F_{tr} = \partial_t A_r - \partial_r A_t &= \frac{-k^2 g^{xx}\partial_r A_t}{\omega^2 g^{tt} + k^2 g^{xx}} \sim \frac{ik^2}{\omega} g^{xx} g_{tt} A_t. \end{aligned} \tag{3.21}$$

Since $g_{tt} \to 0$ near horizon, F_{tr} is also very small there. (Note that the physical electric field $E_r = \sqrt{g^{tt}}\sqrt{g^{rr}}F_{tr}$ is still finite).

3.3.2 Inner product of gauge field

The gauge invariant inner product between two gauge field configurations A_1 and A_2 is

$$(A_1, A_2) = \int \sqrt{h} n^\mu (F_{1\mu\nu}^* A_2{}^\nu - F_{2\mu\nu} A_1^{*\nu}) \tag{3.22}$$

Where the integration is over a Cauchy surface. Following [84], we choose to integrate on constant $u \sim 0$ slice. Then this inner product becomes

$$\int dv d\vec{x} \left(\frac{R}{L}\right)^{-d} g^{uv} (F_{1vu}^* A_{2v} - F_{2vu} A_{1v}^*), \tag{3.23}$$

with u and v related to t and r by

$$\begin{aligned} u &= -e^{\frac{2\pi}{\beta}(r-t)}, \\ v &= e^{\frac{2\pi}{\beta}(t+r)}, \\ (\frac{\beta}{2\pi})^2 g^{uv} &= 2uv g^{tt}. \end{aligned} \tag{3.24}$$

The various components of gauge field are related to the old ones by

$$\begin{aligned} A_v =& \frac{\partial t}{\partial v} A_t + \frac{\partial r}{\partial v} A_r, \\ =& \frac{\beta}{2\pi} \frac{1}{2v} (A_t + A_r), \\ F_{uv} =& \frac{\partial t}{\partial u} \frac{\partial r}{\partial v} F_{tr} + \frac{\partial r}{\partial u} \frac{\partial t}{\partial v} F_{rt}, \\ =& -(\frac{\beta}{2\pi})^2 \frac{1}{2uv} F_{tr}. \end{aligned} \tag{3.25}$$

Following Eq. (3.19) and Eq. (3.21),

$$\begin{aligned} A_v = \frac{\beta}{2\pi}\frac{1}{v}A_t =& \frac{1}{v}v\partial_v\left(\int d\omega d\vec{k}\frac{i}{\omega+iDk^2}v^{-i\frac{\beta\omega}{2\pi}}e^{i\vec{k}\cdot\vec{x}}\right) \\ :=& \partial_v\phi(v,\vec{x}), \\ g_{xx}g^{tt}F_{tr} =& \int d\omega d\vec{k}\frac{ik^2}{\omega+iDk^2}v^{-i\frac{\beta\omega}{2\pi}}e^{i\vec{k}\cdot\vec{x}} = -\vec{\nabla}^2\phi(v,\vec{x}). \end{aligned} \tag{3.26}$$

Plug this into the inner product expression Eq. (3.23), we get

$$\begin{aligned} (A_1,A_2) =& \int dvd^d\vec{x}\left(\frac{R}{L}\right)^{2-d}[-\nabla^2\phi_1^*(v,\vec{x})\partial_v\phi_2(v,\vec{x})+\nabla^2\phi_2(v,\vec{x})\partial_v\phi_1^*(v,\vec{x})] \\ =& \int dvd^d\vec{x}\left(\frac{R}{L}\right)^{2-d}[\vec{\nabla}\phi_1^*(v,\vec{x})\cdot\partial_v\vec{\nabla}\phi_2(v,\vec{x})-\vec{\nabla}\phi_2(v,\vec{x})\cdot\partial_v\vec{\nabla}\phi_1^*(v,\vec{x})] \end{aligned} \tag{3.27}$$

where $\phi(v,\vec{x})$ is the diffusion kernel given in Eq. (3.26). We will see that the inner product written in this way is very convenient when discussing the shockwave.

3.3.3 Scattering states

The original definition of OTOC is complicated by a UV divergence arising from coincident operator insertions. To avoid this, one can consider a regularized version obtained by inserting operators at different values of imaginary time,

$$\mathcal{C}_{reg} = Tr[\rho^{1-\epsilon}V(t_2,\vec{x}_2)W(t_1,\vec{x}_1)\rho^{\epsilon}V(t_2,\vec{x}_2)W(t_1,\vec{x}_1)] \tag{3.28}$$

To simplify the discussion, we choose a symmetric regularization. In the following, we will consider the correlator

$$\mathcal{C}_{\mathcal{J},\mathcal{O}} = Tr[\rho^{\frac{1}{2}} J_0(t_2, \vec{x}_2) O(t_1, \vec{x}_1) \rho^{\frac{1}{2}} J_0(t_2, \vec{x}_2) O(t_1, \vec{x}_1)]. \tag{3.29}$$

It has a representation as an inner product of in and out states

$$\begin{aligned} |in\rangle &= O^L(t_1, \vec{x}_1) J_0^R(t_2, \vec{x}_2) |S - AdS\rangle \\ |out\rangle &= J_0^L(t_2, \vec{x}_2) O^R(t_1, \vec{x_1}) |S - AdS\rangle \end{aligned} \tag{3.30}$$

where $|S - AdS\rangle$ denotes the Schwarzschild-AdS black hole thermal double state,

$$|S - AdS\rangle = \sum_n e^{-\frac{\beta}{2} E_n} |E_n\rangle_L |E_n\rangle_R. \tag{3.31}$$

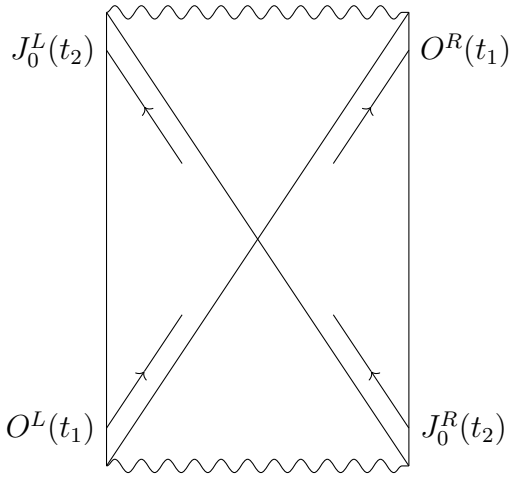

Figure 3.3: in and out sates in a symmetric regularization scheme

The superscript L and R on each operator means that the excitation is created on the left or right side, respectively. For example, $J_0^R(t_2)$ creates a photon on the right. We denote the

corresponding gauge field by A^R_μ. In general it is a linear superposition of in-falling and out-going solutions, depending on the state we are constructing. Following [124][125], we choose the coefficients such that the field has positive Kruskal frequency for in-falling mode and negative Kruskal frequency for out-going mode. For this purpose, we use the following combination

$$A^R_\mu(r,\omega,k) = (1+n(\omega))A^R_{\mu\ \text{in-falling}}(r,\omega,k) - n(\omega)A^{R*}_{\mu\ \text{in-falling}}(r,\omega,k), \tag{3.32}$$

$n(\omega)$ is the Boltzmann factor.

For the in-falling part, we use the ansatz:

$$\begin{aligned} A^R_{v\ \text{in-falling}} &= \partial_v \phi^R_{\text{in-falling}}(v,\vec{x}), \\ \phi^R_{\text{in-falling}}(v,\vec{x}) &= \int \frac{d^dk}{(2\pi)^d} \frac{1}{(ve^{-\frac{2\pi}{\beta}t_2}-1)^{\frac{\beta Dk^2}{2\pi}}} \theta(v-e^{\frac{2\pi}{\beta}t_2}) e^{i\vec{k}\cdot(\vec{x}-\vec{x_2})}. \end{aligned} \tag{3.33}$$

This is just rewritten from Eq. (3.26), except that we have inserted an extra 1 in the denominator. This change doesn't modify the long time behavior of the wave function, but it does provide some convenience in the analysis. On the other hand, the out-going part in A_v is proportional to u. To evaluate the OTOC, we choose to calculate the inner product on the surface $u \sim 0$. Hence, the out-going mode's contribution can be neglected. The thermal factor $(1+n(\omega))$ is proportional to $\frac{1}{2\sin(\frac{\beta Dk^2}{2})}$, evaluated at the diffusive pole[1]. It suggests the following ansatz for A^R_v

$$\begin{aligned} A^R_v &= \partial_v \phi^R(v,\vec{x}), \\ \phi^R(v,\vec{x}) &= \int \frac{d^dk}{(2\pi)^d} \frac{1}{2\sin(\frac{\beta Dk^2}{2})} \frac{1}{(1-ve^{-\frac{2\pi}{\beta}t_2})^{\frac{\beta Dk^2}{2\pi}}} e^{i\vec{k}\cdot(\vec{x}-\vec{x_2})}. \end{aligned} \tag{3.34}$$

[1]The actual pole contains a small real part that is higher order in k which keeps the integrand finite.

A nice property of the above expression is that the real space form of ϕ^R and $\phi^R_{in-falling}$ are related by analytical continuation, if we treat it as a complete solution of equation of motion. To see this, note that

$$\frac{1}{(1-e^{\frac{2\pi}{\beta}(t-t_2+r+i0^+)})^{\frac{\beta Dk^2}{2\pi}}}-\frac{1}{(1-e^{\frac{2\pi}{\beta}(t-t_2+r-i0^+)})^{\frac{\beta Dk^2}{2\pi}}}=2i\sin(\frac{\beta Dk^2}{2})\frac{1}{(ve^{-\frac{2\pi}{\beta}t_2}-1)^{\frac{\beta Dk^2}{2\pi}}}\theta(v-e^{\frac{2\pi}{\beta}t_2}) \tag{3.35}$$

Similarly, on the left side boundary, the operator J_0^L sources a wave function A_v^L. By symmetry, A_v^L is related to A_v^R via the transformation $(u,v)\to(-u,-v)$. Correspondingly, we define $\phi^L(v,\vec{x})=\phi^R(-v,\vec{x})$. Then A_v^L can be written as

$$\begin{aligned} A_v^L &= \partial_v\phi^L(v,\vec{x}),\\ \phi^L(v,\vec{x}) &= \int\frac{d^dk}{(2\pi)^d}\frac{1}{2\sin(\frac{\beta Dk^2}{2})}\frac{1}{(1+ve^{-\frac{2\pi}{\beta}t_2})^{\frac{\beta Dk^2}{2\pi}}}e^{i\vec{k}\cdot(\vec{x}-\vec{x_2})}. \end{aligned} \tag{3.36}$$

The scalar operator O^R and O^L create scalar mode in the bulk. For simplicity, we assume that the scalar operator O has a large conformal dimension, corresponding to a particle in bulk with a large mass. As a consequence, we can treat the scalar particle semi-classically. As it moves deep into the bulk, the scalar mode carries the shockwave along with it, which modifies the photon's wave function as we will analyze in the next section. In contrast, we will neglect the back-reaction from the photon on this scalar mode.

3.3.4 Shockwave geometry

Since we are interested in the large time limit of the OTOC, we will take $t_1\gg\beta$ and $t_2\ll-\beta$. As a result, the geodesic of the scalar particle is approximated by $u=\epsilon\sim 0$. The

shockwave geometry is described by a metric that contains a singularity near the horizon,

$$ds^2 = 2g_{uv}du[dv - \delta(u)h(\vec{x})du] + g_{xx}d\Omega_d, \tag{3.37}$$

where $h(\vec{x}) = \frac{\Delta_O}{N} e^{\frac{2\pi}{\beta}t_1 - \mu|\vec{x}-\vec{x}_1|}$ and $\mu = \sqrt{\frac{2d}{d+1}}\frac{2\pi}{\beta}$.

The Maxwell-Einstein equation in this background is

$$\begin{aligned} \partial_v(\sqrt{\gamma}F_{uv}g^{uv}) + \sum_{i=1}^{d}\partial_i(\sqrt{\gamma}g^{ii}F_{iv}) = 0, \\ \partial_u(\sqrt{\gamma}F_{vi}g^{ii}) + \partial_v(\sqrt{\gamma}F_{ui}g^{ii}) + \partial_v(\sqrt{-g}g^{vv}F_{vi}g^{ii}) = 0, \end{aligned} \tag{3.38}$$

.

where the i's run from 1 to d and label the transverse directions. The effect of the shockwave is encoded in the g^{vv} component. γ is the metric determinant in the transverse directions, so $-g = g_{uv}^2\gamma$.

As before, we simplify the equation by approximating $\frac{R}{R_+} \sim 1$ such that we can set $\gamma = (\frac{L}{R})^{2d}$ and $g^{ii} = (\frac{L}{R})^2$. Then using $g^{vv} = -(g^{uv})^2 g_{uu} = 2g^{uv}h(\vec{x})\delta(u)$, the second equation becomes

$$-\partial_u\partial_i A_v - \partial_v\partial_i A_u - 2\partial_v(\partial_i A_v h(\vec{x})\delta(u)) = 0. \tag{3.39}$$

In the region $u < \epsilon$ and $u > \epsilon$, the first two terms are finite. At $u = \epsilon$, we are searching for a solution where A_v jumps and A_u may contain a delta function $\delta(u)$. On the other hand, from the first equation of Eq. (3.38), F_{uv} must be finite. Therefore the delta functions in $\partial_u A_v$ and $\partial_v A_u$ must cancel each other at $u = \epsilon$. Applying this condition, Eq. (3.39) can be written as

$$-2\partial_u\partial_i A_v - 2\partial_v(\partial_i A_v h(\vec{x})\delta(u)) = 0. \tag{3.40}$$

Integrating over u we obtain

$$\partial_i A_v(v,\vec{x})|_{u=\epsilon+0^+} = \partial_i A_v(v-h(\vec{x}),\vec{x})|_{u=\epsilon-0^+}. \tag{3.41}$$

Note that this shift in v doesn't commute with derivatives in the transverse directions, so this simple shift rule only applies to $\vec{\nabla}A$ instead of A itself. The first equation in Eq. (3.38) gives the same relation between F_{uv} and A as in Eq. (3.21). Comparing with Eq. (3.26), we find that this simple shift rule also applies to $\vec{\nabla}\phi(v,\vec{x})$. Hence,

$$\vec{\nabla}\phi(v,\vec{x})|_{u=\epsilon+0^+} = \vec{\nabla}\phi(v-h(\vec{x}),\vec{x})|_{u=\epsilon-0^+}, \tag{3.42}$$

which is the reason to write the inner product in the form of Eq. (3.27). In summary, after scattering with the shockwave, the wave function sourced by J_0^R is modified according to the rule Eq. (3.42). If we choose to evaluate the inner product, Eq. (3.27), just after the scattering, along $u=\epsilon+0^+$, then ϕ_1 and ϕ_2 (in Eq. (3.27)) should be

$$\begin{aligned}\vec{\nabla}\phi_1(v,\vec{x}) &= \vec{\nabla}\phi^L(v,\vec{x}),\\ \vec{\nabla}\phi_2(v,\vec{x}) &= \vec{\nabla}\phi^R(v-h(\vec{x}-\vec{x_1}),\vec{x}).\end{aligned} \tag{3.43}$$

3.3.5 Calculation of OTOC

In this section, we evaluate the inner product in Eq. (3.27). It turns out that the relevant integral in is easier to do in momentum space. Define

$$\phi(p,\vec{x}) = \int dv e^{ipv}\phi(v,\vec{x}), \tag{3.44}$$

so that

$$\begin{aligned}
\vec{\nabla}\phi_1(p,\vec{x}) &= \int \frac{d^d\vec{k}}{(2\pi)^d}\frac{-i\vec{k}}{2\sin(\frac{\beta Dk^2}{2})}\frac{p^{\frac{\beta Dk^2}{2\pi}-1}e^{Dk^2t_2}}{\Gamma(\frac{\beta}{2\pi}Dk^2)}e^{ipe^{\frac{2\pi}{\beta}t_2}+iph(\vec{x}-\vec{x}_1)}e^{i\vec{k}\cdot(\vec{x}-\vec{x_2})}\theta(p),\\
\vec{\nabla}\phi_2(p,\vec{x}) &= \int \frac{d^d\vec{k}}{(2\pi)^d}\frac{-i\vec{k}}{2\sin(\frac{\beta Dk^2}{2})}\frac{p^{\frac{\beta Dk^2}{2\pi}-1}e^{Dk^2t_2}}{\Gamma(\frac{\beta}{2\pi}Dk^2)}e^{-ipe^{\frac{2\pi}{\beta}t_2}}e^{i\vec{k}\cdot(\vec{x}-\vec{x_2})}\theta(p).
\end{aligned} \tag{3.45}$$

Note that if we only keep the leading order terms in k^2, then the term $\sin(\frac{\beta Dk^2}{2})$ will cancel with $\Gamma(\frac{\beta}{2\pi}Dk^2)$. As long as we are considering large transverse coordinate separation, this approximation should be qualitatively correct. Plugging these into Eq. (3.27) and approximating $\frac{R}{R_+}\sim 1$, we obtain

$$\begin{aligned}
&(A_1,A_2) =\\
&\frac{1}{\pi}\int dp\int d^d\vec{x}\int\frac{d^dk}{(2\pi)^d}\int\frac{d^dk'}{(2\pi)^d}(\vec{k}\cdot\vec{k}')pp^{Dk^2-1}e^{Dk^2t_2}p^{Dk'^2-1}e^{Dk'^2t_2}e^{-2ipe^{t_2}}e^{-iph(\vec{x}-\vec{x_1})}e^{i(\vec{k}'-\vec{k})\cdot(\vec{x}-\vec{x_2})}.
\end{aligned} \tag{3.46}$$

To save space, we have suppressed the factor $\frac{\beta}{2\pi}$ setting the units of time. After some changes of variable and approximations shown in Appendix B.2, we obtain the final expression for the

OTOC as

$$(A_1, A_2) \sim \frac{1}{\left[\ln\left(2 + \frac{\Delta_O}{N} e^{\frac{2\pi}{\beta} t_{12} - \mu|\vec{x}_{12}|}\right)\right]^{\frac{d}{2}}}. \tag{3.47}$$

At early time, this expression admits a large N expansion in which the leading term still grows exponentially with time. Moreover, one can identify the same Lyapunov exponent and butterfly velocity as in the non-conserved OTOC in Eq. (3.8). In the late time limit, the $\ln$ of the exponentially growing part in the denominator gives rise to a power law time decay behavior. Hence, we find a significant difference from the OTOC of non-conserved operators in the late time regime.

3.4 Physical interpretation

In this section we try to understand the result in Eq. (3.47) in a more intuitive way. In the last section, we calculated the OTOC by integrating first over the radial momentum. Although this makes the calculation easier, the physical reason why we expect a power law decay at late time is somewhat obscured. As an alternative approach, we can perform the spatial momentum integral at the beginning and rewrite the integral in Eq. (3.46) as

$$\int_0^{+\infty} ds \int d^d\vec{x} \left| \vec{\nabla} \left(\frac{1}{(Ds)^{\frac{d}{2}}} e^{\frac{-|\vec{x}|^2}{4Ds}} \right) \right|^2 e^{-2ie^{-s}} e^{-i\frac{1}{N} e^{t_{12} - s - \mu|\vec{x} - \vec{x}_{12}|}} \tag{3.48}$$

Here s is defined as $s = \ln(\frac{e^{-t_2}}{p})$ and we have cut-off the large momentum contribution for $p > e^{-t_2}$.

This formula has a direct physical interpretation. The squared term can be viewed as the

photon's wave function. From the solution Eq. (3.20), we see that the photon's wave function is extended both in the radial direction and in the transverse directions. Although we obtain Eq. (3.48) in momentum space, it's more inspiring to think of s as the radial coordinate. Small values of s correspond to regions close to the horizon, while larger values of s correspond to regions further from the horizon. The last term is a phase induced by the gravitational scattering, and $e^{t_{12}-s}$ measures the relative scattering energy of the two particles. Therefore, it is natural to think of the scattering between the photon's large wave-packet and the scalar particle's localized wave-packet as taking place over a large range of radial depths. Then as the scalar particle scans through the photon's wave function, the colliding energy effectively becomes smaller and smaller.

The term in the middle can be thought of as a regulator for large momentum (small s). Since we didn't obtain the complete solution of the photon's wave function in the black hole geometry, the regulator might be replaced by a more general function in the full solution. However, if we're only interested in the late time behavior, meaning $t_{12} - \mu|\vec{x}_{12}| \gg \ln(N)$, then the integral in s receives its dominate contribution from $s > t_{12}$ due to the fast oscillation of the phase term for small s. The regulator is therefore not important, and we can directly see that the result is proportional to $\frac{1}{t_{12}{}^{\frac{d}{2}}}$.

3.5 Correlator with stress-energy tensor

The low energy hydrodynamics of the stress-energy tensor shares some similarity with that of $U(1)$ charge. In this section, we show that the OTOC has the same late time behavior. As shown in [126][127][128], in hydrodynamic limit, small perturbation of stress-energy tensor splits into sound and shear modes. The corresponding graviton wave functions in the bulk have

a sound pole and a diffusive pole, respectively. The shear mode is relatively easier to analyze, as it involves less components of the metric perturbation, but we will see that they have the same qualitative effect on the OTOC in the late time regime.

As above, we take the $\vec{k}$ direction as the x-axis. The shear modes consist of T_{ty}, T_{xy}. Here y can be any direction perpendicular to x, Sound modes are more involved, including T_{tt}, T_{tx}, T_{xx} and T_{yy}. The shear and sound mode operators on the boundary excite bulk metric fluctuation corresponding to vector and scalar perturbations, respectively. Taking the operator T_{ty} as an example, it sources the bulk metric perturbations h_{ty} and h_{yr}. Other choices of non-zero metric components are related to this by a gauge transformation. The spherically symmetric choice of scalar perturbation sourced by T_{tt} involves h_{tt}, h_{tr}, $h_{xx} = h_{yy}$, and h_{rr}. For simplicity, we mainly discuss the shear mode and comment on the sound mode in the end.

3.5.1 Wave function of graviton

For a given momentum $\vec{k}$, choose the coordinate system such that the x-axis is parallel to $\vec{k}$. The shear modes involve the $T^{ty}(\omega, \vec{k})$ and $T^{xy}(\omega, \vec{k})$ components, and are described by

$$\begin{aligned} T^{xy} &= -D_T \partial_x T^{ty}, \\ \partial_t T^{ty} + \partial_x T^{xy} &= 0, \end{aligned} \tag{3.49}$$

which together imply

$$\partial_t T^{ty} = D_T \partial_x^2 T^{ty}. \tag{3.50}$$

In AdS/CFT, the dynamics of these modes can be found by solving the linearized Einstein

equation,

$$\delta R_{\mu\nu} = \frac{2}{d}\Lambda h_{\mu\nu}, \tag{3.51}$$

where d is the spacial dimension of boundary theory. $h_{\mu\nu}$ is the metric perturbation, $\delta g_{\mu\nu} = h_{\mu\nu}$. The equations are simplified if we set to zero all the components except h_{ty} and h_{ry}. Then there are only two independent equations,

$$\begin{aligned}
&(k^2 - \frac{\omega^2}{f(R)})h_r^y + \frac{i\omega}{f(R)}\partial_r h_t^y = 0, \\
&\frac{d}{R}h_r^y + \frac{1}{f(R)}\partial_r h_r^y + \frac{i\omega}{f(R)}h_t^y = 0,
\end{aligned} \tag{3.52}$$

where R is the radial coordinate in the metric Eq. (3.10) and r is the tortoise coordinate defined in Eq. (3.11). The two first order equations then lead to a second order differential equation for h_t^y,

$$\partial_r^2 h_t^y + \partial_r \ln\left(\frac{1}{R^d(\omega^2 - k^2 f)}\right)\partial_r h_t^y + (\omega^2 - k^2 f)h_t^y = 0. \tag{3.53}$$

This equation is the same as equation in $U(1)$ charge case except with $d-2$ replaced by d (see Eq. (B.47)). Thus we have the same solution, except the diffusion constant $D_T = \frac{1}{d+1}R_+$ is different. Also, while the photon wave function excited by J_0 is spherically symmetric in the boundary spatial plane, in this case, since the shear mode operator T_{ty} contains a spatial index, it breaks the spherical symmetry. So we expect that the wave function given by Eq.(3.20) only captures the dependence on directions $\vec{x}$ satisfying $\vec{x} \perp y$. In the y direction, the mode propagates as sound. To avoid the complexity of mixing sound and shear modes, we restrict to consider the string operator living in $d-1$ spatial dimensions, $T^s(t, \vec{x}) := \int_{-\infty}^{+\infty} dy T_{ty}(t, y, \vec{x})$. Note that the choice of line operators over point operators can change late-time exponents by shifting the

effective dimension of space.

3.5.2 Interaction with the shockwave

We continue to focus on the OTOC between energy-momentum tensor and a scalar operator with large conformal dimension. As above, we approximate the shockwave as sourced by the heavy scalar without backreaction from the graviton. Then it remains to consider the evolution of the graviton wave function in the geometry. In the following, to distinguish the metric perturbation from the shockwave, we will use $f(\vec{x})$ as the displacement in the metric,

$$ds^2 = 2g_{uv}du[dv - \delta(u)f(\vec{x})du] + g_{xx}d\Omega_d. \tag{3.54}$$

We solve the linearized equation

$$\frac{1}{2}(D_\rho D_\mu h^\rho_\nu + D_\rho D_\nu h^\rho_\mu - D_\rho D^\rho h_{\mu\nu} - D_\mu D_\nu h^\rho_\rho) - \frac{2}{d}\Lambda h_{\mu\nu} = 0. \tag{3.55}$$

This is a very complicated equation in general. Some other components have to be generated even if we start with only the shear mode perturbation. However, if we restrict the shockwave term g_{uu} to only depend on directions that are perpendicular to y, the equation becomes easier to deal with. So we require S to be a function of x_i with $\vec{x}_i \perp y$. Then the equations are simplified to

$$\begin{aligned} \partial_v[g^{uv}(\partial_v h^y_u - \partial_u h^y_v)] + \text{finite terms} = 0, \\ g^{uv}(\partial_v\partial_i h^y_u + \partial_u\partial_i h^y_v) + 2g^{uv}\partial_v[\partial_i h^y_v f(\vec{x})\delta(u)] + \text{finite terms} = 0, \end{aligned} \tag{3.56}$$

where 'finite terms' denotes terms that don't contain a delta function. Here we are searching for

a solution such that $\partial_u h^y_v$ and h^y_u are proportional to $\delta(u)$. Requiring the cancellation of all $\delta(u)$s, we find that

$$2g^{uv}\partial_u\partial_i h^y_v + 2g^{uv}\partial_v[\partial_i h^y_v f(\vec{x})\delta(u)] = 0. \tag{3.57}$$

Hence, we again have the simple shift rule,

$$\partial_i h^y_v(v,\vec{x}) \to \partial_i h^y_v(v - f(\vec{x}),\vec{x}), \tag{3.58}$$

after the graviton passing the shockwave. Finally, in order for f to only depend on $\vec{x}\perp y$, we have to also consider a string operator built from the scalar $O^s(t,\vec{x}) = \int dy O(t,\vec{x},y)$.

3.5.3 Inner product

As before, we construct the gauge invariant inner product using the symplectic form,

$$\delta\mathcal{L} = \delta\phi\frac{\delta\mathcal{L}}{\delta\phi} + d\theta(\phi,\delta\phi). \tag{3.59}$$

We find that

$$(h_1,h_2) =$$
$$\int \sqrt{g}n^\rho[-h_1^{*\mu\nu}D_\mu h_{2\nu\rho} + \frac{1}{2}h_1^{*\mu\nu}D_\rho h_{2\mu\nu} + \frac{1}{2}h^{*\nu}_{1\rho}D_\nu h_2 + \frac{1}{2}h_1^* D_\nu h_2{}^\nu_\rho - \frac{1}{2}h_1^* D_\rho h_2] - (1\longleftrightarrow 2). \tag{3.60}$$

Knowing that the trace of h_1 and h_2 are zero, we only keep the first two terms. Then, after

some cancellations, a much simpler form remains

$$(h_1, h_2) = \int \sqrt{\gamma} g^{xx} g^{uv} (h_{1v}^{*y} \partial_{[v} h_{2u]}^{\ y} - \Gamma_{yv}^{y} h_{1[v}^{*y} h_{2u]}^{\ y}) - (1 \longleftrightarrow 2). \tag{3.61}$$

We have chosen n to be $\frac{\partial}{\partial_v}$. This expression is very similar to the photon case (see Eq. (3.22)), except for second term, which is proportional to the connection. Then we observe that Γ_{yv}^{y} is of order u near the horizon, so if we choose to evaluate the inner product along the hyper-surface $u \sim 0$, the second term can be neglected.

3.5.4 OTOC of stress-energy tensor

3.5.4.1 Shear mode

Just like the $U(1)$ case, the OTOC,

$$Tr(\rho^{\frac{1}{2}} T_{ty}^{s}(t_2, \vec{x}_2) O^{s}(t_1, \vec{x}_1) \rho^{\frac{1}{2}} T_{ty}^{s}(t_2, \vec{x}_2) O^{s}(t_1, \vec{x}_1)), \tag{3.62}$$

can be written as an inner product between the graviton wave functions, before and after passing the shockwave. Plugging the solution Eq. (3.20) and Eq. (3.58) into Eq. (3.61), we get exactly the same expression as in the $U(1)$ case, and the subsequent calculation is completely parallel. Note that these string operators live in an effective $d-1$ spacial dimension. The exponent of power law tail is also modified to $\frac{d-1}{2}$.

3.5.4.2 Sound mode

We can also consider a local insertion of a stress-tensor operator that creates spherically symmetric wave function propagating in the bulk. At low energy, these modes have the dispersion relation of a sound wave. For instance, we can choose the insertion T_{tt} and $\sum_{i=1}^{d} T_{ii}$. The pole in the Green's function is at

$$\omega = \pm v_s k - i\frac{d-1}{d} D_T k^2, \tag{3.63}$$

where D_T is the diffusion constant (same as that of the shear mode). The quadratic term has the same effect as the shear mode, broadening the wave-packet. Hence, we expect the OTOC to have the same power law tail as in the photon case. Another interesting regime for the sound mode is at early time, where we have the shockwave that propagates at the butterfly velocity v_B as well as the hydrodynamical mode that propagates at the sound speed v_s. For the gravity model we considered in this work, $v_B > v_s$ for physically sensible spatial dimension. However, in other models the sound speed might be larger.[2] In this case we find that the information carried by sound mode can scramble faster, the spreading speed of which is determined by v_s instead. We solve the sound mode gravitaional perturbation equation and provide a detailed analysis of the OTOC in Appendix B.3.

[2]For example, in [41, 110] there is a case where v_B is small at low temperature.

3.6 Discussion and generalization

3.6.1 Higher order corrections

We have calculated the photon wave function by just keeping the leading order in ω and k. This gave an OTOC with a power law dependence on t at large time. We may include higher order terms in the wave function, for example, consider

$$\phi(\omega, k) = \frac{i(1 + A\omega + Bk)}{\omega + iDk^2 + C\omega^2 + Dk^3}. \tag{3.64}$$

The pole is now at

$$\omega = -iDk^2(1 + \gamma k). \tag{3.65}$$

After Fourier transformation with respect to ω, the wave function becomes

$$\begin{aligned} \phi(v, k) =& \int d\omega \phi(\omega, k) e^{-i\omega v}, \\ =& (1 + Bk - iADk^2) v^{-Dk^2(1+\gamma k)}. \end{aligned} \tag{3.66}$$

Following the steps above, we should multiply the integrand of Eq. (3.46) by a factor $(1 + \alpha k + \beta k^2)$. Also we should modify the exponent of $[2 + f(\vec{x})e^{t_{12}}]$ in second equation of Eq. (B.10) to $-Dk^2(1 + \gamma k)$. After performing integration with respect to k, these modifications only contribute factors of higher order in t_{12}^{-1}, and do not change the leading long time behavior. One can also include loop corrections due to a graviton, as we discuss in Appendix B.4. This correction creates a branch cut in the wave function but doesn't modify the long time behavior of the OTOC.

3.6.2 Hydrodynamics and OTOCs of non-conserved operator

In this section, we explore the question of how hydrodynamic modes may affect scrambling of non-conserved operators. In the process shown in Fig 3.4 (with the photon line representing either a photon mode or a sound mode), imagine that a massive scalar particle (created by a non-conserved operator) emits a hydrodynamic mode through a coupling of order $O(g_c)$ in the near boundary region. This mode grows in size as it falls into the black hole. The in state before the shockwave scattering would contain a term $g_s \int f_s(p,x) f_m(p',x) |p,x'\rangle_s |p',x'\rangle_m |q,y\rangle$, where f_s is the sound mode wave function and f_m is the massive scalar wave function. The state with momentum q is the second massive mode. The collidision induces a phase factor $e^{iqph(x,y)+iqp'h(x',y)}$. So we expect the scattering amplitude to be the one that involves hydrodynamic modes (like in Eq. (3.29)) multiplied with the one that involves only massive scalars. As discussed in the previous sections, the hydrodynamic OTOC has a power law tail at late time. However, the non-conserved OTOC is multiplied with it and the combination decays faster. Hence, the complete OTOC at late time is still controlled by massive particle scattering. On the other hand, the early time behavior can be modified, if we consider the non-conserved mode coupling with a sound mode, becuase the scattering amplitude between the sound mode and the second massive particle starts to decay earlier if $v_s > v_B$ (see Appendix B.3 for details). Since the hydrodynamic mode's wave function is created with amplitude $O(g_c)$, its influence on the OTOC is of order $O(g_c^2)$. So even if $v_s > v_B$, the fast propagating wave-front cannot grow to exceed the same order,

$$OTOC \sim 1 - \frac{c_1}{N} e^{t - \frac{|x|}{v_B}} - \frac{c_2 g_c^2}{N} e^{t - \frac{|x|}{v_s}}. \tag{3.67}$$

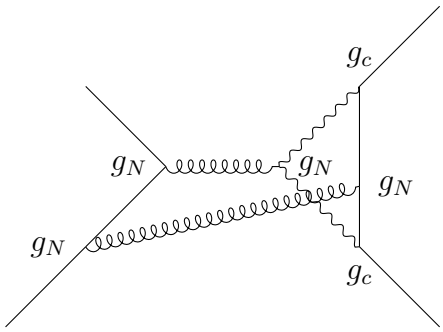

Figure 3.4: intermediate hydrodynamic state in scalar-scalar scattering

Since all modes couple to gravity, they also couple to the sound mode of the gravitational perturbation. In this case, $g_c^2 \sim \frac{1}{N}$, and the last term can grow with time up to order $O(\frac{1}{N})$. A similar situation has been discussed in [109], where they gave a bound on the squared commutator of the form

$$\text{squared commutator} \leq \frac{e^{t-\frac{|x|}{v_B}}}{N} + \frac{a(x,t)}{N} + O(\frac{1}{N^2}), \tag{3.68}$$

where the function $a(x,t)$ is non-zero when $|x| < v_s t$, and is bounded by an $O(1)$ quantity. However, the picture we considered here (Fig 3.4) is slightly different.

3.6.3 Summary

In conclusion, we have explored OTOCs between hydrodynamic operators and generic operators. In the late time regime, these OTOCs obey a power law scaling, while at early time the deviation still grows exponentially. In some models where the sound speed v_s is large, the information near the wave-front scrambles with a velocity that depends on v_s. Finally, when generalizing to OTOCs of generic operators that couple to hydrodynamic modes, we found that the late time power law decay is absent, while there can be a small amount of information scrambling faster than v_B (when $v_s > v_B$) near the wave-front.

We can also understand the conclusion intuitively in the boundary picture. Starting with a non-conserved operator O. A part of it evolves into $g_c JO$, where J represents a hydrodynamic operator. Then a small part of the information is carried by the hydrodynamic mode. A pure hydrodynamic operator J may spread fast (in sound mode case) but release its information slowly (which causes the late time power law tail). Therefore, although the order g_c^2 amount of information may propagate fast and lead to a rapidly moving wave-front in the OTOC, the scalar operator accompanied with J releases most of the information and breaks the power law tail at late time. Due to conservation law constraints, the dynamics prevents O from turning into pure J's. In bulk theory, this is a constraint from gauge symmetry.

3.7 Acknowledgements

This work is supported in part by the Simons Foundation through the It From Qubit Collaboration.

Chapter 4: Large N Matrix Quantum Mechanics as a Quantum Memory

This chapter is based on the publication 'Large N Matrix Model as Quantum Memory' by ChunJun Cao, Gong Cheng and Brian Swingle, published as arxiv: 2211.08448.

4.1 Overview

In this paper, we explore the possibility of building a quantum memory that is robust to thermal noise using large N matrix quantum mechanics models. First, we investigate the gauged $SU(N)$ matrix harmonic oscillator and different ways to encode quantum information in it. By calculating the mutual information between the system and a reference which purifies the encoded information, we identify a transition temperature, T_c, below which the encoded quantum information is protected from thermal noise for a memory time scaling as N^2. Conversely, for temperatures higher than T_c, the information is quickly destroyed by thermal noise. Second, we relax the requirement of gauge invariance and study a matrix harmonic oscillator model with only global symmetry. Finally, we further relax even the symmetry requirement and propose a model that consists of a large number N^2 of qubits, with interactions derived from an approximate $SU(N)$ symmetry. In both ungauged models, we find that the effects of gauging can be mimicked using an energy penalty to give a similar result for the memory time. The final qubit model also has the potential to be realized in the laboratory.

4.2 Introduction

Quantum information is typically fragile when encountered in familiar physical systems, thus giving rise to the intuition that quantum information is inherently hard to preserve at macroscopic scales, e.g. in large systems or at long times. The discovery of quantum error correction showed that this intuition is incomplete: in the right kind of physical system, quantum information can be retained for an arbitrarily long time. Maintaining the information is typically an active process where we keep a vigil for errors and periodically correct them. An error correcting code operating in this mode forms an active quantum memory. Some codes may have the additional capability to preserve the encoded information for a long time naturally, without any active intervention. A code operating in this mode is called a passive or self-correcting quantum memory—it is like a quantum hard drive. In this paper and a forthcoming companion paper, we search for passive quantum memories in the context of quantum gauge theories and models inspired by them.

Why gauge theories? For one thing, some of the most important currently known codes can be viewed as gauge theories. For example, the toric code can be viewed as a Z_2 lattice gauge theory with dynamical electric charges in the extreme deconfined limit. More generally, deconfined lattice discrete gauge theories are associated with a high degree of quantum entanglement and topological order, both of which are linked with quantum error correction [4, 51, 129]. One feature of topological order is a robustness of the ground space to perturbations of the Hamiltonian, which is suggestive of the potential for passive error correction. And while the two-dimensional toric code does not form a passive memory [130], a four-dimensional analog does [58]. Moreover, phases of matter exhibiting topological order associated with a discrete non-Abelian group

can be used for fault tolerant quantum computation, a fact that also hints at a degree of intrinsic protection [131].

From another perspective, quantum error correction has been linked with quantum gravity in the context of holographic duality, also known as the AdS/CFT correspondence [132]. The best understood examples of the correspondence involve continuous non-Abelian gauge theories with large gauge groups, thus providing another connection between non-Abelian gauge symmetry and quantum error correction. In this context, one also finds that the boundary conformal field theory with $SU(N)$ gauge symmetry can possess a low temperature confined phase which is qualitatively distinct from the generic high temperature physics in the deconfined phase. This boundary confinement-deconfinement phase transition is dual to the Hawking-Page transition [133] between a thermal AdS geometry and a AdS black hole geometry in the bulk [134]. It was suggested in [135] that when treating the low energy sector of AdS/CFT as an approximate quantum error-correcting code under the influence of thermal errors, the encoded information living in the bulk thermal AdS geometry can be disturbed by the scattering of thermal particles with probability $O(1/N^2)$. However, in the high temperature phase, the encoded information is scrambled by the black hole, thus inducing a large logical error. In the large N limit, the distinct phases correspond to the existence of a threshold, such that logical information remains robust in the low temperature phase where the errors occur less frequently[1].Therefore, it is natural to explore whether this type of robustness also extends to other theories with such gauge symmetries.

With these motivations, we have undertaken an investigation of quantum error correction

[1]Note that unlike the tensor network constructions [136] where one changes the system size by increasing the number of layers, which roughly corresponds to changing the IR cutoff in the bulk or the UV cutoff on the boundary theory when it is put on a lattice, the size of the physical system in [135] is altered by N of the $SU(N)$ symmetry while keeping the number of "boundary sites" fixed. Heuristically, the physical Hilbert space can be taken as placing $O(N^2)$ qudits on each boundary site.

in non-Abelian gauge theories with large gauge groups. We focus here on $SU(N)$ groups with N taken large. This large N limit is like a thermodynamic limit, and we expect that passive error correction can only emerge in such a thermodynamic limit. We define and study quantum codes in a variety of models, including models inspired by gauge theories but where we relax the gauge constraint. We are seeking to answer two key questions: (1) are there potentially useful lab-constructible quantum memories built from gauge theories or derived models and (2) can naturally occurring systems, e.g. QCD or a hypothetical holographic dual to quantum gravity in our universe, naturally preserve quantum information for a long time? This paper focuses on quantum mechanical systems with large gauge groups, while the companion paper [137] will consider quantum field theories with large gauge groups.

The key results of the present paper are as follows. First, we discuss broadly how a property called large N factorization is related to an approximate version of the Knill-Laflamme error correction condition [45, 138]. Assuming a code space with the right properties can be defined and coupled to a thermal bath satisfying reasonable assumptions, we then prove a theorem establishing the existence of a memory lifetime which scales polynomially with N. We then consider a sequence of models of increasing generality and show how the conditions of the main theorem can be satisfied. For a certain fully gauged model, we find that the conditions of the theorem are immediately satisfied; for models where we do not gauge the symmetry or even make the symmetry approximate, an energy penalty scaling like $\log N$ is needed to meet the conditions of the main theorem. While here we focus on the construction of such quantum memories and their memory times, there are other aspects of the model that are relevant for practical implementation, such as whether quantum information information can be efficiently encoded, recovered, and processed. We will leave these discussions for future work.

In the remainder of the introduction, we first review the basic notions for readers without the necessary background in quantum codes or quantum gauge theories. We then give a high level overview of our results. We also note that a few prior works have considered the role of large N factorization and/or gauge symmetry in defining quantum error correcting codes [139, 140]. There is also a large literature on passive quantum memories from a variety of approaches [51, 57, 58, 141]. See also [59] for a more comprehensive review.

4.2.1 Background on quantum codes

In this subsection, we review the key concepts of quantum error correction needed for our discussion. This section is aimed at readers with a more high energy background.

Mathematically, a quantum error correcting code is a subspace, the *logical space* $\mathcal{C}$, of a larger *physical Hilbert space* $\mathcal{H}$. Errors are modeled by a quantum process $\mathcal{E}$ and error correction is given by another process $\mathcal{R}$ such that

$$\mathcal{R}(\mathcal{E}(\rho)) = \rho \quad \forall \rho \in \mathcal{C}. \tag{4.1}$$

If the error channel is viewed as probabilistically applying errors from a set $\{E_a\}$, then one way to formulate the necessary condition for the existence of an error correction process is the Knill-Laflamme (KL) condition,

$$\langle i|E_a^\dagger E_b|j\rangle = c_{ab}\delta_{ij}, \tag{4.2}$$

where $|i\rangle$ and $|j\rangle$ are any two elements of a basis for $\mathcal{C}$. The intuition behind KL is that errors are unable to cause transitions between distinct states in the code. We can also relax these exact

equalities to obtain instead an approximate quantum code.

In practice, such a code is instantiated within a concrete physical substrate, with $\mathcal{H}$ being some model of the physical space of states of the substrate. For example, a code ($\mathcal{C}$) might be implemented as a subspace of the full energy levels ($\mathcal{H}$) of a superconducting circuit (substrate). In some cases, the code space might correspond to the ground space of some Hamiltonian for the substrate, but this is not required in general.

A code is used as follows. Information is first encoded using some encoding operation. This operation might correspond to a quantum circuit which takes a fixed initial state in $\mathcal{H}$ and produces the desired code state in $\mathcal{C}$. After encoding, the code is subject to errors, corresponding to one application of the error channel $\mathcal{E}$. Then the recovery procedure $\mathcal{R}$ is applied to recover the initially encoded information. The condition above guarantees success provided the encoding prepares a state in $\mathcal{C}$. Finally, the information can be read out by a decoding operation. Note the distinction between recovery, which repairs the information but keeps it encoded, and decoding, which reverses the encoding map when applied to an error free state[2].

To make these ideas more concrete, we can consider the simple goal of information storage for a period of time (as opposed to any active computation on the encoded data). We think of the code during the error part of the protocol as sitting idle in the presence of an undesirable environment. The effect of the environment is what produces errors in the code, so the channel $\mathcal{E}$ implicitly contains information about the nature of the environment and how long the code is exposed to the environment. We denote such an error channel by $\mathcal{E}_t$, where t corresponds to the time for which the code is exposed to the environment. Correspondingly, the recovery operation

[2]Note that somewhat confusingly, decoding in the context of active error correction can also refer to applying some suitably chosen operations to the state based on syndrome measurements. This process typically leave the information encoded, which corresponds to our recovery operation in our current definition.

$\mathcal{R}$ may depend on t and indeed on the whole structure of $\mathcal{E}_t$.

In this paper we consider the environment to be a thermal reservoir at some temperature T. There is still freedom in determining exactly how the reservoir couples to the system, but from an effective theory perspective we should expect all allowed couplings to be present with some strength. In this context, the need for active error correction can be phrased like this. Given a code $\mathcal{C}$, the code requires active error correction if, as $t \to \infty$, there is no $\mathcal{R}$ that can correct $\mathcal{E}_t$. In other words, a code requires active error correction if, given enough time, the error channel will eventually degrade the information beyond the ability of any physically conceivable recovery operation to repair.

More generally, we can define a memory time t_{mem} as the time beyond which $\mathcal{E}_t$ degrades the information beyond any hope of recovery. Of course, this time depends on the code and the error model, but it also depends on what recovery operations we can conceivably perform and on how well we want to be able to recover the information (e.g. the degree of approximation in our approximate code). A perfect passive memory is one for which $t_{\text{mem}} = \infty$. Typically, we can only hope for this sort of behavior in a thermodynamic limit, so we should really view a passive memory as a sequence of codes indexed by the physical size n for which $\lim_{n\to\infty} t_{\text{mem}}(n) = \infty$. Even more practically, what really matters is how t_{mem} scales with n and other parameters of the code.

For the purpose of potentially implementing a quantum memory in the lab, we may also want to impose some additional rules of the game. One variant of such rules are called the Caltech rules [142, 143]. For example, we might obtain a long memory time by sending the energy cost of errors to infinity "by hand", but this could be considered "cheating" unless there is a good physical reason for this large energy penalty. The idea is that we indeed want to effectively

forbid errors, but this should happen naturally without sending any microscopic energy scale to infinity. Of course, if one does have a system where errors are particularly costly, then it might form a good enough passive memory in the sense that t_{mem} is long enough for practical purposes. To give another example, to be able to construct codes in physical three-dimensional space, we might want some restrictions on the kinds of codes we consider, e.g. trying to avoid the need for too many long-range interactions [143]. We note that all the models we consider here do have non-local interactions between the large N degrees of freedom[3].

4.2.2 Background on quantum gauge theories

In this subsection, we review the key concepts of quantum gauge theories needed for our discussion. This section is aimed at readers with a more quantum information background.

At the most basic level, a gauge theory is defined by giving a gauge group $\mathcal{G}$ and a set of degrees of freedom transforming under $\mathcal{G}$ with the requirement that all physical states and operators are invariant under $\mathcal{G}$. This invariance condition is known as Gauss' law, in honor of its roots in electromagnetism. An immediate question is why one would use such a redundant description at all? Experience shows that one can always use a gauge-invariant description of the states and operators, but such a description often hides important underlying features of the physics. For example, loop-like operators known as Wilson lines provide a class of gauge invariant observables in quantum field theories with gauge fields, but the extended nature of these operators can obscure aspects of locality in the theory. In special cases, one can even have an equivalence be-

[3]Note that it is somewhat ambiguous what constitutes the local degrees of freedom in the large N gauged oscillator model as they are not simply tensor product of qubits. We show in later sections that there is a construction where two such gauged oscillators are spatially local with respect to each other. However, each one contains a large N degrees of freedom even though there is no sense in which they occupy an extended region in space. It is in this sense that these degrees of freedom are related to each other non-locally.

tween a local gauge theory and another local theory with no explicit gauge structure, for example, the duality between the 3d statistical Ising model and 3d Z_2 gauge theory.

We study such gauge theories in large part because they form a crucial part of our description of nature. The quantum theory of electromagnetism is a gauge theory where the gauge group is related to the abelian Lie group $U(1)$. The more general Standard Model is also a gauge theory with a non-Abelian gauge group of the form $SU(3) \times SU(2) \times U(1)$. Gauge theories also arise in condensed matter systems, for example, when describing so-called spin liquid phases, and, as we mentioned above, they also have interesting error correction properties.

Apart from the motivations from known models of high-energy particle physics and condensed matter systems, another motivation to consider gauge theories comes from quantum gravity. Since the discovery of AdS/CFT, it is generally believed that certain d dimensional $SU(N)$ gauge theories with large N admit a dual geometric description in terms of a $d+1$ dimensional theory of gravity. From a quantum information perspective, this correspondence provides the possibility of hiding quantum information deep inside the emergent geometry. This has inspired a lot of research in the field of holographic quantum error correcting codes [132], with explicit models such as the HaPPY code [136], the effective field theory code [144], and many other related constructions using tensor networks [145, 146, 147]. Current holographic codes often utilize the extra dimension, such that any local/UV errors can not access the information deep inside along the extra radial direction. However, very little of the error correcting power in these constructions come directly from the gauge symmetries in AdS/CFT. In this work, we will focus on a different kind of protection from the large N gauge symmetries, which can be related to the small Newton's constant in these holographic theories [135, 140]. This opens another possibility to design a new kind of quantum memory.

An interesting structure we exploit in the large N gauge theory is its sparse density of excitations at low energy. Due to Gauss' law, the only allowed excitations of a $SU(N)$ gauge theory on any compact manifold are gluons that combine into gauge singlets. Therefore, the density of states is determined by counting the number of gauge singlets in a given energy level. It is a general feature that the density of states in such model scales exponentially with some power of energy and does not depend on N. As is pointed out in [148], even for a free gauge theory with large N, the projection to the gauge invariant subspace induces effective interactions among the gluons, which is negligible at high energy but dominates at the low energy regime. In fact, for a weakly coupled $SU(N)$ gauge theory, there is a phase transition analogous to the comfinement/deconfinement transition in QCD, in the limit of $N \to \infty$. As we show, this induces a critical temperature, T_c, below which the quantum information can be long-lived but above which the information is quickly destroyed. In the geometric description, this is believed to be dual to the Hawking-Page transition and the high temperature phase can be thought of as a black hole that kills the quantum information [135].

To zero in on just the effects of gauge symmetry, we distill only the necessary ingredients from the above gauge theory intuitions and consider a gauge theory with no spatial geometry at all. It turns out that even the simplest $0+1$-dimensional gauge theory of harmonic oscillators is sufficient for our purposes. The inverted harmonic oscillator has been studied as a dual to a two dimensional string theory and can be considered as toy model of holography [149, 150, 151, 152]. Here we start from a similar but non-inverted harmonic oscillator model and try to build a quantum memory from it.

4.2.3 Organization and overview of results

The rest of this paper is organized as follows. In Section 4.3, we describe in detail the large N matrix quantum mechanics model with $SU(N)$ gauge symmetry. We then discuss how it may be construed as an approximate error correcting code and define various bath models we will use for the rest of the paper. We then discuss the mutual information diagnostic for memory time and distill the core conclusions of our work in the form of Theorem 1. It shows that if a large N system has a sparse low energy spectrum, couples to the bath uniformly, and is an approximate QECC, then it has a memory time polynomial in N at low enough temperatures. In the ensuing Sections, we deploy this theorem to various quantum memory constructions.

In Section 4.4, we study two concrete examples of quantum memories built from two gauged harmonic oscillator models coupled to a thermal reservoir. The memory time scales as N^2 in both models. For the first model, the N^2 life time persists even at high temperature, but the model requires non-local logical operations. We then construct a local model which has a N^2 memory time in the low temperature phase, but requires a large coupling of strength $\sim \log N$ between the gauged oscillators. At zero temperature limit $T \to 0$, the first model has a constant N^2 life time, while the second model has a divergent life time that scales as $N^2 e^{\frac{\omega}{T}}$, where ω is some energy scale of this model.

In Section 4.5, we consider what happens if the gauge constraint is not imposed exactly, but only as an energetic cost in the Hamiltonian. A large number of non-singlet excitations now modify the physics, but the information retention time can be still be quadratic in N if the energy scale of non-singlet excitations is large.

Finally, in Section 4.6, we ask to what extent does robustness depend on the symmetry

being exact and the Hilbert space of quantum systems being infinite dimensional. On the practical level, we want the quantum memories to be implementable on finite dimensional quantum systems like qubits or qudits. To this end, we consider an even more relaxed situation where the $SU(N)$ symmetry itself is not only ungauged but also approximate. We then build a quantum memory consisting of N^2 number of physical qudits that interact non-locally with each other. Qualitatively, this model behaves similarly to the one in Section 4.5 in the low energy sector, except small correction terms that suppressed to order at most $\sim \log N/N$. We find that if we require the total energy of the interaction scales as $\log N$ and a reasonable pattern of coupling strengths, then Theorem 1 again holds to guarantee a N^2 memory time. The zero temperature limit of life times for the last two models also diverge as $N^2 e^{\frac{\omega}{T}}$.

4.3 Matrix model and set up

4.3.1 Matrix Quantum Mechanics

We wish to study a gauged matrix model of harmonic oscillators. First, recall the classical Lagrangian of a single harmonic oscillator,

$$L = \frac{1}{2}(\dot{x}^2 - \omega^2 x^2). \tag{4.3}$$

The canonical momentum is $p = \frac{\partial L}{\partial \dot{x}} = \dot{x}$, in terms of which we also have the Hamiltonian description,

$$H = \frac{1}{2}(p^2 + \omega^2 x^2). \tag{4.4}$$

The system is quantized in the usual way by setting $[x, p] = i\hbar$.

A generalization can be made by promoting the variable $x(t)$ to an $N \times N$ matrix $X(t)$ and promoting products of variables to matrix multiplication. We hasten to emphasize that this $N \times N$ matrix structure does not refer to a quantum Hilbert space; rather it is a way of organizing N^2 variables into a single unit. Then one gets an action for a matrix harmonic oscillator,

$$L = \frac{1}{2}\,\mathrm{Tr}[(\partial_t X)^2 - \omega^2 X^2]. \tag{4.5}$$

Again, let us emphasize that the trace is not a quantum Hilbert space trace but rather a sum over the matrix degrees of freedom. The diagonal elements of X are real variables, while the off-diagonal components are complex variables coming in conjugate pairs.

The momentum conjugate to X^i_j is $P^j_i = \dot{X}^j_i$. We quantize the theory by specifying canonical commutators for all pairs of conjugate variables. If we extend quantum Hermitian conjugation to include a tranpose of the matrix degrees of freedom, then the quantum variable X is Hermitian. In terms of its matrix elements X^i_j, Hermiticity implies that X^i_i are quantum Hermitian while X^i_j and X^j_i are quantum Hermitian conjugates, $(X^i_j)^\dagger = X^j_i$. Note that X^i_j is not quantum Hermitian when $i \neq j$, but the above formula is still correct.

After quantization, it is convenient to work in terms of creation and annihilation operators,

$$\begin{aligned} a^i_j &= \sqrt{\frac{\omega}{2}}(X^i_j + iP^i_j) \\ a^{\dagger j}_i &= \frac{1}{\sqrt{2\omega}}(X^j_i - iP^j_i), \end{aligned} \tag{4.6}$$

which satisfy

$$[a^i_j, a^{\dagger k}_l] = \delta^i_l \delta^k_j. \tag{4.7}$$

The Hamiltonian written in terms of a and $a^\dagger$'s takes the simple form

$$H = \omega \, \mathrm{Tr}(a^\dagger a) \tag{4.8}$$

after subtracting the zero-point energy. There is a unique vacuum state $|0\rangle$ satisfying

$$a^i_j |0\rangle = 0, \ \forall i, j. \tag{4.9}$$

Acting creation operators on this vacumm then generates all the Fock states that span the Hilbert space.

Looking back at the Lagrangian in Eq. (4.5), we see that it has a symmetry under unitary transformations $X(t) \to UX(t)U^\dagger$, with $U \in U(N)$. (This is why we consider complex off-diagonal entries in X.) This can be made into a local symmetry $U(t)$, meaning a symmetry where $U(t)$ can be different at each different time, as follows. We add a matrix gauge field $A(t)$ and promote the time derivative to a covariant derivative, defined as

$$D_t X = \partial_t X - [A, X] \tag{4.10}$$

with $A(t)$ transforming as $A(t) \to U(t)A(t)U(t)^\dagger - iU(t)\partial_t U(t)^\dagger$. One can check that the covariant derivative transforms in the same way as $X(t)$, which is $D_t X \to U(t) D_t X U(t)^\dagger$. Therefore, the Lagrangian is invariant under this transformation. We call this symmetry with respect to the time-dependent transformation the gauge symmetry.

The model equipped with such a symmetry can be regarded as a redundant description of a physical system whose Hilbert space is defined to include only gauge-invariant states. Indeed,

in this model, $A(t)$ can be view as a Lagrange multiplier. Fixing a gauge $A = 0$, and integrating out A in the path integral representation gives the Gauss law constraint:

$$G = [X, \dot{X}] = 0. \tag{4.11}$$

This condition is implemented by requiring that physical states $|\psi\rangle$ be annihilated by G, $G|\psi\rangle = 0$.

One can see that the states satisfying this constraint are the symmetry singlets, generated by traces of operators acting on the vacuum,

$$|\psi\rangle = \mathrm{Tr}(a^{\dagger n_1})\,\mathrm{Tr}(a^{\dagger n_2})\cdots\mathrm{Tr}(a^{\dagger n_k})|0\rangle. \tag{4.12}$$

These states, after being normalized, span a subspace of the ungauged matrix model's Hilbert space. They are also eigenstates of the Hamiltonian (4.8) such that

$$H|\psi\rangle = \omega \sum_{i=1}^{k} n_i |\psi\rangle. \tag{4.13}$$

4.3.2 Physical states and the Knill-Laflamme Condition

We now describe in broad terms how the properties of these gauge-singlet states can be leveraged to generate approximate codes obeying an approximate version of the KL condition. First some terminology. If a gauge invariant operator contains only a single trace, it is called single trace operator. Operators with multiple traces are called multi-trace. Using the commutation relation, Eq. (4.7), one can derive a useful commutator rule for single trace operators, with $n_{1,2}$,

$m_{1,2}$ being $O(1)$ number,

$$[\mathrm{Tr}(a^{n_1}a^{\dagger m_1}), \mathrm{Tr}(a^{n_2}a^{\dagger m_2})] = (n_1 m_2 - n_2 m_1)\,\mathrm{Tr}(a^{n_1+n_2-1}a^{\dagger m_1+m_2-1}) + O\left(\frac{1}{N^2}\right). \quad (4.14)$$

Using these rules, overlaps of states generated by acting multi-trace operators on the ground state can be obtained to leading order in large N. For example, the squared norm of the state $\mathrm{Tr}(a^\dagger)|0\rangle$ is

$$\langle 0|\,\mathrm{Tr}(a^n)\,\mathrm{Tr}(a^{\dagger n})|0\rangle = \langle 0|[\mathrm{Tr}(a^n), \mathrm{Tr}(a^{\dagger n})]|0\rangle = nN^n + O\left(\frac{1}{N^2}\right). \quad (4.15)$$

We also find that states with the same energy are almost orthogonal, with overlaps suppressed by a power of N. For example,

$$\langle 0|\frac{\mathrm{Tr}(a^m)\,\mathrm{Tr}(a^{n-m})}{N^{\frac{m}{2}}}\frac{\mathrm{Tr}(a^{\dagger n})}{N^{\frac{n}{2}}}|0\rangle = O\left(\frac{1}{N}\right). \quad (4.16)$$

Moreover, one can show that a factorization property holds for products of single trace operators. As an example, given four single trace operators with vanishing expectation value, O_i, O_j, O_k and O_l, we have

$$\begin{aligned} \langle 0|O_i O_k O_l^\dagger O_j^\dagger|0\rangle &\sim \langle 0|O_i O_j^\dagger|0\rangle\langle 0|O_k O_l^\dagger|0\rangle + \langle 0|O_i O_l^\dagger|0\rangle\langle 0|O_k O_j^\dagger|0\rangle + O\left(\frac{1}{N^2}\right) \\ \langle 0|O_i O_k O_j^\dagger|0\rangle &\sim O\left(\frac{1}{N}\right). \end{aligned} \quad (4.17)$$

If we could find a way to classify O_i and O_j as logical operators and O_k and O_l as errors, then this equation would be interpreted as an approximate version of Knill-Laflamme condition (aKL).

While one may deviate from KL in many forms, the approximate KL condition we consider in this work could be written as

$$\begin{aligned} \langle i|E_a^\dagger E_b|j\rangle &= f_{ab}\delta_{ij} + \frac{g_{ab}^{ij}}{N^2} \\ \langle i|E_a|j\rangle &= \frac{e_a^{ij}}{N}. \end{aligned} \tag{4.18}$$

In the above formulae, we are imagining that E_a and E_b are some general non-identity error operators. In general, we expect them to be any gauge invariant operators that satisfy some constraints, depending on how we couple the model to a thermal environment. We will give concrete examples in Section 4.4, and explicitly calculate the functions f, g and e. These examples will show such large N matrix quantum mechanics models can used to construct approximate quantum error correcting codes [138].

For later use, we also briefly discuss the counting of gauge invariant operators. If we have only one matrix harmonic oscillator, the general invariant states are in the form of Eq. (4.12). At energy level $n\omega$, the number of distinct states (which are also approximately orthogonal) is equal to the number of partitions of integer $p(n)$. For example, at level $n = 3$. The three partitions are,

$$\begin{aligned} 3 &= 3 + 0 \\ 3 &= 2 + 1 \\ 3 &= 1 + 1 + 1. \end{aligned} \tag{4.19}$$

Correspondingly, we have three gauge invariant states at energy 3ω, which are

$$\mathrm{Tr}(a^{\dagger 3})|0\rangle, \quad \mathrm{Tr}(a^{\dagger 2})\,\mathrm{Tr}(a^\dagger)|0\rangle, \quad \mathrm{Tr}(a^\dagger)^3|0\rangle. \tag{4.20}$$

In general, we can have arbitrary $k \leq n$ number of matrix harmonic oscillators, each carrying energy that is an integer multiple of ω. We label the individual matrix operator by its subindex, a_1, a_2, a_3, $\cdots$. The counting becomes more complicated with multiple oscillators, so let us focus on the states generated by single trace operators. At energy level $n\omega$, these states can be written as

$$\mathrm{Tr}(P\{a_1^{\dagger n_1} a_2^{\dagger n_2} \cdots a_k^{\dagger n_k}\})|0\rangle, \tag{4.21}$$

with $n = \sum_i n_i$. The state $|0\rangle$ is tensor product of k ground states of each oscillator. We use the symbol P to denote a particular permutation of all the operators inside the bracket. By counting how many different ways of splitting n and the number of permutations, one can show that the number of these single trace operators asymptotically scales as k^n when n is large enough. For simplicity, in the concrete models that will be discussed in the following sections, we consider no more than two matrix modes.

4.3.3 Bath model

We have seen that if errors and logical operators can be chosen properly, then an approximate Knill-Laflamme condition holds. Based on this, we expect that a single error operator can only corrupt the logical information at order $\frac{1}{N^2}$. At the same time, gauge invariance constrains the number of possible errors that may occur in the form of excitations. Since the density of states for the gauged oscillator grows with energy but is independent of N below some critical value, we may expect such a system to serve as a good quantum memory even at finite temperature. To show this explicitly, we couple the proposed quantum memory to a thermal reservoir and calculate the memory time t_{mem}.

We make the standard assumption that the bath is Markovian and couples to the system locally. More specifically, we model the bath as collection of bosonic modes b_l, e.g. a collection of oscillators, with the following thermal spectral function [153],

$$\mathrm{Tr}(\rho_B b_k(\nu) b_l^\dagger(-\nu)) = \delta_{kl} \left| \frac{\nu}{1 - e^{-\beta\nu}} \right| := \delta_{kl}\gamma(-\nu). \tag{4.22}$$

Physically, this means that the probability of having a given error that adds energy $\epsilon = -\nu$ to the system is suppressed by a thermal factor $\gamma(\epsilon)$.

We will discuss three scenarios for the structure of the bath. In particular, there is a degree of ambiguity in what constitutes a generic physical bath for these systems, so we consider a number of models of varying levels of generality.

Case 1: Consider two matrix harmonic oscillators, a_1 and a_2, separated by a large distance in space. The reason for introducing two such oscillators will become clear in the next section. We model this setup by assuming that these oscillators couple to the thermal bath independently with order one coupling constants. This means we assume that thermal errors can include any multi-trace operators provide they are uncorrelated between a_1 and a_2. By uncorrelated error, we mean that the modes a_1 and a_2 can not appear inside the same trace; instead errors must be of the form

$$E_{L,R} = \prod_{(r_1,r_2)\in L,\ (s_1,s_2)\in R} \frac{:\mathrm{Tr}(P\{a_1^{\dagger r_1} a_1^{r_2}\}) :: \mathrm{Tr}(P\{a_2^{\dagger s_1} a_2^{s_2}\}) :}{N^{\frac{r_1+r_2+s_1+s_2}{2}}} \tag{4.23}$$

with L and R being some sets of integer 2-tuples. The symbol P denotes the sum over all distinct arrangements of the creation and annihilation operators inside the bracket. The symbol :: means normal ordering and the N-dependent normalization is to ensure that the single trace operator of

each a, $a^\dagger$ arrangement has order one norm (see Eq. (4.15)). In terms of these errors, the thermal Hamiltonian is

$$H_{\text{thermal}} = \sum_{L,R} \lambda_{L,R} b_{L,R} E_{L,R} + h.c., \tag{4.24}$$

where h.c. stands for hermitian conjugate. We will discuss this case in more detail in Section 4.4.1.

Case 2: We assume the coupling with the bath modes b_l are through single-trace operators, with order one coupling constants λ_l's. We still consider modes a_1 and a_2 from two different matrix oscillators. The thermal coupling Hamiltonian is in the form of

$$H_{\text{thermal}} = \sum_{\{n_k\}} \lambda_{\{n_k\}} b_{\{n_k\}} \frac{: \text{Tr}(P\{a_1^{\dagger n_1} a_2^{\dagger n_2} a_1^{n_3} a_2^{n_4}\}) :}{N^{\frac{\sum_{k=1}^4 n_k}{2}}} + h.c., \tag{4.25}$$

At first sight, it appears that coupling only to single-trace operators is a strong assumption, because in general we should allow all gauge invariant operators to couple with the bath. However, this is still general enough since single-trace errors accumulate into multi-trace errors as time increases. We will discuss this scenario in more detail in Section 4.4.2.

Case 3: We consider the most general coupling to the thermal bath where each of the N^2 harmonic oscillator modes can couple to the bath independently without requiring the coupling terms be gauge invariant. In addition, we assume that the coupling constant decays exponentially with the number of creation and annihilation operators involved. This is a reasonable assumption because the correlated errors that involves more operators occur with smaller probability. We explain this in detail in Section 4.5, where we consider the ungauged model.

4.3.4 Mutual information diagnostic

Given the assumptions on the bath described above, the time evolution of our system can be described by a Lindblad equation after tracing out the bath,

$$\dot{\rho}(t) = -i[H, \rho(t)] + \sum_a \lambda_a(\nu_a) E_a \rho(t) E_a^\dagger - \frac{1}{2} \sum_a \lambda_a(\nu_a) \{E_a^\dagger E_a, \rho(t)\}, \tag{4.26}$$

where $\lambda_a(\nu_a) = \lambda_a \gamma(\nu_a)$, is the coupling constant multiplied with thermal factor. ν_a is the energy of excitation, and the $\{E_a\}$ depend on the interaction Hamiltonian.

The generic expectation is that the above system dynamics will lead to rapid information loss within the system. We wish to show that this is not the case for the right kind of code constructed from the matrix degrees of freedom. To quantitatively measure the memory time, we entangle the encoded d-dimensional system with a reference R. The initial state is thus

$$\begin{aligned} \frac{1}{\sqrt{d}} \sum_{i=1}^{d} |i\tilde{i}\rangle &:= \frac{1}{\sqrt{d}} \sum_{i=1}^{d} |i\rangle_S |i\rangle_R \\ \rho_0 &= \frac{1}{d} \sum_{i,j=1}^{d} |i\tilde{i}\rangle\langle j\tilde{j}|, \end{aligned} \tag{4.27}$$

and the correlation between the reference is maximal.

The goal is then to understand how the system-reference correlation evolves with time. The state evolves under the Lindblad dynamics into

$$\begin{aligned} \rho(t) &= e^{\mathcal{L}t} \rho_0, \\ \text{where } \mathcal{L}\mathcal{O} &= \sum_k \lambda_k E_k \mathcal{O} E_k^\dagger - \sum_k \frac{\lambda_k}{2} \{E_k^\dagger E_k, \mathcal{O}\}. \end{aligned} \tag{4.28}$$

In terms of the system and reference reduced density matrices $\rho_S(t) = \mathrm{Tr}_R[\rho(t)]$ and $\rho_R(t) = \mathrm{Tr}_S[\rho(t)]$, we may quantify the correlation using the mutual information,

$$I(S:R)(t) = S(\rho_S(t)) + S(\rho_R(t)) - S(\rho(t)). \tag{4.29}$$

When the mutual information is maximal, $I = 2\ln d$, we say that the quantum information is stored in the quantum memory. However, as $I(S:R)$ decays, the information of the encoded qubit leaves the memory and dissipates into the environment. For the sake of simplicity, we will focus on quantum memory constructions that store a single encoded qubit in the ensuing sections, so $d = 2$.

We now tie together all the ingredients above in a theorem. In general, different couplings with the bath can induce different errors on the system. However, as long as such errors are not too numerous and can be suppressed by the code, i.e., satisfying the aKL condition, then the following theorem guarantees the memory time of the quantum information is relatively long. To be precise, this theorem shows that the mutual information diagnostic decays polynomially with t at a rate suppressed by $\frac{1}{N^2}$, which implies that the memory time can scale polynomially with N.

Theorem 1. *Consider a system whose low energy states form an approximate quantum error correcting code that encodes a logical qudit S and a set of physical errors $\mathcal{E}$ induced by the system-bath coupling (c.f. Section 4.3.3). Provided the following conditions are satisfied,*

1. *(Sparse spectrum) There exists an energy ϵ_0 below which the effective number of errors[4] in $\mathcal{E}$ with energy $\epsilon \leq \epsilon_0$ is independent of N and bounded by $\exp(\mu\epsilon)$ for some $\mu > 0$,*

2. *(Uniform coupling) The thermal Hamiltonian that couples each $E \in \mathcal{E}$ to an independent*

[4]These are errors that contribute non-trivially in the Lindblad equation.

bath operator has coupling constant no larger than $O(1)$*,*

3. *(Approximate error correction)* $\forall E_a, E_b \in \mathcal{E}$*, the approximate Knill-Laflamme condition (Eq. (4.18)) is satisfied,*

then the mutual information $I(S, R)$ *defined in Eq. (4.29) is given by*

$$I(S:R)(t) = 2\ln d - K\left(\frac{t}{N^2}\right), \tag{4.30}$$

where $K(x)$ *is a polynomial function of* t*, for temperature* $T < \frac{1}{\mu}$*.*

Proof. The proof is given in Appendix C.1. □

In the following sections, we will construct different systems coupled via different bath models, as outlined in Section 4.3.3, and prove that they satisfy the assumptions in the theorem, such as the approximate Knill-Laflamme condition (aKL) for a corresponding set of error operators and logical states.

Remark: Note that the above theorem does not require the code subspace to be the ground space of the system. Therefore, the N^2 scaling of memory time holds generally for these models no matter how the code subspace is chosen as long as the requisite conditions are satisfied. Intuitively, this is because the transition rate between states are $1/N^2$ suppressed. However, as excited states can still slowly decay into lower energy states at the same rate, their memory times need not be longer by lowering the temperature.

On the other hand, for quantum memories where we also choose the code subspace to be the ground space, the memory lifetime can be further extended by a multiplicative factor $\exp(\omega/T)$, which is related to the effect of thermal suppression. This renders the total low temperature mem-

ory time to be of $O(N^2 \exp(\omega/T))$ for some energy scale ω as we see in some of the examples below.

4.4 Fully gauged model

4.4.1 Non-local model

As the first example, consider two gauged harmonic oscillators a_1 and a_2 with $SU(N)$ gauge symmetry, separated by a large distance. Their interaction is weak, and each couples to the thermal reservoir locally and independently[5]. The Hamiltonian takes the following form,

$$H = \omega \operatorname{Tr}(a_1^\dagger a_1) + \omega \operatorname{Tr}(a_2^\dagger a_2) + \sum_{L,R} \lambda_{L,R} b_{L,R} E_{L,R} + h.c., \tag{4.31}$$

where $E_{L,R}$'s are the possible errors acting on this model, and $\lambda_{L,R}$'s are $O(1)$ coupling constants.

The general gauge invariant states are given in Eq. (4.21) with $k = 2$. However, since we assume that these modes only couple to the thermal bath locally, the set of possible error operators is a proper subset of all physical operators. These errors are uncorrelated in the sense that each error operator contains only a single trace either the mode a_1 or the mode a_2, but never both. Given two sets of integer 2-tuples L and R, we can define the errors as,

$$E_{L,R} =: \prod_{(r_1,r_2)\in L,\ (s_1,s_2)\in R} \frac{\operatorname{Tr}(P\{a_1^{\dagger r_1} a_1^{r_2}\}) \operatorname{Tr}(P\{a_2^{\dagger s_1} a_2^{s_2}\})}{N^{\frac{r_1+r_2+s_1+s_2}{2}}} : . \tag{4.32}$$

where the symbol P denotes the sum over all distinct arrangements of the $a_i, a_i^\dagger$ operators[6]. In

[5] More realistically, thermal noise can have finite correlation. In such cases, we assume that the distance separating the two oscillators is much larger than the correlation length so our assumptions remain good approximations.

[6] For example, $a^{\dagger 2} a^2$ and $a^\dagger a a^\dagger a$ are counted as two distinct arrangements.

general, $P\{a^{\dagger r_1}a^{r_2}\}$ admits $(r_1+r_2)!/r_1!r_2!$ terms of distinct arrangements. Each operator is brought to normal ordering, and divided by some power of N to make sure that these operators have $O(1)$ norm.

Logical states

Given this set of error operators, we can construct logical states that are protected against them. In general, we may choose the logical states to be

$$|\mathcal{I}\rangle := \prod_{(m,n)\in\mathcal{I}} \frac{\mathrm{Tr}(a_1^{\dagger m}a_2^{\dagger n})}{N^{\frac{m+n}{2}}}|0\rangle_{12}. \tag{4.33}$$

with $m,n \geq 1$ and belonging to some set $\mathcal{I}$ of integer 2-tuples. The state $|0\rangle_{12}$ is the tensor product of the vacuum states of the two oscillators. For simplicity, let us focus on a code subspace spanned by two states and treat it as a logical qubit[7]:

$$\begin{aligned} |\tilde{1}\rangle &= \frac{\mathrm{Tr}(a_1^{\dagger 2}a_2^{\dagger 2})}{N^2}|0\rangle_{12} \\ |\tilde{2}\rangle &= \frac{\mathrm{Tr}(a_1^{\dagger}a_2^{\dagger})^2}{\sqrt{2}N^2}|0\rangle_{12}. \end{aligned} \tag{4.34}$$

They are not orthogonal states, since $\langle\tilde{1}|\tilde{2}\rangle = \frac{\sqrt{2}}{N} + O(\frac{1}{N^3})$. However, it is straightforward to identify an orthonormal basis $|\tilde{\uparrow}\rangle$ and $|\tilde{\downarrow}\rangle$, defined as

$$\begin{aligned} |\tilde{\uparrow}\rangle &= |\tilde{1}\rangle \\ |\tilde{\downarrow}\rangle &= \frac{|\tilde{2}\rangle - \langle\tilde{2}|\tilde{1}\rangle|\tilde{1}\rangle}{\sqrt{1-\langle\tilde{2}|\tilde{1}\rangle^2}}. \end{aligned} \tag{4.35}$$

[7]The logical subspace we use is not the lowest energy subspace of the Hamiltonian, so they have the tendency to decay into lower energy states. However, the decay rate is suppressed by $\frac{1}{N^2}$, as discussed in Appendix C.2.1.

Errors and aKL

Because we assume errors are gauge invariant, they are expressible as single or multi-trace operators (see Eq. (4.32)). For the purpose of invoking Theorem 1, it suffices to check that aKL holds for these errors,

$$\begin{aligned}\langle\tilde{i}|E^{\dagger}_{L',R'}E_{L,R}|\tilde{j}\rangle &= f_{L'R',LR}\delta_{ij}+\frac{g^{ij}_{L'R',LR}}{N^2}+O(\frac{1}{N^4})\\ \langle\tilde{i}|E_{L,R}|\tilde{j}\rangle &= \frac{e^{ij}_{L'R',LR}}{N}+O(\frac{1}{N^3}).\end{aligned} \tag{4.36}$$

To build up some intuition, let us first examine a few instructive examples before we arrive at the more general relation (4.36). To start, one can check that the operator $\frac{\mathrm{Tr}(a_1^{\dagger}a_1)}{N}$ has the logical states as eigenstates,

$$\frac{\mathrm{Tr}(a_1^{\dagger}a_1)}{N}|\tilde{i}\rangle=\frac{2}{N}|\tilde{i}\rangle. \tag{4.37}$$

Therefore, it is a logical identity operator. We can similarly check that the Hamiltonian that generates the system dynamics is proportional to the logical identity, which is necessary for a memory.

Next, let us examine a class of single-trace errors of the form $E_n=\frac{\mathrm{Tr}(a_1^{\dagger n})}{\sqrt{n}N^{\frac{n}{2}}}$. As a potential bit flip error, we check the transition amplitude,

$$\langle\tilde{\downarrow}|E_m^{\dagger}E_n|\tilde{\uparrow}\rangle=O(\frac{1}{N^3}). \tag{4.38}$$

The bit flip error only carries n dependence at order $O(\frac{1}{N^3})$. Similarly, the phase errors are also

suppressed,

$$\begin{aligned}\langle\tilde{\uparrow}|E_m^\dagger E_n|\tilde{\uparrow}\rangle &= \delta_{nm}\left[1+\frac{3n}{N^2}+O\left(\frac{1}{N^4}\right)\right]\\ \langle\tilde{\downarrow}|E_m^\dagger E_n|\tilde{\downarrow}\rangle &= \delta_{nm}\left[1+\frac{2n}{N^2}+O\left(\frac{1}{N^4}\right)\right].\end{aligned} \tag{4.39}$$

Note that the leading order terms of these equations come from factorized two point functions $\langle 0|E_m^\dagger E_n|0\rangle\langle\tilde{i}|\tilde{j}\rangle$, and they represent the non-connected contribution to the four point correlator. The sub-leading corrections are from the connected part, shown diagrammatically in Figure 4.1. It is this part that induces phase and bit-flip errors between the two logical states. In a similar way, one can check that the aKL condition holds for other single-trace errors. We present the more comprehensive calculations in Appendix C.2.1.

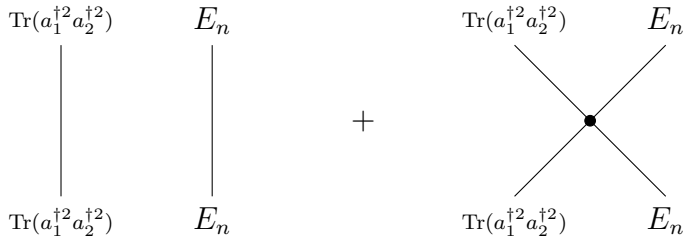

Figure 4.1: The inner product can be viewed as scattering between two particles. $(1,0)$ represents the logical state $|\tilde{\uparrow}\rangle$. The connected part is suppressed by $\frac{1}{N^2}$.

The conclusion of this analysis is that single-trace operators can only produce $1/N$ suppressed errors, thus giving rise to the approximate Knill-Laflamme condition (aKL). Using the results for single-trace errors, one can also derive the aKL conditions for any multi-trace errors. As an example,

$$\begin{aligned}\langle\tilde{\uparrow}|E_p^\dagger E_q^\dagger E_m E_n|\tilde{\uparrow}\rangle &= F(m,n,p,q)+\frac{G_\uparrow(m,n,p,q)}{N^2}+O(\frac{1}{N^4})\\ \langle\tilde{\downarrow}|E_p^\dagger E_q^\dagger E_m E_n|\tilde{\downarrow}\rangle &= F(m,n,p,q)+\frac{G_\downarrow(m,n,p,q)}{N^2}+O(\frac{1}{N^4}).\end{aligned} \tag{4.40}$$

The function F is the same in both correlators, so it represents a correctable error. In contrast, different G functions appear in the two equations. Their difference, $G_\uparrow - G_\downarrow$, represents a small uncorrectable error. They both have simple diagrammatic representation as shown in Figure 4.2 and Figure 4.3, from which we can read off the function $F(m,n,p,q)$. It must take the form

$$F(m,n,p,q) = (\delta^p_m \delta^q_n + \delta^q_m \delta^p_n) + \delta^{p+q}_{m+n} \frac{f(p,q,m,n)}{N^2}, \tag{4.41}$$

where the $O(\frac{1}{N^2})$ term comes from the partly connected diagram in Figure 4.2. Since F does not depend on the logical information and will not contribute to uncorrectable errors, it is not pertinent to the subsequent discussion. Therefore, we will not determine f explicitly.

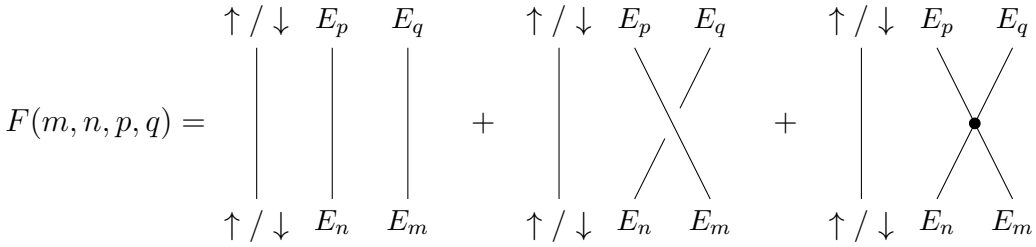

Figure 4.2: The first two diagrams are totally disconnected. The third is partly connected and represents the $O(\frac{1}{N^2})$ term in $F(m,n,p,q)$.

The function G can be read off from Figure 4.3. Using the results for single-trace errors in Eq. (4.39), we can show that,

$$\begin{aligned} G_\uparrow(m,n,p,q) &= (\delta^p_m \delta^q_n + \delta^q_m \delta^p_n)(3n+3m) \\ G_\downarrow(m,n,p,q) &= (\delta^p_m \delta^q_n + \delta^q_m \delta^p_n)(2n+2m). \end{aligned} \tag{4.42}$$

From this explicit form, we see that there is indeed a difference between the these functions, so the logical states are connected by multi-trace operators, again with $1/N$ suppressed amplitudes

provided the indices m, n, p, q are not too large.

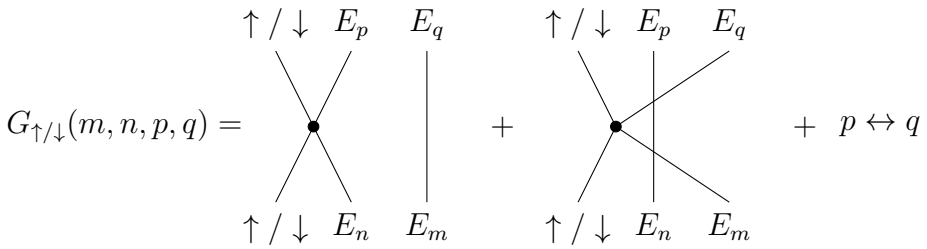

Figure 4.3: The G functions arise from connected diagrams of order $O(\frac{1}{N^2})$ that involve the state $\mathrm{Tr}(a_1^\dagger)|0\rangle$.

Now, although we only explicitly calculated a particular class of multi-trace errors, the algorithm generalizes directly to more general cases. The analog of the G function always consists of connected scattering diagram of logical states and single-trace operators. In other words, the uncorrectable part of any multi-trace error can be written as a sum over contributions of the single-trace errors, due to the factorization property of large N matrix models (Eq (4.17)). Therefore, if the aKL condition is satisfied for the single-trace operators, it will also hold for these multi-trace errors. Note that if a diagram has four legs connected, then it must be suppressed by $\frac{1}{N^2}$. In special cases we also have three-leg diagrams, where the error operators involve $\frac{\mathrm{Tr}(a_{1,2}^{\dagger 2})}{\sqrt{2}N}$ or $\frac{\mathrm{Tr}(a_{1,2}^\dagger)}{\sqrt{N}}$. For example, the G function in the correlator $\langle\tilde{\uparrow}|\frac{\mathrm{Tr}(a_1^2)}{\sqrt{2}N}\frac{\mathrm{Tr}(a_2^2)}{\sqrt{2}N}\frac{\mathrm{Tr}(a_1^{\dagger 2})}{\sqrt{2}N}\frac{\mathrm{Tr}(a_2^{\dagger 2})}{\sqrt{2}N}|\tilde{\uparrow}\rangle$ contains the product of two three-leg diagrams, as shown in Figure 4.4. Each of them is proportional to $\frac{1}{N}$, so the term involving G that depends on the logical state is still suppressed by $\frac{1}{N^2}$.

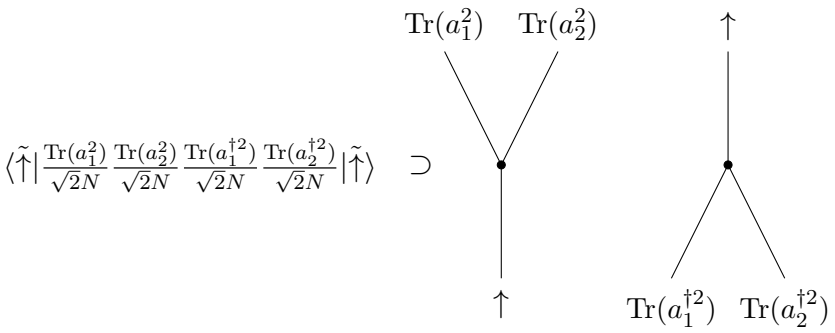

Figure 4.4: Contribution of connected diagram with three legs. Each is suppressed by $\frac{1}{N}$.

Mutual information diagnostic

Now we couple this quantum memory to a single-qubit reference system R, and calculate the mutual information between them (Eq. (4.29)). At $t = 0$, ρ_0 is a pure state,

$$\rho_0 = \frac{1}{2}\sum_{i,j=1}^{2} |i\tilde{i}\rangle_{SR}\langle j\tilde{j}|. \tag{4.43}$$

The system and reference are maximally entangled, so the initial mutual information is $I(S : R)(0) = 2\ln 2$.

Next we count the effective number of error operators which will contribute non-trivially to logical errors under the Lindblad dynamics. Operators that contain more than two a_1 or a_2 trivially annihilate the logical states, so we only need to count the error operators with $r_2, s_2 \leq 2$. The number of gauge invariant error operators with energy $n\omega$ that satisfy this requirement is bounded by $n^2 p(n)$, where $p(n)$ is the number of integer partitions of n. So the number of effective errors is sub-exponential asymptotically.

By construction, the bath model has uniform coupling as required by condition 2 in theorem 1. Together with the aKL condition above, we apply Theorem 1 and conclude the mutual

information decays in the following way,

$$I(S:R)(t) = 2\ln 2 - K(\frac{t}{N^2}), \tag{4.44}$$

where $K(t)$ is linear in t at early time. More specifically, when $\lambda t \ll N^2$, $K(t) \sim \frac{\sum_n n\lambda_n t}{N^2}$. It develops a dependence on higher powers of t at late time $\lambda t \sim N^2$, where $K(t) \sim \sum_p (\frac{\sum_n n\lambda_n t}{N^2})^p$.

Details of the proof for Eq. (4.44) and more rigorous results can be found in Appendix C.1, but here we briefly sketch the general ideas behind the proof. The dominant errors in the early-time regime are the single trace errors. In contrast, in the late time regime, the dominant errors are multi-trace. In fact, the average size k of errors, defined as the number of traces in an error operator, grows linearly with time. These errors, when acting on logical states, cause a loss of quantum information proportional to $\frac{k^p}{N^{2p}}$, leading to the $(\frac{t}{N^2})^p$ growth behavior at late time.

Note that the rate of information loss here is captured by the sum over λ_n, which can be approximated by

$$\begin{aligned} \sum_n n^q \lambda_n &= \sum_n n^q d_n e^{-n\beta\omega} \\ &\sim \sum_n n^{q+2} p(n) e^{-n\beta\omega}, \end{aligned} \tag{4.45}$$

where $q = 1$, and d_n is the number of distinct states at the nth level. In this model, $d_n \sim n^2 p(n)$, which grows sub-exponentially with n. As the sum is always finite, it follows that the memory time scales like $t_{\text{mem}} \sim N^2$. From the above discussion, we conclude that this model serves as a good passive quantum memory.

Now we discuss the zero temperature limit. Since the thermal fluctuation is suppressed,

the relevant error operators are only those which lower the energy when acting on logical states. In this model, they are $\frac{\mathrm{Tr}(a_{1,2})}{\sqrt{N}}$ and $\frac{\mathrm{Tr}(a_{1,2}^2)}{N}$, whose aKL conditions are given in Appendix C.2.1. They lead to a spontaneous decay of quantum information at a constant rate of $O(\frac{1}{N^2})$ at zero temperature. There are also operators that don't change energy of the system, but they have no contribution to the information loss since their thermal spectral functions (Eq. (4.22)) vanish at zero temperature limit, $lim_{\beta\to\infty}\gamma(\nu=0)=0$.

To modify the encoded information, we need to apply logical operators, which involve $\mathrm{Tr}(a_1^\dagger a_2^\dagger)$ or $\mathrm{Tr}(a_1^{\dagger 2} a_2^{\dagger 2})$. This requires us to perform non-local operations (or a series of local operations) by bringing the two modes together and turning on some local coupling, as shown in Figure 4.5. We assume this procedure to be accurate. After the logical operations, we can separate the two modes so that the system again behaves like a passive memory that protects the encoded information.

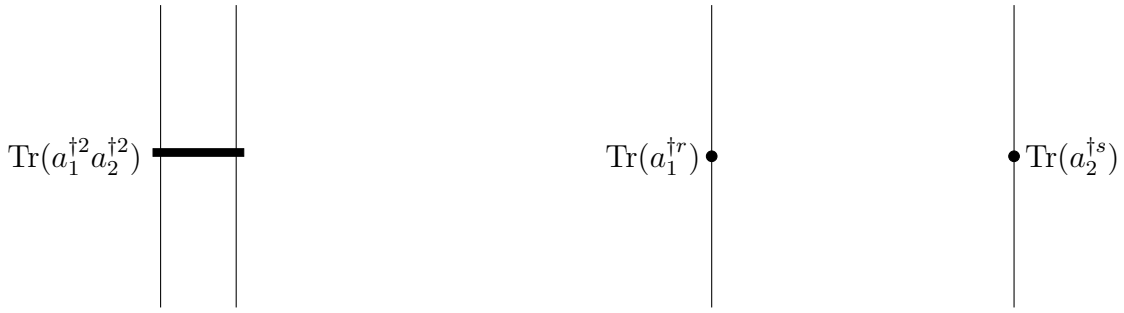

(a) Logical operators (b) Thermal errors

Figure 4.5: In (a), two modes are brought together to implement a logical operator. In (b), two modes are separated far away. Thermal fluctuation are sufficiently local so the quantum information is preserved.

We can also implement logical operations without bringing the two modes together. Instead, we may induce a coupling mediated by a third ancillary mode c. The procedure is that we first bring the mode c close enough to the mode a_1 and implement the operator $\mathrm{Tr}(a_1^{\dagger m} c^\dagger)$. Then

we bring together the intermediate mode and the mode a_2 and implement the operator $\mathrm{Tr}(a_2^{\dagger n}c)$. These two moves can be combined together to give the desired logical operation,

$$\mathrm{Tr}(a_2^{\dagger 2}c)\,\mathrm{Tr}(a_1^{\dagger 2}c^\dagger)|0\rangle \propto \mathrm{Tr}(a_1^{\dagger 2}a_2^{\dagger 2})|0\rangle. \tag{4.46}$$

In summary, this model achieves the power law scaling of memory time with system size. However, it has some drawbacks. First, it requires a gauge symmetry that acts consistently on the two matrix modes separated by a large distance. Second, the logical operation is non-local, and thus can be difficult to implement. For these reasons, we construct another model, where the two matrix modes are put together, but with the added price that a high energy penalty is required.

4.4.2 Local model

In this model, we still consider two matrix harmonic oscillators, but we put them together and turn on a large coupling between them. The full Hamiltonian is

$$H = \omega\,\mathrm{Tr}(a_1^\dagger a_1) + \omega\,\mathrm{Tr}(a_2^\dagger a_2) + J[\frac{\mathrm{Tr}(a_1^\dagger)\,\mathrm{Tr}(a_1)}{N} + \frac{\mathrm{Tr}(a_2^\dagger)\,\mathrm{Tr}(a_2)}{N} - 1]^2 + H_{\text{thermal}} \tag{4.47}$$

with $J \sim 2\omega \ln N$. The ground space of this Hamiltonian is spanned by the following two states,

$$\begin{aligned} |\tilde{\uparrow}\rangle &= \frac{\mathrm{Tr}(a_1^\dagger)}{\sqrt{N}}|0\rangle_{12} \\ |\tilde{\downarrow}\rangle &= \frac{\mathrm{Tr}(a_2^\dagger)}{\sqrt{N}}|0\rangle_{12}. \end{aligned} \tag{4.48}$$

where $|0\rangle_{12}$ is again the tensor product of the vacuum states of the two oscillators. These states span the code subspace of the model.

We assume that H_{thermal} contains only single trace operators:

$$H_{\text{thermal}} = \sum_{\{n_k\}} \lambda_{\{n_k\}} b_{\{n_k\}} \frac{: \mathrm{Tr}(P\{a_1^{\dagger n_1} a_2^{\dagger n_2} a_1^{n_3} a_2^{n_4}\}) :}{N^{\frac{\sum_{k=1}^4 n_k}{2}}} + h.c.. \tag{4.49}$$

where P again denotes the sum over distinct arrangements of the operators inside the curly bracket, and all the operators are then normal ordered. In general, $\mathrm{Tr}(P\{a_1^{\dagger n_1} a_2^{\dagger n_2} a_1^{n_3} a_2^{n_4}\})$ is a sum over $\frac{(n_1+n_2+n_3+n_4)!}{n_1!n_2!n_3!n_4!}$ terms.

The interaction term in the Hamiltonian Eq. (4.47) incurs an energy penalty for any logical errors that involve $\mathrm{Tr}(a_1^\dagger)$ or $\mathrm{Tr}(a_2^\dagger)$, so their probability to appear are suppressed due to the thermal factor. For example, the probability of the error operator $\mathrm{Tr}(a_1^\dagger)\,\mathrm{Tr}(a_2)$ is $\gamma(J)\gamma(-J) \sim e^{-\frac{J}{T}}$. We set the energy scale J to be $2\omega \ln N$, which guarantees that these uncorrectable errors are unlikely to occur when N is large enough. All the other operators generated by the coupling in Eq. (4.49) are treated as possible errors that could act on the logical state. To show that these errors are approximately correctable, and to invoke Theorem 1, it suffices to check that aKL holds for single-trace errors, $E_{\{n_k\}} := \frac{:\mathrm{Tr}(P\{a_1^{\dagger n_1} a_2^{\dagger n_2} a_1^{n_3} a_2^{n_4}\}):}{N^{\frac{\sum_{k=1}^4 n_k}{2}}}$,

$$\begin{aligned} \langle\tilde{i}|E^\dagger_{\{n'_k\}} E_{\{n_k\}}|\tilde{j}\rangle &= f_{\{n'_k\},\{n_k\}}\delta_{ij} + \frac{g^{ij}_{\{n'_k\},\{n_k\}}}{N^2} + O(\frac{1}{N^4}) \\ \langle\tilde{i}|E_{\{n_k\}}|\tilde{j}\rangle &= \frac{e^{ij}_{\{n_k\}}}{N} + O(\frac{1}{N^3}). \end{aligned} \tag{4.50}$$

Applying the argument we discussed in Section 4.4.1, one can again derive the aKL equation for general multi-trace operators using the above relations for single-trace operators. This

guarantees that the aKL condition holds for all the error operators generated in this model. A proof of the aKL condition for the most general error is given in Appendix C.2.2. Here we discuss a few helpful examples to show that these errors indeed conform with the aKL condition.

Again, let us first check operators of the form $\frac{\mathrm{Tr}(a_{1,2}^\dagger a_{1,2})}{N}$. They induce a phase error of size $O(\frac{1}{N})$,

$$\begin{aligned}\langle\tilde{\uparrow}|\frac{\mathrm{Tr}(a_1^\dagger a_1)}{N}|\tilde{\uparrow}\rangle &= \frac{1}{N}\\ \langle\tilde{\downarrow}|\frac{\mathrm{Tr}(a_1^\dagger a_1)}{N}|\tilde{\downarrow}\rangle &= 0,\end{aligned} \tag{4.51}$$

which is consistent with the aKL condition in Eq. (4.50). Next, we check the aKL conditions for single-trace errors of the form $E_{(n,m)} = \frac{\mathrm{Tr}(a_1^{\dagger n} a_2^{\dagger m})}{N^{\frac{m+n}{2}}}$, with $n \geq 1, m \geq 1$. For the bit flip errors, we can show that

$$\langle\tilde{\downarrow}|E_{(n'+1,m'-1)}^\dagger E_{(n,m)}|\tilde{\uparrow}\rangle = \delta_{nn'}\delta_{mm'}\frac{(n+1)m}{N^2} + O(\frac{1}{N^4}), \tag{4.52}$$

and for the phase errors, we have

$$\begin{aligned}\langle\tilde{\uparrow}|E_{(n',m')}^\dagger E_{(n,m)}|\tilde{\uparrow}\rangle &= \delta_{nn'}\delta_{mm'}[1 + \frac{n^2-m^2}{N^2} + O(\frac{1}{N^4})]\\ \langle\tilde{\downarrow}|E_{(n',m')}^\dagger E_{(n,m)}|\tilde{\downarrow}\rangle &= \delta_{nn'}\delta_{mm'}[1 + \frac{m^2-n^2}{N^2} + O(\frac{1}{N^4})].\end{aligned} \tag{4.53}$$

When m or n equals to 0, the equations are slightly different. For instance, when $m = 0, n \geq 2$, the matrix elements are,

$$\begin{aligned}\langle\tilde{\uparrow}|E_{(n',0)}^\dagger E_{(n,0)}|\tilde{\uparrow}\rangle &= \delta_{nn'}[1 + \frac{n(n-1)}{N^2} + O(\frac{1}{N^4})]\\ \langle\tilde{\downarrow}|E_{(n',0)}^\dagger E_{(n,0)}|\tilde{\downarrow}\rangle &= \delta_{nn'}\\ \langle\tilde{\uparrow}|E_{(n',0)}^\dagger E_{(n,0)}|\tilde{\downarrow}\rangle &= 0.\end{aligned} \tag{4.54}$$

Although H_{thermal} only contains single-trace operators, the expansion in Eq. (4.28) involves multi-trace operators acting on the state. To see the effect of these multi-trace errors, we evaluate an example:

$$\begin{aligned}\langle\tilde{\uparrow}|E^\dagger_{(p,0)}E^\dagger_{(q,0)}E_{(m,0)}E_{(n,0)}|\tilde{\uparrow}\rangle &= F(m,n,p,q)+\frac{G(m,n,p,q)}{N^2}+O(\frac{1}{N^4})]\\ \langle\tilde{\downarrow}|E^\dagger_{(p,0)}E^\dagger_{(q,0)}E_{(m,0)}E_{(n,0)}|\tilde{\downarrow}\rangle &= F(m,n,p,q)+O(\frac{1}{N^4}).\end{aligned} \tag{4.55}$$

If the Knill-Laflamme conditions are satisfied, then the above expressions should yield matrix elements that only depend on the errors. We see that the presence of the G function does allow one to distinguish the logical states, but the effect is suppressed by $1/N^2$. These correlation functions both have simple diagrammatic representations similar to those shown in Figure 4.2 and Figure 4.3, but the explicit form of these two functions are complicated,

$$\begin{aligned}F(m,n,p,q) &= (\delta^p_m\delta^q_n+\delta^q_m\delta^p_n)+\delta^{p+q}_{m+n}\frac{f(p,q,m,n)}{N^2}\\ G(m,n,p,q) &= (\delta^p_m\delta^q_n+\delta^q_m\delta^p_n)[n(n-1)+m(m-1)]+(\delta^p_{m\pm1}\delta^q_{n\mp1}+\delta^q_{m\pm1}\delta^p_{n\mp1})\sqrt{pqmn}.\end{aligned} \tag{4.56}$$

with some function f whose exact form is not essential for our argument.

Again all the errors discussed above are approximately correctable errors, because they can only corrupt the logical information up to $O(\frac{1}{N^2})$. The uncorrectable errors or logical operators are those that contain $\mathrm{Tr}(a_1^\dagger)$ and $\mathrm{Tr}(a_2^\dagger)$. However, recall that we have tuned the coupling J to be proportional to $2\omega\ln N$ so that these uncorrectable errors have a similar $1/N$ suppressed effect comparable in size to the approximately correctable errors.

By construction, the bath model has uniform coupling as required by condition 2 of Theo-

rem 1. In addition, the number of gauge invariant error operators with energy $n\omega$ that are induced by Eq. (4.49) grows asymptotically as 2^n. In particular, the number of effective error operators that act non-trivially on the logical state, i.e., ones contributing to the information leak in the Lindblad equation, must have $n_2, n_4 \leq 1$. Therefore, the total number of effective errors with energy ωn is bounded by an exponential function, as required by condition 1.

Because the aKL condition holds and the bath model only generates errors which are protected by the code, we again invoke the Theorem 1. The mutual information between the encoded qubit S and a reference R is

$$I(S:R)(t) = 2\ln 2 - K_{\text{local}}(\frac{t}{N^2}). \tag{4.57}$$

The expression $K_{\text{local}}(t)$ in this model is slightly different from $K(t)$, since the $O(\frac{1}{N^2})$ term in the aKL condition depends quadratically on n (see Eq. (4.52)). When $\lambda t \ll N^2$, $K_{\text{local}}(\frac{t}{N^2}) \sim \frac{\sum_n n^2 \lambda_n t}{N^2}$. At late time $\lambda t \sim N^2$, $K_{\text{local}}(t) \sim (\sum_n n^2 \lambda_n t)^2$.

More importantly, note that the rate of information loss is given by

$$\begin{aligned} \sum_n n^q \lambda_n &= \sum_n n^q d_n e^{-n\beta\omega} \\ &\sim \sum_n n^q 2^n e^{-n\beta\omega}, \end{aligned} \tag{4.58}$$

where $q = 2$, and $d_n \sim 2^n$ is the number of single trace states at the nth energy level. A crucial distinction from the previous model is the Hagedorn-like transition with a critical temperature $T_c = \frac{\omega}{\ln 2}$ [148]. In the low temperature phase where $T < T_c$, the rate of information loss (4.58) is finite and N-independent. Therefore the large N gauged matrix model has a long memory

time $t_{\text{mem}} \sim N^2$. However, for $T > T_c$, (4.58) exhibits a Hagedorn-like behaviour[8]. As a result, $K_{\text{local}}(t)$ now also scales with N. This N dependence cancels out the large N suppression, and the memory time no longer scales with the system size. This behaviour is similar to the holographic code [135], where the temperature needs to be lower than a critical value to maintain the robustness of the encoded information.

Since the logical states are within the ground space of this model, there are no operators that can lower the energy. The zero energy error operators do not contribute to information loss at zero temperature limit, due to the vanishing thermal spectral function $\lim_{\beta\to\infty}\gamma(\nu = 0)$. Therefore, when $\beta \to \infty$, we expect the information decay rate to scale as $\frac{1}{N^2}e^{-\beta\omega}$ according to Eq. (4.58).

4.5 Relaxing the gauge constraint

We now relax the gauge constraint to a global symmetry, which we then impose energetically. The purpose of this is two-fold — (i) we want to understand how the stability of quantum memory is tied to the gauge symmetry specifically, and (ii) there are very few models in nature that are known to have gauge symmetries. For example, Quantum ElectroDynamics (QED) has a $U(1)$ symmetry and Quantum ChromoDynamics (QCD) has an $SU(3)$ symmetry. However, there is no known $SU(N)$ gauged model that can be realized in the laboratory, especially for arbitrarily large N. Therefore, in this section, we consider a single oscillator model with only a

[8]Note that for finite N, the Hagedorn behaviour does not continue to arbitrary energies, but only to order N^2, the total number of gauge invariant degrees of freedom. The counting of gauge invariant operators can be found in Section 4.3.4.

global $SU(N)$ symmetry. The system of interest has Hamiltonian

$$\begin{aligned} H_{\text{Gauss}} &= \frac{\mathcal{J}}{N}\sum_{ij} G_j^i G_i^j \\ G_j^i &= \sum_k a_k^{\dagger i} a_j^k - a_j^{\dagger k} a_k^i, \end{aligned} \tag{4.59}$$

where $G_j^i|\psi\rangle = 0$ is the Gauss law constraint associated with the gauge symmetry. The energy penalty term plays the role of a Casimir operator in the group $SU(N)$, with eigenvalues proportional to $\mathcal{J}$ and being the same for all states in an irreducible representation. This term in the Hamiltonian forces the low energy states to be singlets of the symmetry group.

In the absence of gauge symmetry, we allow the modes a_j^i's to couple independently with the thermal bath operator. Let us consider the following thermal coupling Hamiltonian,

$$\begin{aligned} H_{\text{thermal}} =& \lambda_1 \sum_{ij} b_j^i a_i^{j(\dagger)} + \lambda_2 \sum_{ijkl} b_{jl}^{ik} a_i^{j(\dagger)} a_k^{l(\dagger)} + \lambda_3 \sum_{ijklpq} b_{jlq}^{ikp} a_i^{j(\dagger)} a_k^{l(\dagger)} a_p^{q(\dagger)} + \cdots \\ &+ h.c.. \end{aligned} \tag{4.60}$$

One can show that the Lindblad Master equation takes the form of

$$\dot{\rho}(t) = \lambda_1 \frac{\text{Tr}(a^\dagger)}{\sqrt{N}} \rho \frac{\text{Tr}(a)}{\sqrt{N}} + \lambda_1 e^{-\frac{\mathcal{J}}{T}} \sum_{ij} \tilde{a}_j^{\dagger i} \rho \tilde{a}_i^j + \cdots, \tag{4.61}$$

where $\tilde{a}_j^i$ represents the component that transforms in the adjoint representation of $SU(N)$, such that

$$\tilde{a}_j^{\dagger i} = a_j^{\dagger i} - \frac{\text{Tr}(a^\dagger)}{N} \delta_j^i. \tag{4.62}$$

We show in Appendix C.3 that it is a consequence of the H_{Gauss} term in the Hamiltonian.

These non-singlet errors acting on the "gauge invariant" logical states, *i.e.*, logical states satisfying the Gauss law constraint, only corrupt quantum information at $O(\frac{1}{N^2})$, which we show in Appendix C.2.3. The summation in Eq. (4.61) is over N^2 number of such errors and therefore the total effect of these non-singlet errors is proportional to $N^2 e^{-\frac{\mathcal{J}}{T}}$. Hence the coupling strength $\mathcal{J}$ has to be at least $\sim 2T \log N$ in order to suppress their effects to the same order as those from the the singlet errors. Note that this model effectively contains one such matrix oscillator and does not exhibit a Hagedorn-like transition. Nevertheless, it is clear that stability is only ensured when $T\mathcal{J}$, hence can also depend on the system size[9]. In the following, we will assume their suppression with a strong enough coupling. As for the singlet error operators, they are defined as,

$$E_{(\{n_k,m_k)\}} := \prod_k \frac{\text{Tr}(P\{a^{\dagger n_k} a^{m_k}\})}{N^{\frac{\sum_k n_k+m_k}{2}}}. \tag{4.63}$$

The logical states we choose in this model are (divided by proper normalization constant),

$$\begin{aligned} |\tilde{1}\rangle &= \frac{\text{Tr}(a^{\dagger L})^2}{\mathcal{N}(L)}|0\rangle \\ |\tilde{2}\rangle &= \frac{\text{Tr}(a^{\dagger L+1})\,\text{Tr}(a^{\dagger L-1})}{\mathcal{N}(L)}|0\rangle. \end{aligned} \tag{4.64}$$

We also define the orthogonormal basis,

$$\begin{aligned} |\tilde{\uparrow}\rangle &= \frac{|\tilde{1}\rangle + |\tilde{2}\rangle}{2(1+\langle\tilde{1}|\tilde{2}\rangle)} \\ |\tilde{\downarrow}\rangle &= \frac{|\tilde{1}\rangle - |\tilde{2}\rangle}{2(1-\langle\tilde{1}|\tilde{2}\rangle)}. \end{aligned} \tag{4.65}$$

[9]This should be contrasted with the models with exact gauge symmetry, where the temperature that sets apart a stable and an unstable memory only depends on the natural frequency of the system. Note that in the local model with gauge symmetry, there is an additional scale introduced by J which has to satisfy $J\omega \log N$ to to ensure stability. However, as long as we have tuned $J > T_c$, then T_c will be the relevant energy scale for the low energy stability.

In order to recast the code subspace as a lower energy subspace, let us consider a shifted version of the system Hamiltonian and write the full Hamiltonian as

$$H = \frac{\mathcal{J}}{N}\sum_{ij} G_j^i G_i^j + \omega(\mathrm{Tr}(a^\dagger a) - L)^2 + H_{\text{thermal}}, \tag{4.66}$$

where $L > 0$ is some arbitrary integer.

One can check that the aKL condition,

$$\begin{aligned}\langle\tilde{i}|E^\dagger_{\{(n'_k,m'_k)\}}E_{\{(n_k,m_k)\}}|\tilde{j}\rangle &= f_{\{(n'_k,m'_k)\},\{(n_k,m_k)\}}\delta_{ij} + \frac{g^{ij}_{\{(n'_k,m'_k)\},\{(n_k,m_k)\}}}{N^2} + O(\frac{1}{N^4})\\ \langle\tilde{i}|E_{\{(n_k,m_k)\}}|\tilde{j}\rangle &= \frac{e^{ij}_{\{(n_k,m_k)\}}}{N} + O(\frac{1}{N^3}),\end{aligned} \tag{4.67}$$

holds for all relevant errors induced by (4.63) as long as they do not contain $\mathrm{Tr}(a^{\dagger L})$ or $\mathrm{Tr}(a^{\dagger L\pm 1})$ as a factor. For example, consider the class of error operators $E_n = \frac{\mathrm{Tr}(a^{\dagger n})}{\sqrt{n}N^{\frac{n}{2}}}$. The relevant matrix elements are

$$\begin{aligned}\langle\tilde{\uparrow}|E_m^\dagger E_n|\tilde{\downarrow}\rangle &= \delta_{mn}[\frac{2n}{N^2} + O(\frac{1}{N^4})]\\ \langle\tilde{\uparrow}|E_m^\dagger E_n|\tilde{\uparrow}\rangle - \langle\tilde{\downarrow}|E_m^\dagger E_n|\tilde{\downarrow}\rangle &= O(\frac{1}{N^4}).\end{aligned} \tag{4.68}$$

Note that although the Hamiltonian and logical states depend on L, the error induced by a low energy operator has no such dependence (the $O(\frac{1}{N^2})$ term does not depend on L); ergo, the aKL conditon in the standard form Eq. (4.18) holds for such singlet errors (4.63). We present the details of the proof in Appendix C.2.3).

Similar to the discussion in Section 4.4.1, the number of singlet errors with the energy $n^2\omega$

scales as the number of integer partitions $p(n)$. This is clearly slower than exponential growth. Therefore, if the thermal coupling in (4.60) does not contain $\mathrm{Tr}(a^{\dagger L})$ and $\mathrm{Tr}(a^{\dagger L\pm 1})$ as factors, and $\lambda \sim O(1)$, then Theorem 1 applies and we again attain a memory time quadratic in N. Since the logical states are within the ground space, there are no spontaneous decay of quantum information. So the memory time is proportional to $N^2 e^{\frac{\omega}{T}}$ at zero temperature limit.

However, the low energy errors like $\mathrm{Tr}(a^{\dagger L})\,\mathrm{Tr}(a^{L})$ do appear, which means that the aKL condition does not hold for these operators. Nevertheless, it is possible to retain this long memory time in this model as long as we also suppress the singlet errors containing such terms. One way to achieve this is to assume that the coupling constants are exponentially suppressed with respect to the number of modes involved, i.e., $\lambda_k \sim \lambda^k$ for some $\lambda < 1$. This gaps out the dangerous error for large $L \sim \log N$ by suppressing the error probability to order $\frac{1}{N^2}$. In the meantime, it is also a natural requirement in this model because the thermal bath mode couples to each oscillator individually.

One potential drawback in this model (and also the fully gauged model in Section 4.4.2) is that the coupling constants $\mathcal{J}, J \propto \ln N$ depend on the system size. However, this is not as unreasonable as it looks because the interaction energy per harmonic oscillator mode is small[10] and is proportional to $\frac{\ln N}{N^2}\omega$. For reference, let us contrast this N-dependence with that of the toric code model with system size equal to N. Recall that the toric code is a Z_2 lattice gauge theory and the Hamiltonian also involves terms that are proportional to the Gauss's law operators, with coupling constant Δ. When it is coupled to a bath with fixed temperature T, the memory time is proportional to $\frac{1}{N} e^{\frac{\Delta}{T}}$. It becomes a viable quantum memory if one can tune the coupling Δ to $T \ln N$, which corresponds to an energy density much larger than that required in our matrix

[10]The energy for thermal state at temperature $T \sim \omega \ll \mathcal{J}$ is $O(1)$ times $\mathcal{J}$. See Appendix C.4 for more detail.

model.

4.6 Large N spin model

In the previous sections, we saw that exact $SU(N)$ symmetries in oscillator models can lead to robust quantum memories, both when the symmetry is fully gauged and when the singlet restriction is enforced energetically. It is natural to ask whether such exact symmetries and infinite dimensional Hilbert spaces are truly necessary for robustness. In other words, can we realize an analogous phenomenon with finite dimensional systems, e.g. involving qubits, that only have an approximate $SU(N)$ symmetry? In this section, we propose one such model and show that the requisite large N factorization properties are mostly preserved up to small corrections in the low energy sector. As a result, the general conclusions of Theorem 1 still apply to this system in a way that is similar to Section 4.

To motivate the model, let us first review how one can approximately embed the low-energy states of an oscillator into a spin Hilbert space. Consider a spin-j representation of $SU(2)$. When acting on states with S^z eigenvalue close to maximal, mj, the spin commutator becomes

$$[S^x, S^y] = i\hbar S^z \approx i\hbar^2 j + \cdots . \tag{4.69}$$

This suggest that S^x and S^y can be approximately mapped to a canonical pair. Setting

$$Q = \frac{\ell}{\hbar\sqrt{j}} S^x, \quad P = \frac{1}{\ell\sqrt{j}} S^y \tag{4.70}$$

for some as yet undetermined length ℓ, we see that

$$[Q, P] \approx i\hbar + \cdots . \tag{4.71}$$

Now considering the harmonic oscillator Hamiltonian

$$H = \frac{1}{2}(P^2 + \omega^2 Q^2) = \frac{1}{2}\left(\frac{1}{\ell^2 j}(S^y)^2 + \frac{\omega^2 \ell^2}{\hbar^2 j}(S^x)^2\right), \tag{4.72}$$

we may set $\ell^2 = \hbar/\omega$ to obtain

$$H = \frac{\omega}{2\hbar j}\left((S^x)^2 + (S^y)^2\right) = \frac{\omega}{2\hbar j}(S^2 - (S^z)^2). \tag{4.73}$$

Using the standard spectrum of S^2 and S^z with $m = j - \Delta$, the spectrum of H is

$$\frac{\hbar\omega}{2j}\left(j(j+1) - (j-\Delta)^2\right) = \hbar\omega\left(\Delta + \frac{1}{2} + O(\Delta^2/j)\right). \tag{4.74}$$

From this discussion, we expect that the physics of our oscillator models may be suitably extended by replacing the oscillators with qudits of dimension d ($d = 2j + 1$ in the above mapping). At large d we have a nearly identical low-energy spectrum, but the models make sense for any d and we will show that even $d = 2$ ($j = 1/2$) suffices.

Specifically, we can construct a system of N^2 spins, which can be thought of as qudits with local dimension d. It is tempting to write each spin operator in the adjoint representation of

$SU(N)$, meaning each spin operator carries indices i, j running from 1 to N and transforms as

$$S_j^{i\pm} \to \sum_{kl} U_k^i S_l^{k\pm} U_j^{\dagger l}. \tag{4.75}$$

Each spin also satisfies the following $SU(2)$ algebra,

$$\begin{aligned} [S_i^{j+}, S_j^{i-}] &= 2S_i^{jz} \\ [S_i^{jz}, S_i^{j+}] &= S_i^{j+} \\ [S_i^{jz}, S_j^{i-}] &= -S_j^{i-}, \end{aligned} \tag{4.76}$$

where i, j again label the different spins or qudits. However, the $SU(N)$ symmetry does not act consistently on the spin algebra due to the first line above: we cannot interpret S_i^{jz} as being in the adjoint of $SU(N)$ while also obeying the commutation relation. Moreover, even if we grant that S_i^{jz} is not in the adjoint representation, it is impossible to construct $SU(N)$ generators G_i^j with the desired commutation relations with $S_i^{j\pm}$, i.e. there is no G_i^j obeying[11]

$$[G_i^j, S_k^{l\pm}] = \delta_i^l S_k^{j\pm} - \delta_k^j S_i^{l\pm}. \tag{4.77}$$

However, it is still possible to realize an approximate symmetry in terms of the pseudo-generators,

$$\begin{aligned} \tilde{G}_i^j &= \sum_k S_k^{j+} S_i^{k-} - S_i^{k+} S_k^{i-} \\ [\tilde{G}_i^j, S_k^{l\pm}] &= (\delta_i^l S_k^{j\pm} - \delta_k^j S_i^{l\pm}) S_k^{lz}. \end{aligned} \tag{4.78}$$

[11] The inconsistency of $SU(N)$ and the $SU(2)$ algebra can be seen from the equation $\sum_k [[S_k^{i+}, S_j^{k-}], S_h^{l+}] = \delta_j^i \delta_h^j S_h^{l+}$, where the right hand side transforms differently from the left hand side.

Indeed, if S^z could be approximated as a constant operator, then we would have the desired commutators. This approximate algebra thus connects back with the oscillator models of the previous sections where the symmetry becomes exact. In what follows, we work with the pseudo-generators $\tilde{G}_i^j$ and set $d = 2$.

Similar to our recipe in the previous sections, one can construct the analogs of the gauge invariant states by acting multi-trace operators on the tensor product of spin down states

$$\begin{aligned} &\mathrm{Tr}(S^{+n_1})\,\mathrm{Tr}(S^{+n_2})\cdots\mathrm{Tr}(S^{+n_k})|0\rangle \\ &|0\rangle := |\downarrow\downarrow\cdots\downarrow\rangle. \end{aligned} \tag{4.79}$$

For convenience, we still refer to these analogues of the gauge invariant operators (states) singlet operators (states). Indeed, one can see that the desired symmetry is only approximate because the algebra of such operators is not closed. For example,

$$\mathrm{Tr}(S^{-2})\,\mathrm{Tr}(S^{+2})\,\mathrm{Tr}(S^{+2})|0\rangle = (4N^2 - 4N - 8)\,\mathrm{Tr}(S^{+2})|0\rangle + 32\sum_i S_i^{i+}S_i^{i+}|0\rangle. \tag{4.80}$$

Generally, the product of such singlet terms can produce non-singlet terms that are only sub-leading in N [12].

Now let us consider a system Hamiltonian $H_S = hH_0 + \mathcal{J}H_G$, where

$$H_0 = (\sum_{ij} S_j^{iz} - S_{\mathrm{tot}})^2, \tag{4.81}$$

[12] If we further restrict ourselves to only consider spin-$\frac{1}{2}$,i.e., $d = 2$, then the non-singlet terms also vanishes. This can be a convenient simplification when the local systems are exactly qubits, however, our analysis of robustness will also hold for systems with $d > 2$.

and $-\frac{N^2}{2} \leq S_{\text{tot}} \leq \frac{N^2}{2}$ is some N-dependent offset. H_G is an energy penalty term similar to the Gauss law constraint; it corresponds to the Casimir operator that enforces the approximate $SU(N)$ symmetry for low energy states[13],

$$H_G = \frac{1}{N}\tilde{G}^2 := \frac{1}{N}\sum_{ij} \tilde{G}_i^j \tilde{G}_j^i. \tag{4.82}$$

When $\mathcal{J}$ is large, it creates a large gap in the spectrum. We define the low energy sector as the states with eigenvalues suppressed by $\frac{1}{N}$. The energy eigenstates of H_S are generally superpositions of the singlet and non-singlet states, but it can be shown that the low energy sector is isomorphic to the singlet subspace. For example, the following are four states created by product of three S^+'s, which are simultaneous eigenstates of both H_0 and H_G,

$$\begin{aligned}
|\psi_1\rangle &= \mathrm{Tr}(S^{+3})|0\rangle \\
|\psi_2\rangle &= [\mathrm{Tr}(S^+)^3 - 3\,\mathrm{Tr}(S^{+2})\,\mathrm{Tr}(S^+)]|0\rangle \\
|\psi_3\rangle &= [\mathrm{Tr}(S^{+2})\,\mathrm{Tr}(S^+) + (1+\frac{2}{N})\,\mathrm{Tr}(S^+)^3 - \frac{19}{2N}\sum_i (S^{+2})_i^i S_i^{+i}]|0\rangle \\
|\psi_4\rangle &= [\sum_i (S^{+2})_i^i S_i^{+i} - \frac{1}{N}\,\mathrm{Tr}(S^{+2})\,\mathrm{Tr}(S^+)]|0\rangle.
\end{aligned} \tag{4.83}$$

The first three states are in the low energy sector, since they are eigenstates of H_G with eigenvalues $E_1^G = E_2^G = 0$ and $E_3^G = \frac{7\mathcal{J}}{2N}$. The fourth state has eigenvalue $E_4^G = \mathcal{J}$, and hence a high energy excitation.

There are two potential causes for this model to deviate from the one in Section 4.5 —

[13]The Casimir operator $C = \sum_{ij} G_j^i G_i^j$ for an exact $SU(N)$ symmetry has a spectrum of the form NwJ, where w is the highest weight of given representation. Analogously, the Hamiltonian H_G also has an energy spectrum of the form of wJ up to $\frac{1}{N}$ corrections.

effects from the symmetry being approximate and finite dimensionality of each spin. Formally, we should still expect the low energy states, *i.e.*, ones with energy $\ll \mathcal{J}$, to have a one-to-one correspondence with the multi-trace operators formed by S^+'s. More precisely, their low energy spectra should coincide up to corrections that are $1/N$ suppressed and the multiplicity, when we ignore such corrections, should be identical.

We see this by noting that their energy only depend on number of S^+ involved, with small corrections proportional to $\frac{\mathcal{J}}{N}$ (Figure 4.6). Therefore, up to these small corrections introduced by the deviations from the exact symmetry, the operator counting at each energy level is the same as that in Section 4.5. These corrections can be connected to the break down of the exact symmetry.

As for the correction from finite dimensionality, thanks to the "Gauss law" constraint H_G and the form of H_0, these corrections would only significantly modify this counting when the total number of S^+ involved is of $O(N)$. Therefore, in the low energy regime where we operate, both effects are suppressed by having a large enough N.

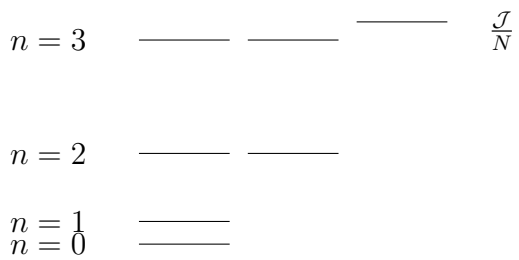

Figure 4.6: Specturm of the low energy states. The ground state has energy zero. Excited states has energy proportional to $n^2 h$. Note that due to the non-exactness of symmetry, there are small energy splitting proportional to $\frac{\mathcal{J}}{N}$. For sufficiently large N, this small gap can be neglected and the degeneracy at each level is the same as in harmonic oscillator model. Non-singlet excitations have energy $O(\mathcal{J})$, which we do not count as low energy.

Similar to the harmonic oscillator model, we consider the full Hamiltonian,

$$H = hH_0 + \mathcal{J}H_G + H_{\text{thermal}} \tag{4.84}$$

with H_{thermal} being

$$\begin{aligned} H_{\text{thermal}} =& \lambda_1 \sum_{ij} b_j^i S_i^{j\pm} + \lambda_2 \sum_{ijkl} b_{jl}^{ik} S_i^{j\pm} S_k^{l\pm} + \lambda_3 \sum_{ijklpq} b_{jlq}^{ikp} S_i^{j\pm} S_k^{l\pm} S_p^{q\pm} + \cdots \\ &+ h.c.. \end{aligned} \tag{4.85}$$

The lowest energy states must have total spin equal to S_{tot}. Let us define $L = \frac{S_{\text{tot}}+N^2/2}{2}$ and pick a two dimensional subspace as the code subspace. With proper normalization,

$$\begin{aligned} |\tilde{1}\rangle &= \frac{\text{Tr}(S^{+L})^2}{\mathcal{N}}|0\rangle \\ |\tilde{2}\rangle &= \frac{\text{Tr}(S^{+L+1})\,\text{Tr}(S^{+L-1})}{\mathcal{N}}|0\rangle. \end{aligned} \tag{4.86}$$

Again, we define the orthogonormal basis in this logical subspace as,

$$\begin{aligned} |\tilde{\uparrow}\rangle &= \frac{|\tilde{1}\rangle + |\tilde{2}\rangle}{2(1+\langle\tilde{1}|\tilde{2}\rangle)} \\ |\tilde{\downarrow}\rangle &= \frac{|\tilde{1}\rangle - |\tilde{2}\rangle}{2(1-\langle\tilde{1}|\tilde{2}\rangle)}. \end{aligned} \tag{4.87}$$

with the overlap $\langle\tilde{1}|\tilde{2}\rangle = \frac{f(L)L\sqrt{L^2-1}}{\sqrt{2}N^2}$, where $f(L)$ is a complicated function defined in Appendix C.2.4.

Let us couple this system to a thermal bath at temperature T. First note that the non-singlet excitations are again suppressed by a factor of $e^{-\frac{\mathcal{J}}{T}}$ because of the energy penalty term H_G, while the singlet interaction has no such suppression. Then let us reorganize the system-bath

interactions by the approximate symmetry such that

$$\begin{aligned} H_{\text{thermal}} &= \lambda_1 \sum_{ij} b_j^i S_i^{j\pm} + \lambda_2 \sum_{ijkl} b_{jl}^{ik} S_i^{j\pm} S_k^{l\pm} + \cdots + h.c. \\ &= \lambda_1 \sum_{ij} b_j^i (S_i^{j+} - \frac{\text{Tr}(S^+)}{N} \delta_i^j) + \lambda_1 \frac{\text{Tr}(b)}{\sqrt{N}} \frac{\text{Tr}(S^+)}{\sqrt{N}} + \cdots . \end{aligned} \tag{4.88}$$

Similar to the discussion in last section, this interaction induces an order N^2 number of non-singlet errors. Therefore, the total error contribution from non-singlet excitations is $\sim N^2 e^{-\frac{\mathcal{J}}{T}}$ times that of singlet excitations. To suppress both types of errors to the same order, we require the coupling $\mathcal{J}$ to be greater than $2h \log N$.

More precisely, the singlet error operators are defined as

$$E_{(\{n_k,m_k)\}} := \prod_k \frac{\text{Tr}(P\{S^{+n_k} S^{-m_k}\})}{N^{\frac{\sum_k n_k + m_k}{2}}}. \tag{4.89}$$

Again, we show that the aKL condition

$$\begin{aligned} \langle \tilde{i} | E^\dagger_{\{(n'_k,m'_k)\}} E_{\{(n_k,m_k)\}} | \tilde{j} \rangle &= f_{\{(n'_k,m'_k)\},\{(n_k,m_k)\}} \delta_{ij} + \frac{g^{ij}_{\{(n'_k,m'_k)\},\{(n_k,m_k)\}}}{N^2} + O(\frac{1}{N^4}) \\ \langle \tilde{i} | E_{\{(n_k,m_k)\}} | \tilde{j} \rangle &= \frac{e^{ij}_{\{(n_k,m_k)\}}}{N} + O(\frac{1}{N^3}) \end{aligned} \tag{4.90}$$

is satisfied in Appendix C.2.4. For example, one can see that the operator $\frac{\text{Tr}(S^+S^-)}{N} = \frac{\sum_{ij} S_j^{iz}}{N}$ acts as the logical identity, since the logical states have the same total spin in z direction. For another example, the aKL conditions for errors $E_n = \frac{\text{Tr}(S^{+n})}{\sqrt{n} N^{\frac{n}{2}}}$ are

$$\begin{aligned}\langle\tilde{\uparrow}|E_m^\dagger E_n|\tilde{\downarrow}\rangle &= \delta_{mn}[\frac{2n}{N^2}+O(\frac{1}{N^4})]\\ \langle\tilde{\uparrow}|E_m^\dagger E_n|\tilde{\uparrow}\rangle - \langle\tilde{\downarrow}|E_m^\dagger E_n|\tilde{\downarrow}\rangle &= O(\frac{1}{N^4}).\end{aligned} \tag{4.91}$$

Note that in these examples, and more generally in Appendix C.2.4, deviations from the KL condition only depend on n but not on L. Therefore, the aKL condition remains valid even for very large L. Similar to the last section, we can pick $L\log N$ to make sure uncorrectable errors are suppressed for large N. For instance, one may consider choosing $L = N^2/4$ such that $S_{\text{tot}} = 0$.

Since this spin model has a structure very similar to the ungauged harmonic oscillator model, we can follow the same argument in Section 4.5. In the low energy sector with $\epsilon \ll \mathcal{J} \sim \log N$, (approximate) singlet errors are the dominant error modes. The number of such error operators grows sub-exponentially with energy because these operators still have the multi-trace structure whose counting are the same as the one in Section 4. There are small corrections because of the approximate symmetry, however they are proportional to $\frac{\mathcal{J}}{N}$, and therefore for large N, they do not affect the overall structure of the spectrum for the purpose of our analysis (Figure 4.6). Similarly, we also need the thermal coupling strength to decay exponentially with number of spins to suppress the singlet error operators such as $\text{Tr}(S^{-L})\,\text{Tr}(S^{+L})$. As argued in the previous section, this is a natural assumption since the bath mode couples to each spin individually. Since the rest of the argument is identical to those in Section 4.5, we can then invoke Theorem 1 to conclude that the memory time t_m scales quadratically with N. There is no operator that can lower the logical states' energy, so the zero temperature limit of memory

time is still proportional to $N^2 e^{\frac{\omega}{T}}$. We remark that this model also has the same drawback as the ungauged harmonic oscillator model, that is, the interactions remain non-local and we need the coupling strength $\mathcal{J}$ to scale as at least $\log N$.

4.7 Discussion and Conclusion

Motivated by connections between error correction and phenomena in gauge theory and quantum gravity, we have taken a first step in understanding how $SU(N)$ gauge symmetries at large N can be used to construct stable quantum memories. In particular, we construct a gauged matrix quantum mechanics toy model with non-local logical operations that is a self-correcting quantum memory. The memory time of this model is polynomial in N when coupled to a thermal bath at non-zero temperature. The presence of gauge symmetry induces approximate quantum error correcting codes that become exact in the large N limit, thanks to the large N factorization property. Furthermore, gauge invariance limits the number of error patterns that can be excited up to a certain energy scale. The combination of these factors suppresses the proliferation of memory errors under thermal noise. A similar model with local logical operation is also possible, but as a trade off, we impose an additional energy penalty with a coupling of strength $\sim \log N$. The memory time is again polynomial in N, but only for temperatures below a critical value.

As large N gauge symmetries are not known to occur in nature, we relax the gauge symmetries and impose only large N global symmetries energetically on a single matrix oscillator. We also construct a non-local finite dimensional spin model which further relaxes the symmetry constraint where we only enforce approximate large N symmetries energetically. Interestingly, these constructions remain robust in both scenarios under the assumed system-bath coupling as long as

the symmetry constraints can be energetically enforced with a penalty that scales as $O(\log N)$.

Stepping back from these particular examples, our work provides one set of guidelines for building large N passive quantum memories in which the encoded information remains robust when coupled to a thermal bath. Sufficient conditions on the quantum system and its coupling to the bath are captured in Theorem 1. We hope to extend our current work in a number of future directions. Let us roughly categorize these potential generalizations in the direction of optimality, dimensionality, symmetries, variety, and practicality.

Although we can construct models that have poly(N) memory time, they also often come with other features that are practically difficult, such as non-local interactions and $\log N$ coupling strengths. However, we by no means claim that these are the optimal constructions. Indeed, it is possible that a more careful design can produce better self-correcting memories. For example, an interesting theoretical problem is whether there exists a gauged $SU(N)$ oscillator model with local coupling for which the quantum memory is stable against thermal noise.

It is also natural to generalize these findings to systems with gauge symmetries in higher dimensions by considering geometrically coupled oscillators, lattice gauge theories, and concatenations with other quantum error correcting codes. We will take a first step towards tackling a subset of these problems in an upcoming work [137]. Although we enforce global symmetries energetically in our work, one can similarly ask whether there are advantages in considering systems with emergent gauge symmetries at low energies, which is better understood in higher dimensional systems. Relatedly, one can examine what aspects of the $SU(N)$ symmetry are actually essential. For instance, does a similar result hold for discrete, instead of continuous, non-abelian symmetries?

Drawing intuition from gauge theories, we can also examine how to generalize such models

by coupling the "pure gauge" degrees of freedom to fundamental degrees of freedom like matter fields and defects. In particular, how does the configuration of these other degrees of freedom impact our conclusions? One may, for instance, introduce a variety of fields that may interact under these gauge couplings. Extensions in this direction draw heavy parallels with traditional theoretical particle physics, and can open up new connections with quantum information in this area.

Lastly, as a practical aspect of any quantum memory, information needs to be encoded and extracted relatively easily. This is yet unexplored for both the infinite dimensional oscillator and the finite dimensional spin system. As a standalone quantum code, the gauged matrix oscillator is a continuous variable system that resembles bosonic codes [48] in many ways. However, we have barely begun to analyze its code properties. It is desirable to understand its similarities and differences with existing bosonic codes, its robustness against different kinds of errors, and how active error correction like syndrome extraction can be performed.

Acknowledgement

We thank Alexey Milehkin, John Preskill for helpful comments and discussions. C.C. acknowledges the support by the U.S. Department of Defense and NIST through the Hartree Postdoctoral Fellowship at QuICS, the Air Force Office of Scientific Research (FA9550-19-1-0360), and the National Science Foundation (PHY-1733907). G.C. acknowledges support from the U.S. Department of Energy, Office of Science, Office of Advanced Scientific Computing Research, Accelerated Research for Quantum Computing program "FAR-QC". B.G.S. acknowledges support from the AFOSR under grant number FA9550-19-1-0360.

Appendix A: Supplementary Material for Chapter 2

A.1 Propagator for λ field

Since there is no dynamical terms for the auxiliary field λ in the Lagrangian, the leading contribution to the λ propagator must comes from a loop correction as in Figure 2.1. The polarization function is

$$\begin{aligned} M\Pi(i\omega_n) = &\sum_{\mu=1}^{M} \frac{1}{2} T \sum_{\nu_n} G(i\nu_n) G(-i\nu_n + i\omega_n) \\ =&M\frac{1}{2} \oint \frac{dz}{2\pi i} \int dx \frac{A(x)}{z-x} \int dy \frac{A(y)}{-z + i\tilde{\omega}_n - y} n_B(z) \\ =&M\frac{1}{2} \int dx \int dy \frac{A(x)A(y)}{i\tilde{\omega}_n - x - y} [n_B(-y) - n_B(x)] \end{aligned} \tag{A.1}$$

$A(x)$ is the spectral function for the rotor field. So the integration is performed on the region where $A(x)A(y)$ is non-zero. In particular, at critical point $A(\tilde{\omega}) = \frac{2}{\pi J}\tilde{\omega}\sqrt{1-\tilde{\omega}^2}$, with $\tilde{\omega} \in [-1, 1]$. In general, the expression above cannot be simplified further, but if we look at the strong coupling limit, which amounts to taking $\tilde{\omega}$ to be small, an analytic expression can be obtained. First, we rewrite Eq. (A.1) as

$$\Pi(i\omega_n) = -\int dt \frac{f(t)}{i\tilde{\omega}_n - t} \tag{A.2}$$

where

$$\begin{aligned} f(t) =& \frac{1}{2}\int dx A(x)A(t-x)[n_B(x)-n_B(x-t)] \\ =& \frac{2\sqrt{Jg}}{\pi^2 J^2}\left(\frac{1}{3}\tilde{t}^3+\frac{4}{3}\pi^2\tilde{T}^2\tilde{t}+\cdots\right) \end{aligned} \tag{A.3}$$

This gives the non-analytic part of $\Pi(i\omega_n)$,

$$\Pi(i\omega_n) = \frac{2\sqrt{Jg}}{\pi J^2}\left(\frac{1}{3}|\tilde{\omega}_n|^3-\frac{4}{3}\pi^2\tilde{T}^2|\tilde{\omega}_n|+\cdots\right)+\text{analytic part.} \tag{A.4}$$

The non-analytic part of $G_\lambda(i\omega_n)$ can also be expanded in $|\tilde{\omega}_n|$ and $\tilde{T}$,

$$\begin{aligned} G_\lambda(i\omega_n) =& -\frac{1}{M\Pi(i\tilde{\omega}_n)} \\ =& \frac{1}{M}\frac{1}{\Pi(0)^2}\frac{2\sqrt{Jg}}{\pi J^2}(\frac{1}{3}|\tilde{\omega}_n|^3-\frac{4}{3}\pi^2\tilde{T}^2|\tilde{\omega}_n|+\cdots)+\text{analytic part.} \end{aligned} \tag{A.5}$$

Finally, by Fourier transformation we obtain the imaginary time propagator of λ field at strong coupling limit,

$$T\sum_n G_\lambda(i\omega_n)e^{-i\omega_n\tau} = J^2\frac{c}{\sin^4(\frac{\pi\tau}{\beta})}. \tag{A.6}$$

A.2 Self-energy correction

In this section, we compute the self-energy correction (see Figure 2.7),

$$\frac{1}{M}\Sigma(i\omega_n) = T\sum_n G(i\omega_n-i\nu_n)G_\lambda(i\nu_n) \tag{A.7}$$

where

$$G_\lambda(i\nu_n) = -\frac{1}{M\Pi(i\nu_n)}. \tag{A.8}$$

Note that the summation in Eq. (A.7) is not convergent since G_λ(z) defined in Eq. (A.8)) diverges like $\frac{z^2}{a}$ for some constant a as z goes to ∞. So we regularize G_λ by multiplying to it a factor $\frac{1}{1-\epsilon z^2}$ with a small ϵ. Physically, this means we soften the delta function constraint in Eq. (2.5) by adding a small quadratic term for λ in the Lagrangian

$$Z = \int D\lambda Dn e^{\sum_i \frac{1}{2}(\epsilon a M\lambda_i^2 - \lambda_i n_i n_i) + \ldots} \tag{A.9}$$

and finally take ϵ to zero. When we convert the summation in Eq. (A.7) to contour integral, the effect of this factor is to introduce two poles at $\pm\frac{1}{\sqrt{\epsilon}}$ in the integrand. Now we first evaluate the integral around branch cuts of function G_λ(z) and $G(z)$. Denoting this part by $\Sigma_1(i\omega_n)$

$$\begin{aligned}
\frac{1}{M}\Sigma_1(i\omega_n) &= \oint \frac{dz}{2\pi i} G(i\omega_n - z)G_\lambda(z)n_B(z) \\
&= -\oint \frac{dz}{2\pi i}\int dx \frac{A(x)}{z - i\omega_n - x} G_\lambda(z)n_B(z) + \frac{2i}{2\pi i}\int dx \Im[G_\lambda(x + i0^+)]G(x - i\omega_n)n_B(x) \\
&= \int dx [A(x)G_\lambda(x + i\omega_n)n_B(x) + \frac{1}{\pi}\Im[G_\lambda(x + i0^+)]G(x - i\omega_n)n_B(x)]
\end{aligned} \tag{A.10}$$

In the second line, we integrated around the branch cut of $G(i\omega_n + z)$ and $G_\lambda(z)$ respectively. Define

$$\frac{1}{M}A_\lambda(x) = \frac{1}{\pi}\Im G_\lambda(x + i0^+) \tag{A.11}$$

Then from Eq. (A.10), we have that

$$\frac{1}{M}\Sigma_1(i\omega_n) = \int dx A(x) G_\lambda(x + i\omega_n) n_B(x) - \frac{1}{M}\int dx \int dy \frac{A_\lambda(x)A(y)n_B(x)}{i\omega_n - x - y} \tag{A.12}$$

The integration in x and y are over regions on real axis, where $A(y)$ and $A_\lambda(x)$ are non-zero. Note that we didn't express G_λ in terms of $A_\lambda(x)$ in the first term. In fact G_λ cannot be represented by it's spectral function in the usual way, since from Eq. (A.8) $G_\lambda(z)$ is divergent as $z \to \infty$. Then we include in Eq. (A.12) the contribution from the two poles at $z = \pm\frac{1}{\sqrt{\epsilon}}$. Denoting this part by Σ_2, we have

$$\begin{aligned}\frac{1}{M}\Sigma_2(i\omega_n) =& \frac{1}{2\sqrt{\epsilon}} G\left(i\omega_n - \frac{1}{\sqrt{\epsilon}}\right) G_\lambda\left(\frac{1}{\sqrt{\epsilon}}\right) n_B\left(\frac{1}{\sqrt{\epsilon}}\right) - \frac{1}{2\sqrt{\epsilon}} G\left(i\omega_n + \frac{1}{\sqrt{\epsilon}}\right) G_\lambda\left(-\frac{1}{\sqrt{\epsilon}}\right) n_B\left(-\frac{1}{\sqrt{\epsilon}}\right) \\ \xrightarrow{\epsilon\to 0}& \frac{1}{2\sqrt{\epsilon}} G\left(\frac{1}{\sqrt{\epsilon}}\right) G_\lambda\left(\frac{1}{\sqrt{\epsilon}}\right) \coth\left(\frac{\beta}{2}\frac{1}{\sqrt{\epsilon}}\right) + \frac{i\omega_n}{2\sqrt{\epsilon}} G'\left(\frac{1}{\sqrt{\epsilon}}\right) G_\lambda\left(\frac{1}{\sqrt{\epsilon}}\right)\end{aligned} \tag{A.13}$$

Since $\frac{1}{\sqrt{\epsilon}}$ is very large, the $\coth$ function can be set to one. So the leading order term is proportional to $\frac{1}{\sqrt{\epsilon}}$ and divergent as $\epsilon \to 0$. Adding Eq. (A.12) and Eq. (A.13) we get

$$\begin{aligned}\frac{1}{M}\Sigma_R(\omega) =& \int dx A(x) G_\lambda(x + \omega + i0^+) n_B(x) - \frac{1}{M}\int dx \int dy \frac{A_\lambda(x)A(y)n_B(x)}{\omega - x - y + i0^+} \\ &+ \lim_{\epsilon\to 0} \frac{1}{2\sqrt{\epsilon}} G'\left(\frac{1}{\sqrt{\epsilon}}\right) G_\lambda\left(\frac{1}{\sqrt{\epsilon}}\right) \omega + O\left(\frac{1}{M\sqrt{\epsilon}}\right).\end{aligned} \tag{A.14}$$

The divergent part is not a problem, since it will be canceled when we add the self-energy diagrams in Figure A.1.

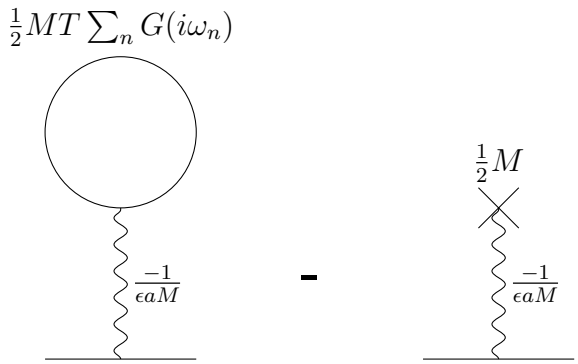

Figure A.1: Other diagrams contributing to the self-energy.

After including the self-energy correction, the Schwinger-Dyson equation for the rotor field two point function is modified to

$$G(i\omega_n)^{-1} = \frac{\omega_n^2}{g} + \lambda - J^2 G(i\omega_n) - \frac{1}{M}\tilde{\Sigma}(i\omega_n) \tag{A.15}$$

Solving this equation we obtain

$$\begin{aligned} G(i\omega_n) =& G^{(0)}(i\omega_n) + \frac{1}{M} G^{(1)}(i\omega_n) \\ =& G^{(0)}(i\omega_n) + \frac{1}{M}\frac{c - \tilde{\Sigma}(i\omega_n)}{J^2 - G^{(0)}(i\omega_n)^{-2}} \end{aligned} \tag{A.16}$$

where $\frac{c}{M} = \lambda - \lambda^{(0)}$ is a constant. $\tilde{\Sigma}(i\omega_n)$ is the finite part of $\Sigma(i\omega_n)$ after subtracting the $O(\frac{1}{\sqrt{\epsilon}})$ term. The pole in Eq. (2.32) is modified to

$$J^2 \frac{G_R(\omega)^2 G_R(\nu-\omega)^2}{1 - J^2 G_R(\omega) G_R(\nu-\omega)} \xrightarrow{\nu\to 0} \frac{1}{J^2}\frac{\pi}{4}\frac{JA(\omega)}{\omega}\frac{1}{-i\tilde{\nu} - \frac{\pi}{2}\frac{1}{M}\frac{JA(\omega)}{\omega} J^2 \Re(G_R^{(0)}(-\omega) G_R^{(1)}(\omega))} \tag{A.17}$$

When ω lies in the interval such that $A(\omega) \neq 0$, we have

$$\begin{aligned}\Re(G_R^{(0)}(-\omega)G_R^{(1)}(\omega)) = \frac{1}{J^4}\Re\left(\frac{c-\tilde{\Sigma}_R(\omega)}{G_R(\omega)-G_R(-\omega)}\right)\\ =\frac{1}{J^4}\frac{-\Im\tilde{\Sigma}_R(\omega)}{2\Im G_R(\omega)}\end{aligned} \tag{A.18}$$

This function is always non-positive since both the denominator and numerator are non-negative functions. The constant c need not to be determined for our purposes, but it can be fixed by demanding

$$T\sum_n G(i\omega_n) = 1. \tag{A.19}$$

A.3 Details of numerical calculation

In Eq. (2.37), we redefine $f'(\omega,\nu) = \sqrt{\frac{A(\omega)}{\omega}}f(\omega,\nu)$. Then it is converted to an eigenvalue problem with a symmetric kernel,

$$K(\omega,\omega') := \frac{\pi}{4}\frac{1}{M}\left[\sqrt{\frac{JA(\omega)}{\omega}}\sqrt{\frac{JA(\omega')}{\omega'}}G_{\text{rung}}(\omega,\omega') + 2\frac{JA(\omega)}{\omega}\Re(G_R^{(0)}(-\omega)G_R^{(1)}(\omega))(2\pi)\delta(\omega-\omega')\right] \tag{A.20}$$

and

$$\partial_t f'(\omega,t) = \int\frac{d\omega'}{2\pi}K(\omega,\omega')f'(\omega',t). \tag{A.21}$$

In the practical calculations, we only deal with the normalized frequency $\tilde{\omega} := \frac{\omega}{2\sqrt{gJ}}$. Since $A(\tilde{\omega})$ is non-zero only when $|\tilde{\omega}|$ lies in finite interval $\mathcal{I} = [\sqrt{\lambda'-\frac{1}{2}}, \sqrt{\lambda'+\frac{1}{2}}]$, approximately we can say that $f(\omega,\nu)$ is only non-zero on $\mathcal{I}$. Then we discretize this interval and diagonalize the kernel numerically by treating Eq. (A.21) as a matrix equation,

$$\partial_t \hat{f}(t) = \hat{K}\hat{f}(t) \tag{A.22}$$

where $\hat{f}(t)$ is a vector whose components are $f(\tilde{\omega} = \frac{i}{m}, t)$. $\hat{K}$ is a matrix with matrix elements $\hat{K}_{ij} = \frac{1}{m}\frac{1}{2\pi}K(\frac{i}{m}, \frac{j}{m})$. $\frac{1}{m}$ is the step size. In our calculation, we take it to be $\frac{1}{100}$. At low temperature, we refine the gridding in the region where $n_B(x)$ varies fast, in order to improve the precision. Then we found the maximal eigenvalue λ_m of $\hat{K}$ by diagonalizing it using Mathematica. If λ_m is positive, the corresponding growing mode will dominate for large t. So we identify the chaos exponent $\tilde{\lambda}_c$ as λ_m.

Appendix B: Supplementary Material for Chapter 3

B.1 Solution to the Maxwell-Einstein differential equation

In our metric, $-g^{tt} = g^{rr} = \frac{R^2}{f}$ and $\sqrt{-g} = R^{-(d+2)} f$. The Maxwell equation simplifies to

$$\partial_r^2 A_t + \partial_r \ln\left(\frac{1}{R^{d-2}(\omega^2 - k^2 f)}\right) \partial_r A_t + (\omega^2 - k^2 f) A_t = 0 \tag{B.1}$$

There is a singular point at $f \to 0$, where the equation becomes

$$\partial_r^2 A_t + \omega^2 A_t = 0 \tag{B.2}$$

with solution $A_t(r, \omega, k) \sim e^{-i\omega r}$. We have picked the in-falling mode on this boundary. The ansatz

$$A_t(r, \omega, k) = e^{-i\omega r} F(r, \omega, k) \tag{B.3}$$

yields an equation for F,

$$F'' - 2i\lambda\hat{\omega} F' - \partial_r \ln[R^{d-2}(\hat{\omega}^2 - \hat{k}^2 f)](F' - i\lambda\hat{\omega} F) + \lambda^2(\hat{\omega}^2 - \hat{k}^2 f)F = 0, \tag{B.4}$$

where $(\omega, k) = (\lambda\hat{\omega}, \lambda\hat{k})$ and $\lambda \ll 1$.

The solution F should have an expansion in the form $F = F_0 + \lambda F_1 + \cdots$. The leading F_0 satisfies

$$\begin{aligned} F_0'' - \partial_r \ln[R^{d-2}(\hat{\omega}^2 - \hat{k}^2 f)] F_0' = 0, \\ \implies F_0 = C_0 + C_1 \int_0^r dr' R'^{d-2}(\hat{\omega}^2 - \hat{k}^2 f). \end{aligned} \tag{B.5}$$

F_0 goes like $C_1 \hat{\omega}^2 r$ as $r \to -\infty$, so a regular solution should have $C_1 = 0$. Similarly, the first order term F_1 should satisfy

$$F_1'' - 2i\hat{\omega} F_0' - \partial_r \ln[R^{d-2}(\hat{\omega}^2 - \hat{k}^2 f)](F_1' - i\hat{\omega} F_0) = 0. \tag{B.6}$$

The integration constant can be fixed by requiring regularity at horizon, then one obtains

$$F_1 = i\hat{\omega} C_0 \int_{r_0}^r dr' [1 - R'^{d-2}(1 - \frac{\hat{k}^2}{\hat{\omega}^2}) f]. \tag{B.7}$$

To first order in λ, we find

$$A_t(r, \omega, k) = C_0 \{1 + i\omega \int_{r_0}^r dr' [1 - R'^{d-2}(1 - \frac{\hat{k}^2}{\hat{\omega}^2}) f]\}. \tag{B.8}$$

B.2 Details of the OTOC calculation

Start from the inner product,

$$
\begin{aligned}
&(A_1, A_2) \\
&= \int dp \int d^d\vec{x} \int \frac{d^dk}{(2\pi)^d} \int \frac{d^dk'}{(2\pi)^d} (\vec{k}\cdot\vec{k'}) p p^{Dk^2-1} p^{Dk'^2-1} e^{-ip\left[2+\frac{\Delta_O}{N}e^{t_{12}-\mu|\vec{x}-\vec{x}_{12}|}\right]} e^{i(\vec{k'}-\vec{k})\cdot\vec{x}} \\
&= \int d^d\vec{x} \int \frac{d^dk}{(2\pi)^d} \int \frac{d^dk'}{(2\pi)^d} (\vec{k}\cdot\vec{k'}) \Gamma[D(k^2+k'^2)] \left[2+\frac{\Delta_O}{N}e^{t_{12}-\mu|\vec{x}-\vec{x}_{12}|}\right]^{-D(k^2+k'^2)} e^{i(\vec{k'}-\vec{k})\cdot\vec{x}}.
\end{aligned}
\tag{B.9}
$$

As in the main text, we will just keep the leading order dependence in k for the gamma function. We change the integration variables to $K = \frac{k+k'}{2}$ and $\kappa = \frac{k-k'}{2}$. This gives

$$
\begin{aligned}
(A_1, A_2) &\sim \int d^d\vec{x} \int \frac{d^dK}{(2\pi)^d} \int \frac{d^d\kappa}{(2\pi)^d} 2^d \frac{K^2-\kappa^2}{2D(K^2+\kappa^2)} \left[2+\frac{\Delta_O}{N}e^{t_{12}-\mu|\vec{x}-\vec{x}_{12}|}\right]^{-2D(K^2+\kappa^2)} e^{-2i\kappa\cdot\vec{x}} \\
&= \int \frac{d^dx}{(4\pi)^d} \left[\frac{d}{D^{d+1}} E(\ln g, \frac{|\vec{x}|^2}{2D}) - \frac{1}{2D^{d+1}} \frac{1}{(\ln g)^d} e^{-\frac{|\vec{x}|^2}{2D\ln g}}\right],
\end{aligned}
\tag{B.10}
$$

where g and E are defined as

$$
\begin{aligned}
g &= 2 + \frac{\Delta_O}{N} e^{t_{12}-\mu|\vec{x}-\vec{x}_{12}|}, \\
E(z,a) &= \int_z^\infty dy \frac{1}{y^{d+1}} e^{-\frac{a}{y}}.
\end{aligned}
\tag{B.11}
$$

Since both of the two terms contain $e^{-\frac{|\vec{x}|^2}{2D\ln g}}$, we expect the integral to receive its dominant contribution from $|x| \sim 0$. Integrating $\vec{x}$ over this saddle point gives a factor of $(2D\ln g)^{\frac{d}{2}}$. Therefore, we finally obtain

$$
(A_1, A_2) \propto \frac{1}{[\ln(2+\frac{\Delta_O}{N}e^{\frac{2\pi}{\beta}t-\mu|x_{12}|})]^{\frac{d}{2}}}.
\tag{B.12}
$$

In fact, the saddle point approximation in last step is only valid for very small diffusion constant D and for not too large values of the function $g(x)$. Thus it is necessary to discuss the late and early time limits separately from the above treatment. Looking back at Eq. (B.10), in the large t_{12} limit, $t_{12} \gg LnN + \frac{|\vec{x}_{12}|}{v_B}$. We can expand the function $\ln g \sim t_{12}(1 - \frac{|\vec{x}|}{v_B t_{12}})$, for $|x| < cv_B t$, where c is some finite constant smaller than 1. Then the integral over x can be evaluated as

$$\begin{aligned} &\int d^d\vec{x} \frac{1}{(\ln g)^\alpha} e^{-\frac{|x|^2}{2D \ln g}}, \\ &= \int^{|x|<cv_B t} d^d\vec{x} \frac{1}{t_{12}^\alpha (1 - \frac{|x|}{t_{12}})^\alpha} e^{-\frac{|x|^2}{2Dt_{12}}[1+O(\frac{|x|}{t_{12}}))]} + \int_{|x|>cv_B t} d^d\vec{x} \frac{1}{(\ln g)^\alpha} e^{-\frac{|x|^2}{2D \ln g}}. \end{aligned} \tag{B.13}$$

For the first part, the change of variable to $x \to \frac{x}{\sqrt{2Dt_{12}}}$ gives

$$\int^{|x|<c\frac{v_B}{\sqrt{2D}}\sqrt{t}} d^d\vec{x}\, t_{12}^{\frac{d}{2}-\alpha} (1 + O(\frac{|x|}{\sqrt{t_{12}}})) e^{-|x|^2(1+O(\frac{|x|}{\sqrt{t_{12}}}))} \sim t_{12}^{\frac{d}{2}-\alpha}(1 + O(t_{12}^{-\frac{1}{2}})). \tag{B.14}$$

The second part is bounded by

$$\int_{|x|>cv_B t} d^d\vec{x} \frac{1}{(\ln 2)^\alpha} e^{-\frac{|x|^2}{2Dt_{12}}} \sim O(e^{-\frac{v_B^2 t_{12}}{D}}). \tag{B.15}$$

From these results, the late time amplitude indeed decays in a power law manner, and is consistent with the result Eq. (B.12).

$$(A_1, A_2) \sim \frac{1}{|t_{12}|^{\frac{d}{2}}}. \tag{B.16}$$

On the other hand, when $t_{12} - \frac{|\vec{x}_{21}|}{v_B} \ll \ln N$, we expand $\ln g \sim \ln 2 + \frac{\Delta_\mathcal{O}}{2N} e^{t_{12} - \frac{|\vec{x}-\vec{x}_{12}|}{v_B}}$, as

well as

$$\begin{aligned} E(\ln g, a) \sim & E(\ln 2, a) + \frac{\Delta_{\mathcal{O}}}{2N} e^{t_{12} - \frac{|\vec{x}-\vec{x}_{12}|}{v_B}} \frac{d}{dz} E(z, a)|_{z=\ln 2}, \\ \sim & E(\ln 2, a) - \frac{1}{2N} e^{t_{12} - \frac{|\vec{x}-\vec{x}_{12}|}{v_B}} \frac{1}{(\ln 2)^{d+1}} e^{-\frac{a}{\ln 2}}. \end{aligned} \tag{B.17}$$

The leading order deviation is

$$(A_1, A_2) \sim \frac{1}{(\ln 2)^{\frac{d}{2}}} \left[1 - \frac{1}{2N} \frac{\frac{d}{2}}{\ln 2} e^{t_{12}} \int d^d \tilde{x} \frac{2}{3} \left(1 + \frac{|x|^2}{d} \right) e^{-\frac{|\tilde{x}-\tilde{x}_{12}/\sqrt{D}|}{v_B/\sqrt{D}} - |\tilde{x}|^2} \right] \tag{B.18}$$

This matches with the result Eq. (B.12), when expanding around small values of D, because the integral in Eq. (B.18) is approximated by $e^{-\frac{|x_{12}|}{v_B}} + e^{-\frac{|x_{12}|^2}{D}}$. We can see that the velocity of the wave-front is still given by v_B. For completeness, we give the exact result of this integral in 1d,

$$e^{-\frac{|x_{12}|}{v_B} + \frac{D}{4v_B^2}} \text{erf} \left(\frac{\sqrt{D}}{2v_B} - \frac{|x_{12}|}{\sqrt{D}} \right) \left(\frac{1}{2} + \frac{D}{12v_B^2} \right) - \left(\frac{\sqrt{D}}{6v_B} + \frac{1}{3} \frac{|x_{12}|}{\sqrt{D}} \right) e^{-\frac{|x_{12}|^2}{D}}. \tag{B.19}$$

B.3 OTOCs of sound mode operators

In this section, we evaluate the OTOC between a sound mode operator (eg. T_{tt}, $T_{xx} + T_{yy}$) and a scalar operator with large conformal dimension Δ. For this purpose, we first solve the sound mode equation in a symmetric gauge to second order of ω and k. By doing this, we obtain the dispersion relation as in [154] and the near horizon form of the wave function. Unlike in [154], we apply a gauge fixing condition that preserves boundary spatial rotational symmetry.

If the boundary source respects rotational symmetry (for example, consider a boundary insertion of T_{tt} or $\sum_{i=1}^{d} T_{ii}$), we expect a bulk configuration satisfying $h_{ti} = h_{ri} = 0$ and h_{ij}

proportional to identity matrix, for $i, j \in \{1, \cdots, d\}$. Without loss of generality, we will take $d = 2$ in the following. Then the non-zero components are h_{tt},h_{tr}, h_{rr} and $h_{xx} = h_{yy}$. They satisfy a set of differential equations. Using the tortoise coordinate $r = -\int \frac{dR}{f(R)}$, and the Fourier decomposition $h_{MN}(r,t,x) = \int d\omega dk h_{MN}(r,\omega,k)e^{-i\omega t+ikx}$, these equations are written as

$$-i(f+3)R\omega h_{\text{xx}} + k^2R^2h_{\text{tr}} + 2iR^2\omega h'_{\text{xx}} - 2iR\omega h_{\text{rr}} = 0, \tag{B.20}$$

$$-\frac{kR^2\omega h_{\text{rr}}}{f} + \frac{ikR^2h'_{\text{tr}}}{f} - kR^2\omega h_{\text{xx}} = 0, \tag{B.21}$$

$$\frac{kR\left(h_{\text{rr}} - h_{\text{tt}}\right)}{f} = 0, \tag{B.22}$$

$$\frac{2f^2h_{\text{xx}}}{R} + \frac{(f+3)h_{\text{rr}}}{2R} - \frac{(f+3)h_{\text{tt}}}{2R} - fh'_{\text{xx}} + i\omega h_{\text{tr}} + h'_{\text{tt}} = 0, \tag{B.23}$$

$$-\frac{\left(f+k^2R^2+3\right)h_{\text{rr}}}{R^2} + \left(\frac{3-f}{R^2}+k^2\right)h_{\text{tt}} + \left(-fk^2 - \frac{6f}{R^2} + \omega^2\right)h_{\text{xx}} - \frac{h'_{\text{rr}}}{R} - \frac{2i\omega h_{\text{tr}}}{R} - \frac{h'_{\text{tt}}}{R} + h''_{\text{xx}} = 0, \tag{B.24}$$

$$h''_{\text{tt}} + \frac{(7f-9)h'_{\text{tt}}}{2R} + \frac{(f-3)fh'_{\text{xx}}}{R} - \frac{(f-3)h'_{\text{rr}}}{2R} + 2i\omega h'_{\text{tr}} + \cdots = 0, \tag{B.25}$$

$$h''_{\rm tt} - 2f h''_{\rm xx} + \frac{3(f-3)h'_{\rm tt}}{2R} + \frac{3f(f+1)h'_{\rm xx}}{R} + \frac{3(f+1)h'_{\rm rr}}{2R} + 2i\omega h'_{\rm tr} + \cdots = 0. \tag{B.26}$$

These seven equations are not independent. They reduce to three independent first order differential equations together with an algebraic equation, Eq. (B.22). Then the last three equations, Eq. (B.24)-(B.26), give an algebraic constraint,

$$\omega h_{xx}(r)\left(3f^2 - 2f\left(k^2R^2+6\right) + 4R^2\omega^2 + 9\right) + \omega h_{tt}(r)\left(-6f + 2k^2R^2 + 6\right) - iRh_{tr}(r)\left((f-3)k^2 + 4\omega^2\right) = 0 \tag{B.27}$$

There are two independent solutions, with out-going and in-falling conditions near the horizon. To see this, make the substitution $\lim_{r\to-\infty} h_{\mu\nu}(r) = e^{\nu r}F_{\mu\nu}$ to the equations and take the limit $R \to 1$. The equations become

$$\nu \begin{pmatrix} F_{xx} \\ F_{tr} \\ F_{tt} \end{pmatrix} = \begin{pmatrix} \frac{3}{2} & \frac{ik^2}{2\omega} & 1 \\ 0 & 0 & -i\omega \\ 0 & -i\omega & 0 \end{pmatrix} \begin{pmatrix} F_{xx} \\ F_{tr} \\ F_{tt} \end{pmatrix} \tag{B.28}$$

There are three eigenvalues, $(\frac{3}{2}, i\omega, -i\omega)$, corresponding to a spurious solution, out-going, and in-falling solutions, respectively. The eigenvalue $\frac{3}{2}$ is discarded, since the corresponding eigenvector is not compatible with the constraint Eq. (B.27). The eigenvector of the in-falling solution tells

us that

$$\begin{pmatrix} F_{xx} \\ F_{tr} \\ F_{tt} \end{pmatrix} = C(\omega,k) \begin{pmatrix} -\frac{k^2-2i\omega}{\omega(2\omega-3i)} \\ 1 \\ 1 \end{pmatrix}. \tag{B.29}$$

One can check that the gauge condition fixes the gauge completely. As a result, the in-falling solution is unique. To second order in momentum, we find the solution for h_{xx}

$$\begin{aligned} h_{xx}(r,\omega,k) &= C(\omega,k)e^{-i\omega r}[-\frac{2}{3R} + \lambda\int_{c_x^1}^{R} dR' \frac{i(k^2 f - 2\omega^2(1-R'^2))}{3R'^2 f\omega} + \lambda^2 h_{xx}^{(2)} + O(\lambda^3)] \\ h_{xx}^{(2)} &= \frac{1}{R}\int_{c_x^2}^{R} dR'[\frac{k^2 f - 2\omega^2}{9R'^2 f} Ln(\frac{f}{3}) + \frac{4(k^2-\omega^2) - k^2 R'^3}{9R'^2 f}] - \left(\frac{4\omega^2}{9} - \frac{k^2}{3}\right) r - \frac{\omega^2 r^2}{3} \end{aligned} \tag{B.30}$$

The integration constants c_x^1 and c_x^2 are fixed by requiring that the $r \to -\infty$ limit of h_{xx} matches with Eq. (B.29).

The solution for h_{tt} is

$$h_{tt}(r.\omega,k) = C(\omega,k)e^{-i\omega r}[\frac{1}{3}R^2 + \frac{2}{3R} + \lambda\frac{2+R^3}{R}\int_{c_t^1}^{R} dR' \frac{3i\omega R'^4}{(2+R'^3)^2 f} + \lambda^2 h_{tt}^{(2)} + O(\lambda^3)], \tag{B.31}$$

where $h_{tt}^{(2)}$ is a complicated function. Again, the integration constants can be chosen according to Eq. (B.29). Finally, solution for h_{tr} is

$$h_{tr}(\omega,k) = C(\omega,k)e^{-i\omega r}[1 - i\lambda\omega\int_1^R dR' \frac{1-R'^2}{f} + \lambda^2(-i\omega\int dR' \frac{h_{tt}^{(1)} + f h_{xx}^{(1)}}{f} + \frac{1}{2}\omega^2 r^2) + O(\lambda^3)]. \tag{B.32}$$

Close to the boundary ($r \to 0$), $h_{tt} \sim O(\frac{1}{r})$, and h_{xx} has the asymptotic form

$$h_{xx} \to \frac{(1+\frac{i\omega}{3}Ln(3))(2\omega^2-k^2)+\frac{4i\omega}{3}(k^2-\omega^2)}{-3i\omega r^2}+O(\frac{1}{r}). \tag{B.33}$$

Therefore, for the boundary souce $h^0_{xx}(\omega,k) = h^0_{yy}(\omega,k) = 1$, we obtain the overall constant $C(\omega,k) = \frac{-3i\omega}{(1+\frac{i\omega}{3}Ln(3))(2\omega^2-k^2)+\frac{4i\omega}{3}(k^2-\omega^2)}$. The near horizon limit of all the components is also clear. Due to rotational symmetry, the x-axis can be any direction. So we have the following ansatz for the wave function, with the correct sound pole,

$$h_{tt}(r,t,\vec{x}) = h_{rr}(r,t,\vec{x}) \sim \int d\omega d^2\vec{k} \frac{-\frac{3}{2}i\omega(\frac{1}{3}R^3+\frac{2}{3R})}{(\omega^2-\frac{1}{2}k^2)+\frac{i\omega}{3}k^2} e^{-i\omega(t+r)+i\vec{k}\cdot\vec{x}}, \tag{B.34}$$

$$h_{xx}(r,t,\vec{x}) \sim \int d\omega d^2\vec{k} \frac{1}{R} \frac{i\omega}{(\omega^2-\frac{1}{2}k^2)+\frac{i\omega}{3}k^2} e^{-i\omega(t+r)+i\vec{k}\cdot\vec{x}}, \tag{B.35}$$

$$h_{tr}(r,t,\vec{x}) \sim \int d\omega d^2\vec{k} \frac{-\frac{3}{2}i\omega}{(\omega^2-\frac{1}{2}k^2)+\frac{i\omega}{3}k^2} e^{-i\omega(t+r)+i\vec{k}\cdot\vec{x}}. \tag{B.36}$$

Using this, we can estimate the late time tail of the sound mode OTOC, given that the inner product contains a term

$$\int \sqrt{\gamma} dv n^v (h^*_{1xx}(v)\partial_v h_{2xx}(v) - h_{2xx}(v)\partial_v h^*_{1xx}(v)), \tag{B.37}$$

where $h_{2xx}(v) = h_{1xx}(v-h)$ is a solution to the linearized Einstein equation on the shockwave background. The calculation is slightly different from the previous one due to the linear in k term

in the sound pole dispersion. In the end, it becomes the following integral

$$
\begin{aligned}
&(h_1, h_2) \\
&\propto \int d^d\vec{x} \int \frac{d^d\vec{k}}{(2\pi)^d} \frac{d^d\vec{k'}}{(2\pi)^d} \int \frac{dp}{2\pi} p p^{Dk^2-1} \cos[v_s k \ln(p)] p^{Dk'^2-1} \cos[v_s k' Ln(p)] G(p) e^{-\frac{\Delta}{N} e^{t_{12}-\mu|\vec{x}-\vec{x}_{12}|}} e^{-i(\vec{k}-\vec{k'})\cdot\vec{x}},
\end{aligned}
\tag{B.38}
$$

where we have introduced an unknown cutoff factor $G(p)$ to regulate the large momentum behavior. Similar to the method in Section 3.4, one defines $s = -\ln(p)$ and performs the integral over the transverse momentum first. Then the inner product can be written as

$$
\begin{aligned}
&\int d^d\vec{x} \int_0^{+\infty} ds \frac{1}{s^{d+1}} (e^{-\frac{(|\vec{x}|-v_s s)^2}{4Ds}} + e^{-\frac{(|\vec{x}|+v_s s)^2}{4Ds}})^2 e^{-i\frac{\Delta}{N} e^{t_{12}-s-\frac{|\vec{x}-\vec{x}_{12}|}{v_B}}} G(s), \\
\sim &\int d\Omega_d \int_0^{+\infty} ds \frac{1}{s^{\frac{d}{2}+1}} e^{-i\frac{\Delta}{N} e^{t_{12}-s-\frac{|v_s s\hat{n}-\vec{x}_{12}|}{v_B}}} G(s).
\end{aligned}
\tag{B.39}
$$

In the final, we performed the integral over $|\vec{x}|$ assuming that it receives its dominant contribution around $|\vec{x}| \sim v_s s$. The factor $G(s)$ regulates small s region. When t_{12} is large, the integral in s becomes significant only when $s > t_{12}$. So we conclude that the late time OTOC has a power law tail.

It's also interesting to discuss the early time regime, where we can expand the integrand in $\frac{1}{N}$, and obtain

$$
\text{OTOC} \sim \int d\Omega_d \int_0^{+\infty} ds \frac{1}{s^{\frac{d}{2}+1}} G(s) \left(1 - \frac{i\Delta}{N} e^{t_{12}-s-\frac{|v_s s\hat{n}-\vec{x}_{12}|}{v_B}} + \cdots\right) \tag{B.40}
$$

We need to analyze the integral over s. Denote the angle between $\hat{n}$ and $\vec{x}_{12}$ by θ. The exponential reaches its maximum at $s_* = \frac{x_{12}}{v_s}(\cos\theta - \sin\theta \tan\varphi)$, with $\varphi = \arcsin\frac{v_B}{v_s}$. So for $v_B > v_s$, or

$\cos\theta < \frac{v_B}{v_s}$, then $s_* = 0$, and we conclude that the information still scrambles at the speed v_B. On the other hand, for $\cos\theta > \frac{v_B}{v_s}$, we expand $s = s_* + l$ and approximate the exponential factor as

$$e^{t_{12}-s-\frac{|v_s s\hat{n}-\vec{x}_{12}|}{v_B}} \approx e^{t_{12}-\frac{x_{12}}{v_s}(\cos\theta+\sin\theta\cot\varphi)} e^{-\frac{v_s\cos^3\varphi}{2x_{12}\sin\theta\sin\varphi}l^2}. \tag{B.41}$$

After integrating over l, the $O(\frac{1}{N})$ term becomes [1]

$$\sim \frac{1}{N}(\frac{x_{12}}{v_s})^{-\frac{d+1}{2}} e^{t_{12}-\frac{x_{12}}{v_s}(\cos\theta+\sin\theta\cot\varphi)}. \tag{B.42}$$

From this expression, we learn that when $v_s > v_B$, a portion of the information, corresponding to solid angle θ_0, can scramble at a speed $\frac{v_s}{\cos\theta_0+\sin\theta_0\cot\varphi} > v_B$, with $\cos\theta_0 < \sin\varphi = \frac{v_B}{v_s}$. For θ_0 sufficiently small, the information spreading speed is close to speed of sound.

B.4 Non-linear corrections

In this section, we consider the leading non-linear correction to the photon's propogator. The correction is from graviton dressing, as shown in Fig. B.1. Expanding the Einstein-Maxwell action, one obtains a gauge-gauge-graviton vertex of the following form,

$$\frac{1}{g_c^2}\int d^{d+2}x A_\mu \partial_\nu [\sqrt{-g}(F^{\rho\nu}h^\mu_\rho + F^{\mu\rho}h^\nu_\rho - \frac{1}{2}F^{\mu\nu}h^\rho_\rho)]. \tag{B.43}$$

Following [155], we consider the gravitational dressing in the near horizon region, and only include the interaction between the photon and the diffusive mode of the graviton. In other

[1] Since s_* can be very large, this result is not sensitive to the regulator $G(s)$. However, the constant term does depend on it, which will change the $O(\frac{1}{N})$ term's prefactor after normalization.

words, we only keep h_{tx} and h_{rx} non-zero. Many terms in Eq. (B.43) are suppressed by small ω and k, so the leading order term involving A_t is

$$\frac{1}{g_c^2}\int d^{d+2}x\sqrt{-g}g^{tt}g^{rr}\partial_r A_t F_{rx}h_t^x. \tag{B.44}$$

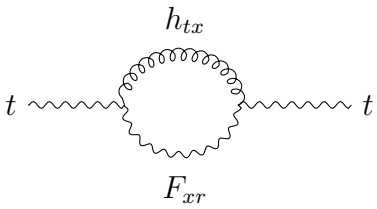

Figure B.1: gravitational dressing to photon's wave function

To be consistent with the main text, we still use the gauge $A_x = 0$. To find the bulk correlators, we have to solve the Maxwell-Einstein equation, Eq. (3.12), with a source term such that

$$\begin{aligned} A_t &= \int d^{d+2}\vec{x}\, G_{tt}(\vec{r}-\vec{r}')J^t(\vec{r}'), \\ A_r &= \int d^{d+2}\vec{x}\, G_{rr}(\vec{r}-\vec{r}')J^r(\vec{r}'), \end{aligned} \tag{B.45}$$

where J^t and J^r are 4-vectors that satisfy

$$\partial_t J^t + \partial_r J^r + \partial_x J^x = 0. \tag{B.46}$$

To obtain G_{tt}, we require $J^r = 0$, and $J^t(r,\omega,k) = \delta(r-r')$. Then $J^x(r,\omega,k) = \frac{\omega}{k}\delta(r-$

r'). One can thenderive the following equation,

$$\partial_r^2 A_t + \partial_r \ln\left(\frac{1}{R^{d-2}(\omega^2 - k^2 f)}\right)\partial_r A_t + (\omega^2 - k^2 f)A_t = \frac{(\omega^2 - k^2 f)R^{d-2}}{k^2}\delta(r - r'). \quad \text{(B.47)}$$

Applying the in-falling condition at the horizon and a Neumann boundary condition on the boundary, we obtain an approximate solution by expanding in small ω and k. Moreover, if we focus on the near horizon region, the solution takes a simple form,

$$\begin{aligned} G_{tt}(\omega, k, r, r') &\sim \frac{\frac{\omega^2}{k^2}}{i\omega - Dk^2}(1 + O(\omega r)), \\ G_{tx,tx}(\omega, k, r, r') &\sim \frac{\frac{\omega^2}{k^2}}{i\omega - D_T k^2}(1 + O(\omega r)). \end{aligned} \quad \text{(B.48)}$$

Similarly, to solve for G_{rr}, we use a source such that $J_t = 0$, and $J_r(r, \omega, k) = \delta(r - r')$. So we have $J^x(r, \omega, k) = \frac{1}{-ik}\delta(r - r')$, as well as the equation

$$\partial_r^2 \tilde{A}_r + \partial_r Log(R^{d-2})\partial_r \tilde{A}_r + (\omega^2 - k^2 f)\tilde{A}_r = \frac{\omega^2}{k^2}\delta(r - r'), \quad \text{(B.49)}$$

where $\tilde{A}_r$ contains a contact term and is defined as $\frac{1}{R^{d-2}}A_r + \frac{1}{k^2}\delta(r - r')$. In the near horizon region, one can also find that

$$G_{rr}(r, r', \omega.k) \sim \frac{\frac{\omega^2}{k^2}}{i\omega - Dk^2}(1 + O(\omega r)). \quad \text{(B.50)}$$

To simplify the calculation, we replace ω by its value at the pole and set $\frac{\omega^2}{k^2}$ to Dk^2. Then we evaluate the bubble diagram by summing over imaginary frequencies and continuing to real

frequency in the end,

$$\Sigma_{tt}(i\omega_n \to \omega + i0^+, k) = \frac{1}{N}\int \frac{d^d k'}{(2\pi)^d} k'^2 T \sum_n \mathcal{G}_{rr}(i\omega'_n, k')\mathcal{G}_{xt,xt}(i\omega_n - i\omega'_n, k-k')|_{i\omega_n \to \omega + i0^+}$$
$$\approx \frac{1}{N}\int \frac{d^d k'}{(2\pi)^d}\int \frac{d\omega'}{2\pi} k'^2 [\frac{\Im G_{rr}(\omega', k')}{\omega'} G_{tx,tx}(\omega-\omega', k-k') + G_{rr}(\omega', k')\frac{\Im G_{tx,tx}(\omega-\omega', k-k')}{\omega-\omega'}]$$
$$\sim \frac{c}{N} k^2 \omega [-i\omega + D_m k^2]^{\frac{d}{2}-1}, \tag{B.51}$$

where $D_m = \frac{DD_T}{D+D_T}$ is a mixed diffusion constant. The loop correction creates a branch cut along $-i\omega < -D_m k^2$, as expected by considering the on-shell condition of the two internal states. Then we suppose that the wave function in the near horizon region also receives a correction in the denominator, of the form

$$A_t \sim \frac{\omega}{\omega + iDk^2 - \frac{c}{N}k^4\omega[-i\omega + D_m k^2]^{\frac{d}{2}-1}}. \tag{B.52}$$

The branch cut structure is similar to that considered in [156]. Close to the line $-i\omega < -D_m k^2$, the pole is split into two poles, at $\omega = -iDk^2 \pm \frac{\alpha}{N}|k|^{d+4}$. So the modification to real time functions is sub-leading in $1/|t|$. When going to the real time, we need to add a integral along a contour that circulates the branch cut. This integral is proportional to

$$\int_{D_m k^2}^{+\infty} ds \frac{c\frac{k^4}{N} s(s-D_m k^2)^{\frac{d}{2}-1} e^{-st}}{(s-Dk^2)^2 + c^2\frac{k^8 s^2}{N^2}(s-D_m k^2)^{d-2}}. \tag{B.53}$$

The integrand is like a Lorentzian function, so we can estimate it by multiplying its peak height and width, which is again $e^{-Dk^2 t}(1+O(k^2))$. So we conclude that the loop correction doesn't

change the conclusion in the main text.

Appendix C: Supplementary Material for Chapter 4

C.1 Proof of Theorem 1

In this section, we will prove that the mutual information decays polynomially in t when coupled to a thermal bath of suitably low temperature, as long as the conditions in Theorem 1 are satisfied. We first set up some useful notations for later use.

Let $\mathcal{E}$ be the set of operators that generate the errors. For all operators $E_a \in \mathcal{E}$ satisfying the aKL equation, we can always diagonalize the matrix f_{ab} by a basis transformation inside $\mathcal{E}$, such that $\langle \tilde{i}|E_b^\dagger E_a|\tilde{i}\rangle = f_a\delta_{ab} + O(\frac{1}{N^2})$. The matrix elements here are taken with respect to the d dimensional code words. Then the aKL equation can be written as

$$\langle \tilde{j}|E_b^\dagger E_a|\tilde{i}\rangle = f_a\delta_{ab}\delta_{ij} + \frac{g_{ab}^{ij}}{N^2}, \tag{C.1}$$

where $f_a \geq 0$ is some $O(1)$ number that depends on the error indices.

Now we define two classes of errors according to whether f_a is 0 or not. *The first class of errors*, labeled by E_α and E_β, satisfies $f_\alpha, f_\beta \neq 0$. *The second class of errors*, labeled by E_σ and E_ν, satisfies $f_\sigma = f_\nu = 0$. Note that we will label the errors with Greek indices, α, β for the first class, σ, ν for the second class, when we distinguish their classes. When we do not need to treat them in different classes, we use Latin indices like a, b to label these errors. For the first class

of errors, we can define an orthonormal basis $\{|\mu_\alpha^i\rangle\}$ by acting error operators E_α on the logical states $|\tilde{i}\rangle$ such that

$$E_\alpha|\tilde{i}\rangle = \sqrt{f_\alpha}|\mu_\alpha^i\rangle + \sum_\beta \frac{c_{\alpha\beta}}{2\sqrt{f_\beta}N^2}|\mu_\beta^i\rangle + \sum_\beta \frac{\Delta_{\alpha\beta}^i}{2\sqrt{f_\beta}N^2}|\mu_\beta^i\rangle + \sum_{\beta,j\neq i} \frac{h_{\alpha\beta}^{ij}}{2\sqrt{f_\beta}N^2}|\mu_\beta^j\rangle. \tag{C.2}$$

The states $|\mu_\alpha^i\rangle$'s can be read off from the $O(1)$ term in above equations. All the other coefficients can be read off from the aKL equations as,

$$\begin{aligned} c_{\alpha\beta} &= \frac{1}{d}\sum_{i=1}^{d} g_{\alpha\beta}^{ii} \\ \Delta_{\alpha\beta}^i &= g_{\alpha\beta}^{ii} - c_{\alpha\beta} \\ h_{\alpha\beta}^{ij} &= \begin{cases} g_{\alpha\beta}^{ij}, & \text{if } i \neq j \\ 0, & \text{if } i = j \end{cases}. \end{aligned} \tag{C.3}$$

One can see that there is a clear separation between the phase errors that are captured by $\Delta_{\alpha\beta}^i$, and the bit flip errors that are captured by $h_{\alpha\beta}^{ij}$. So far we have discussed the first class of errors with non-zero $O(1)$ norm $\sqrt{f_\alpha}$. However, the second class of error operators have vanishing $O(1)$ norm and let us label them by E_σ and E_ν. so $\langle E_\sigma^\dagger E_\sigma\rangle = O(\frac{1}{N^2})$. Generally, the aKL equations for these operators take the form of

$$\langle\tilde{j}|E_\sigma^\dagger E_\nu|\tilde{i}\rangle = \frac{g_{\sigma\nu}^{ij}}{N^2} + O(\frac{1}{N^3}). \tag{C.4}$$

These operators in the second class of errors map the logical states to states with norms propor-

tional to $O(\frac{1}{N})$. More generally, they are operators that satisfy the following equation:

$$E_\sigma|\tilde{i}\rangle = \sum_\nu \frac{s^i_{\sigma\nu}}{N}|\mu^i_\nu\rangle, \tag{C.5}$$

for some $O(1)$ coefficients s's. The states $|\mu^i_\nu\rangle$'s are another set of normalized basis, orthogonal to the states $|\mu^i_\alpha\rangle$'s up to $O(\frac{1}{N})$ overlap. The errors that satisfy

$$\langle\tilde{i}|E_\sigma|\tilde{j}\rangle = \frac{e^{ij}_\sigma}{N} + O(\frac{1}{N^3}), \tag{C.6}$$

also belong to the second class of errors, since they are consistent with Eq. (C.5).

For some calculations, we do not need to differentiate the two types of errors. In that case, we use Latin indices and simply label all of them by E_a. Let us denote the KL matrix element by $\langle\tilde{j}|E^\dagger_b E_a|\tilde{i}\rangle = G^{ij}_{ab}$; one can write down a general relation

$$E_a|\tilde{i}\rangle = \sum_A u^i_{aA}|\mu_A\rangle, \tag{C.7}$$

where $\{|\mu_A\rangle\}$ is a set of orthonormal states, and u^i_{aA} are coefficients that satisfy

$$\sum_A u^i_{aA}u^j_{bA} = G^{ij}_{ab}. \tag{C.8}$$

C.1.1 Early time approximation

Recall that we model our open system dynamics as a Markovian process. At early time, we approximate the evolution by only including the first order perturbation of errors.[1]

$$\rho(t) \approx \rho_0 - \sum_a \frac{\lambda_a(\epsilon_a)t}{2}\{E_a^\dagger E_a, \rho_0\} + \sum_a \lambda_a(\epsilon_a) t E_a \rho_0 E_a^\dagger + \cdots , \tag{C.9}$$

where the sum over E_a includes both the first and second class of errors, and ρ_0 is the maximally entangled state between reference R and system S at $t = 0$,

$$\rho_0 = \frac{1}{d}\sum_{ij} |\tilde{i}i\rangle_{RS}\langle\tilde{j}j|. \tag{C.10}$$

We proceed to compute the mutual information $I(R:S) = S(\rho^R) + S(\rho^S) - S(\rho)$ at early times. Since the non-trivial unitary dynamics that induces the above Markovian evolution only occurs between the system and the bath, the entropy of R should remain invariant over time, *i.e.* $S(\rho^R) = \ln d$. Therefore, it suffices to calculate the entropies of S and the RS joint system.

Generally, the density matrix is block-diagonal. We can generate each block matrix using the operators E_a, with $a \in B_n$, such that for any $a, b \in B_n$, $G_{ab} \neq 0$. Here B_n is an index set that captures the error operators used to generate a particular block matrix. Sometimes we will also refer to this set as a block, since it defines the corresponding block matrix. We write the density

[1] The coupling $\lambda_a(\epsilon_a)$ for each error operator E_a is defined as $\lambda_a\gamma(\epsilon_a)$,, with $\gamma(\epsilon_a)$ defined in Eq.4.22.

matrix associated to the block B_n as,

$$\begin{aligned}\rho_n =& \sum_{a\in B_n} E_a \rho_0 E_a^\dagger \\ =& \frac{1}{d}\sum_{aABij} u_{aA}^i u_{aB}^{j*} |\mu_A\rangle_S\langle\mu_B| \otimes |i\rangle_R\langle j|.\end{aligned} \tag{C.11}$$

The eigenvalues of matrix $\frac{1}{d}\sum_a u_{aA}^i u_{aB}^{j*}$ is the same as that of the matrix $\frac{1}{d}\sum_{iA} u_{aA}^i u_{bA}^{i*} = \frac{1}{d}\sum_i G_{ab}^{ii}$. After tracing out the reference R, the density matrix of system becomes

$$\rho_n^S = \frac{1}{d}\sum_{aiAB} u_{aA}^i u_{aB}^{i*} |\mu_A\rangle_S\langle\mu_B|. \tag{C.12}$$

The eigenvalues of matrix $\frac{1}{d}\sum_{ai} u_{aA}^i u_{aB}^{i*}$ is the same as that of the matrix $\frac{1}{d}\sum_A u_{aA}^i u_{bA}^{j*} = \frac{1}{d}G_{ab}^{ij}$.

Therefore, to evaluate the entropy, we need to calculate the eigenvalues of the matrix $\frac{1}{d}G_{ab}^{ij}$. Generally, inside a block, we have both the first and the second class of errors. Their overlap $G_{\alpha\sigma}$ scales as $\frac{1}{N^2}$ by the aKL condition. However, we can always diagonalize the matrix G, where the diagonal form $\tilde{G}$ has vanishing matrix elements for the overlaps $\tilde{G}_{\alpha\sigma} = 0$ and $\tilde{G}_{\alpha\beta} - G_{\alpha\beta} = O(\frac{1}{N^4}), \tilde{G}_{\sigma\nu} - G_{\sigma\nu} = O(\frac{1}{N^4})$ such that the correction is at subleading order. Therefore, in the following, we can neglect the overlap between the first and the second class of errors, and always treat them as different blocks.

For our following discussion, we use $\rho_n^{(1)}, \rho_n^{(2)}$ to denote the state created purely by the first and the second class of errors, respectively. The entropy for $\rho_n^{(1)}$ is,

$$
\begin{aligned}
S(\rho_n^{(1)}) &= -\operatorname{Tr}(\rho_n^{(1)} \ln \rho_n^{(1)}) \\
&= -\operatorname{Tr}[(f + \frac{c}{N^2}) \ln(f + \frac{c}{N^2})] \\
&= -\operatorname{Tr}(f \ln f) - \frac{1}{N^2} \operatorname{Tr}(c \ln f) - \frac{1}{N^2} \operatorname{Tr}(c) - \frac{1}{2N^4} \operatorname{Tr}(c f^{-1} c) + O(\frac{1}{N^6}).
\end{aligned}
\tag{C.13}
$$

In the second step we used that the eigenvalues of the density matrix are the same as those of the KL overlap matrix $\frac{1}{d}\sum_i G^{ii}$. f is the diagonal matrix $f_\alpha \delta_{\alpha\beta}$ and the matrix elements of c are given by Eq. (C.3). For the reduced density matrix of system S, $\rho_n^S = \operatorname{Tr}_R(\rho_n)$, its entropy is

$$
\begin{aligned}
S(\rho_n^{(1)S}) &= -\operatorname{Tr}[\frac{1}{d}(f \otimes I + \frac{g}{N^2}) \ln(f \otimes I + \frac{g}{N^2})] + \frac{1}{d} \operatorname{Tr}(f \otimes I + \frac{g}{N^2}) \ln d \\
&= \operatorname{Tr}(\rho_n) \ln d - \frac{1}{d} \operatorname{Tr}[(f \otimes I) \ln(f \otimes I)] - \frac{1}{dN^2} \operatorname{Tr}[g \ln(f \otimes I)] - \frac{1}{dN^2} \operatorname{Tr}(g) \\
&\quad - \frac{1}{2dN^4} \operatorname{Tr}[g(f^{-1} \otimes I)g] + O(\frac{1}{N^6}).
\end{aligned}
\tag{C.14}
$$

where f is the matrix with element being $f_{\alpha\beta}$, and I is the $d \times d$ identity matrix. After subtracting $S(\rho_n^{(1)})$ from $S(\rho_n^{(1)S})$, we finally obtain

$$
\begin{aligned}
S(\rho_n^{(1)S}) - S(\rho_n^{(1)}) &= \operatorname{Tr}(\rho_n^{(1)}) \ln d - \frac{1}{2dN^4} \operatorname{Tr}[g(f^{-1} \otimes I)g] + \frac{1}{2N^4} \operatorname{Tr}(c f^{-1} c) + O(\frac{1}{N^6}) \\
&= \operatorname{Tr}(\rho_n^{(1)}) \ln d - \frac{1}{2dN^4} (\sum_i \operatorname{Tr}[\Delta^i f^{-1} \Delta^i] + \sum_{ij} \operatorname{Tr}[h_{ij} f^{-1} h_{ij}^T]) + O(\frac{1}{N^6}),
\end{aligned}
\tag{C.15}
$$

where matrices Δ^i and $h_{ij} := h^{ij}$ are defined in Eq. (C.3). We see that the decay rate of mutual information is suppressed by $\frac{1}{N^4}$. Repeating the same subtractions but for the second class of errors, the difference in entropy is

$$
\begin{aligned}
S(\rho_n^{(2)S}) - S(\rho_n^{(2)}) =& \frac{1}{N^2}[S(\frac{1}{d}g_{\sigma\nu}^{ij}) - S(\frac{1}{d}\sum_i g_{\sigma\nu}^{ii})]|_{\sigma,\nu\in B_n} + O(\frac{1}{N^4}) \\
=& \operatorname{Tr}(\rho_n^{(2)}) \ln d - \frac{1}{N^2}[S(\frac{1}{d}\sum_i g_{\sigma\nu}^{ii}) - \frac{1}{d}S(g_{\sigma\nu}^{ij})]|_{\sigma,\nu\in B_n'} + O(\frac{1}{N^4}),
\end{aligned}
\tag{C.16}
$$

where $S(g_{\sigma\nu}^{ij})$ means that we are calculating entropy of the matrix whose elements are $g_{\sigma i,\nu j}$. On the other hand, in $S(\frac{1}{d}\sum_i g_{\sigma\nu}^{ii})$, we compute the entropy of the matrix with elements proportional to $\frac{1}{d}\sum_i g_{\sigma\nu}^{ii}$. The decay rate is only suppressed in $\frac{1}{N^2}$. The entropy difference in the second term depends on the matrix elements $g_{\sigma\nu}^{ij}$ in a complicated way. Instead of calculating it explicitly, we just provide an upper bound for this expression. Suppose that in each block B_n, the matrix $g_{\sigma\nu}^{ij}$ has a rank of $r(n)$ with its elements bounded by a function $f(n)$, then the second term is bounded by $\frac{r(n)f(n)\log d}{N^2}$.

For $n \geq 1$, define $\alpha_n = \lambda_n t$. The early time density matrix can be written as[2]

$$
\rho(t) = \bigoplus_{n=0}^{\infty}(\alpha_n \rho_n). \tag{C.17}
$$

Applying the relation $\sum_n \alpha_n \operatorname{Tr}(\rho_n) = 1$, one find that the difference of total entropy is

$$
\begin{aligned}
S(\rho^S(t)) - S(\rho(t)) =& \ln d - \sum_{n=1}^{\infty}\frac{\lambda_n t}{N^2}[S(\frac{1}{d}\sum_i g_{\sigma\nu}^{ii}) - \frac{1}{d}S(g_{\sigma\nu}^{ij})]|_{\sigma,\nu\in B_n'} \\
& - \sum_{n=1}^{\infty}\frac{\lambda_n t}{2dN^4}\sum_{\alpha\beta\in B_n}[\sum_i \Delta_{\alpha\beta}^{i2} + \sum_{i\neq j}(h_{\alpha\beta}^{ij})^2] + O(\frac{1}{N^6}).
\end{aligned}
\tag{C.18}
$$

For early time, i.e., $\lambda_n t \ll 1$, the dominant contribution to information decay is from the

[2]To keep the notation tractable, we absorbed any a-dependence of the coupling λ_a into the operators E_a such that the couplings λ only retain the n dependence. To be more precise, one can redefine the couplings and errors such that $\lambda(\epsilon_a)$ only depends on the energy of each error operator ϵ_a. Because $\epsilon_a = \epsilon_n$ for all $a \in B_n$, we can rewrite $\lambda(\epsilon_a)$ as λ_n.

second class of errors.

C.1.2 Finite time

In this section, we look at the finite time behavior of density matrix up to $O(\frac{1}{N^2})$ contributions. We will see that, although the early-time effect of the first class of errors is sub-dominant, it becomes more relevant at later times since it grows quadratically in time. Recall that the overlap between the different classes of errors are suppressed, we can split the Lindbladian operator into two parts associated with the first class and the second class of errors,

$$\rho(t) = e^{\mathcal{L}t}\rho(0) = e^{\mathcal{L}^{(1)}t+\mathcal{L}^{(2)}t}\rho(0) + O(\frac{1}{N^4}). \tag{C.19}$$

From Eq. (C.5), the second class of Lindblad operator creates a term of $O(\frac{1}{N^2})$ each time it acts on the density matrix. Therefore, the state can be approximated by

$$\rho(t) = \rho^{(1)}(t) + t\mathcal{L}^{(2)}[\rho^{(1)}(t)] + O(\frac{1}{N^4}), \tag{C.20}$$

with $\rho^{(1)}(t) = e^{\mathcal{L}^{(1)}t}\rho(0)$ being the state evolved under the first class of errors. Here we only keep the commuting contributions from $\mathcal{L}^{(1)}$ and $\mathcal{L}^{(2)}$, since their commutator only contributes at higher orders of $\frac{1}{N}$.

To simplify the discussion, we will look at an approximation, which we claim is sufficient to capture the behavior of information decay in our discussion. Let us first look at the case with only one type of error E in the first class,

$$\dot{\rho}(t) = \lambda E\rho E^\dagger + \lambda E^\dagger \rho E - \frac{\lambda}{2}\{E^\dagger E, \rho\} - \frac{\lambda}{2}\{EE^\dagger, \rho\}. \tag{C.21}$$

For low energy operators E, we can make the approximation where the coupling of E and its conjugate has the same strength λ, which in general should be different due to the thermal factor. In this large N model, we observe that $E^\dagger E$ acts trivially in the leading order,

$$\begin{aligned} E^\dagger E E^p \rho &= (p+1)E^p\rho + O(\frac{1}{N^2}) \\ E E^\dagger E^p \rho &= pE^p\rho + O(\frac{1}{N^2}). \end{aligned} \tag{C.22}$$

where p is some integer power.

The order $\frac{1}{N^2}$ correctons can be captured by an operator Z, which acts on the code state in the following way:

$$Z|\mu_\alpha^i\rangle = (1 + \frac{g^{ii}}{2N^2})|\mu_\alpha^i\rangle. \tag{C.23}$$

It is not hard to find the solution up to order $\frac{1}{N^2}$,

$$\rho(t) = \sum_{k=0}^{\infty} \frac{(\lambda t)^k}{(1+\lambda Z t)^{k+1}} \frac{E^k \rho_0 E^{\dagger k}}{k!} + O(\frac{1}{N^4}). \tag{C.24}$$

One might generalize this equation to include all the first class error operators E_α. We denote the density matrix dressed by the first class of errors as $\rho^{(1)}(t)$, which is

$$\rho^{(1)}(t) = \sum_{\{k_\alpha\}} w(\{k_\alpha\}) \prod_\alpha \frac{E_\alpha^{k_\alpha} \rho(0) E_\alpha^{\dagger k_\alpha}}{k_\alpha!} + O(\frac{1}{N^4}), \tag{C.25}$$

where the weight function can be upper bounded by,

$$
\begin{aligned}
&w(\{k_\alpha\}) = \prod_\alpha w(k_\alpha), \\
&\text{where } w(k_\alpha) \leq \frac{(\lambda_\alpha t)^{k_\alpha}}{(1+\lambda_\alpha Z_\alpha t)^{k_\alpha+1}}, \quad \text{for } k_\alpha \geq 1.
\end{aligned}
\tag{C.26}
$$

The bound is only saturated if we could neglect the difference between the coupling constants of E_α and $E_\alpha^\dagger$. While said difference is negligible for low energy errors, it is not for high energy ones. In fact, the coupling constant goes down exponentially with the energy ϵ_α of the operator E_α,

$$
\lambda_\alpha \propto \gamma(\epsilon_\alpha) \sim e^{-\beta\epsilon_\alpha}, \tag{C.27}
$$

for $\epsilon_\alpha > 0$. However, the coupling constant λ'_α for $E_\alpha^\dagger$ barely depends on energy, since $\gamma(\epsilon_\alpha) \sim 1$, for $\epsilon_\alpha < 0$. We only bound the weight function for $k_\alpha \geq 1$, since the $k_\alpha = 0$ component does not contribute to the mutual information decay, and it is determined by the constraint $\sum_{k_\alpha=0}^{\infty} w(k_\alpha) = 1$ of the weight function.

Given the density matrix, we calculate the entropy difference by the equation,

$$
S(\rho^{(1)S}) - S(\rho^{(1)}) = \mathrm{Tr}(\rho^{(1)}) \ln 2 - \frac{1}{2dN^4} \sum_{\mathcal{AB}} w_{\mathcal{A}} (\sum_i (\Delta^i_{\mathcal{AB}})^2 + \sum_{i\neq j} (h^{ij}_{\mathcal{AB}})^2) + O(\frac{1}{N^6}), \tag{C.28}
$$

where we use $\mathcal{A}$ and $\mathcal{B}$ as a shorthand notation for the product of first class operators, so that $E_{\mathcal{A}} := \prod_{\alpha_i \in \mathcal{A}} E_{\alpha_i}$. $w_{\mathcal{A}}$ is a number obtained by setting all the Z_α's to identity in Eq. (C.26). The d-function and h-function scale linearly with k_n, and are proportional to some power q of

n_α, with $n_\alpha = \frac{\epsilon_\alpha}{\Omega}$ being the energy level of E_α, where Ω has dimension of energy. For example, $\Omega = \omega$ for our oscillator model. Thus we can upper bound the information decay rate by (up to $\frac{1}{N^4}$),

$$\begin{aligned} K^{(1)}(t) &= \frac{1}{N^4} \sum_{k_\alpha=1}^{\infty} w(\{k_\alpha\})(\sum_\alpha n_\alpha^q k_\alpha)^2 \\ &\leq \frac{1}{N^4}[2(\sum_\alpha \lambda_\alpha n_\alpha^q t)^2 + \sum_\alpha \lambda_\alpha n_\alpha^{2q} t]. \end{aligned} \tag{C.29}$$

Note that the coefficient λ_α scales as $e^{-\beta\epsilon_\alpha}$, and the density of errors with energy ϵ is bounded by $e^{\mu\epsilon}$ by our sparsity condition. By the same argument we have for Eq.(4.58) in Section 4.4.2, one can show that the quantity inside the square bracket does not scale as N as long as $T < \frac{1}{\mu}$.

The decay rate due to the first class of errors is suppressed by N^4 and grows quadratically with time for $\lambda t \gg 1$. Similar arguments also apply for higher orders of $\frac{1}{N^2}$. In general, the decay rate at order $\frac{1}{N^{2m}}$ is proportional to Δ^m and h^m (defined in Eq. (C.3)) of the corresponding error operators, which scales as k^m for the error operator E_α^k. Therefore, the general decay rate takes the form of $\frac{t^m}{N^{2m}}$ at each order with $m \geq 2$.

The second class of errors of the form E_ν^k is suppressed by $\frac{t^k}{N^{2k}}$ in the Lindblad equation, where the leading order term is linear in t,

$$\begin{aligned} \rho^{(2)}(t) &:= t\mathcal{L}^{(2)}[\rho^{(1)}(t)] \\ &= \sum_\nu \lambda_\nu t[E_\nu \rho^{(1)}(t) E_\nu^\dagger - \frac{1}{2}\{\rho^{(1)}(t), E_\nu^\dagger E_\nu\}]. \end{aligned} \tag{C.30}$$

Recall that $\rho^{(1)}(t)$ is the density matrix induced by the first class of errors, explicitly given by Eq. (C.25). For the sake of clarity, let us rewrite $\rho^{(1)}(t)$ as

$$\rho^{(1)}(t) = \sum_{\mathcal{A}} w_{\mathcal{A}}(t) E_{\mathcal{A}} \rho_0 E_{\mathcal{A}}^\dagger. \tag{C.31}$$

Like our discussion in Appendix C.1.1, we convert the entropy of the state to the entropy of the matrix $g^{ij}_{\sigma\mathcal{A},\nu\mathcal{B}}$, which can be read off from

$$\langle \tilde{j}| E_{\mathcal{B}}^\dagger E_\nu^\dagger E_\sigma E_{\mathcal{A}} |\tilde{i}\rangle = \frac{g^{ij}_{\mathcal{A}\sigma,\mathcal{B}\nu}}{N^2} + O(\frac{1}{N^4}). \tag{C.32}$$

Being the product of a second class error and a first class error, this composite operator belongs to the second class of errors, but it has $O(\frac{1}{N})$ overlap with some operators in the first class,

$$\langle \tilde{j}| E_{\mathcal{B}}^\dagger E_\sigma E_{\mathcal{A}} |\tilde{i}\rangle = \frac{\delta_{ij} g_{\sigma\mathcal{A},\mathcal{B}}}{N} + O(\frac{1}{N^3}). \tag{C.33}$$

Due to the factorization property, $\langle \tilde{j}| E_{\mathcal{B}}^\dagger E_\nu^\dagger E_\sigma E_{\mathcal{A}} |\tilde{i}\rangle = \langle \tilde{j}| E_\nu^\dagger E_\sigma |\tilde{i}\rangle \langle 0| E_{\mathcal{B}}^\dagger E_{\mathcal{A}} |0\rangle + \langle \tilde{j}|\tilde{i}\rangle \langle 0| E_{\mathcal{B}}^\dagger E_\nu^\dagger E_\sigma E_{\mathcal{A}} |0\rangle$, the matrix element can be written as sum of two terms,

$$g^{ij}_{\mathcal{A}\sigma,\mathcal{B}\nu} = g^{ij}_{\sigma\nu} f_{\mathcal{A}\mathcal{B}} + \delta^{ij} g_{\sigma\mathcal{A},\nu\mathcal{B}}. \tag{C.34}$$

where $f_{\mathcal{A}\mathcal{B}} := \langle 0| E_{\mathcal{B}}^\dagger E_{\mathcal{A}} |0\rangle$, and $|0\rangle$ is the vacuum state of our system. The matrix $g^{ij}_{\sigma\nu}$ is identical to the one in Eq. (C.4). $g_{\sigma\mathcal{A},\nu\mathcal{B}}$ is positive definite where each element is equal to the four point function $\langle 0| E_{\mathcal{B}}^\dagger E_\nu^\dagger E_\sigma E_{\mathcal{A}} |0\rangle$, modulo the $\frac{1}{N^2}$ factor. The overlap between the composite operators and some first class operators (Eq. (C.33)) can be removed by a basis transformation, which also

cancels the second term in Eq. (C.34). Therefore, similar to Eq. (C.16), we conclude that the entropy difference is

$$\begin{aligned} S(\rho^{(2)S}(t)) - S(\rho^{(2)}(t)) =& \frac{1}{N^2}[S(\frac{1}{d}g^{ij}_{\sigma\nu}(t)f_{\mathcal{AB}}(t)) - S(\frac{1}{d}\sum_i g^{ii}_{\sigma\nu}(t)f_{\mathcal{AB}}(t))] \\ =& \frac{\mathrm{Tr}(f_{\mathcal{AB}}(t))}{N^2}[S(\frac{1}{d}g^{ij}_{\sigma\nu}(t)) - S(\frac{1}{d}\sum_i g^{ii}_{\sigma\nu}(t))] \\ =& \sum_n \frac{\lambda_n t}{N^2}[S(\frac{1}{d}g^{ij}_{\sigma\nu}) - S(\frac{1}{d}\sum_i g^{ii}_{\sigma\nu})]|_{\sigma,\nu\in B'_n}, \end{aligned} \tag{C.35}$$

where $S(\frac{1}{d}g^{ij}_{\sigma\nu}(t)f_{\mathcal{AB}}(t))$ denotes the entropy of the matrix whose element is $\frac{1}{d}g_{\sigma\mathcal{A}i,\nu\mathcal{B}j}(t) = \frac{1}{d}g^{ij}_{\sigma\nu}(t)f_{\mathcal{AB}}(t)$. We have absorbed the factor $\lambda_\nu t$ into the matrix $g^{ij}_{\sigma\nu}(t) := \sqrt{\lambda_\nu\lambda_\sigma}tg^{ij}_{\sigma\nu}$, and the weight function $w_{\mathcal{A}}(t)$ into the function $f_{\mathcal{AB}}(t) := \sqrt{w_{\mathcal{A}}(t)w_{\mathcal{B}}(t)}f_{\mathcal{AB}}$. By definition, $\mathrm{Tr}(f_{\mathcal{AB}}) = \sum_{\mathcal{A}} w_{\mathcal{A}}(t)\langle 0|E^\dagger_{\mathcal{A}}E_{\mathcal{A}}|0\rangle = \mathrm{Tr}(\rho^{(1)}(t)) + O(\frac{1}{N^2}) = 1 + O(\frac{1}{N^2})$. In the last step, we again utilized the block diagonal form of the matrix $g^{ij}_{\sigma\nu}$ to write the result as a sum of each block's contribution, with blocks being labeled by B'_n, such that the matrix elements are non-zero only for σ and ν in the same block. Note that the entropy difference is the same as in Eq. (C.16). We can bound the decay rate induced by the second class of errors with the following function at leading order of $\frac{\lambda t}{N^2}$,

$$K^{(2)}(t) \leq \sum_n \frac{\lambda_n t}{N^2} f(n)r(n)\log d, \tag{C.36}$$

where $f(n)$ is a upper bound for each matrix element $g^{ij}_{\sigma\nu}$ in the block B_n, and $r(n)$ is the rank of the block.

At higher order, we can continue to expand the second class of Lindbladian operator and one can repeat these calculations following the same procedure. Errors of the form E^m_σ then

induce information decay at $O(\frac{1}{N^{2m}})$, with magnitude proportional to $(\lambda t)^m$.

In summary, we find that both the first class of errors and the second class of errors contribute to the information decay with some rate function $K_m(t) \propto \frac{t^m}{N^{2m}}$ as long as the assumptions of Theorem 1 are satisfied. For $N^2 \gg \lambda t \gg 1$,

$$I(S:R) = 2\ln d - \sum_{m=1}^{\infty} K_m(t). \tag{C.37}$$

C.2 aKL condition for single trace errors

C.2.1 non-local model

In this section, we present the aKL equations for the most general single-trace error operators. Since the logical states (Eq.4.35) are symmetric in $a_1^\dagger$ and $a_2^\dagger$, we only need to consider the single-trace operators involving a_1 and $a_1^\dagger$. In the following, we will only keep track of the terms up to $O(\frac{1}{N^2})$.

Let us define a class of error operators

$$E^P_{n,m} = \frac{:\mathrm{Tr}(P\{a_1^{\dagger n} a_1^m\}):}{N^{\frac{n+m}{2}}}, \tag{C.38}$$

where P denotes a particular permutation of the operators inside the curly brackets. Acting it on the logical states, one obtains,

$$E^P_{n,m}|\tilde{i}\rangle = f|\mu^i\rangle + \frac{g}{N^2}|\mu\rangle + O(\frac{1}{N^4}). \tag{C.39}$$

To extract these coefficients, we calculate the overlap

$$\langle\tilde{i}|E^{P'\dagger}_{n',m'}E^{P}_{n,m}|\tilde{j}\rangle, \tag{C.40}$$

which is essentially a four-point function that factorizes into,

$$\langle\tilde{O}^{\dagger}_{i}E^{P'\dagger}_{n',m'}E^{P}_{n,m}\tilde{O}_{j}\rangle = \langle\tilde{O}_{i}{}^{\dagger}\tilde{O}_{j}\rangle\langle E^{P'\dagger}_{n',m'}E^{P}_{n,m}\rangle + O(\frac{1}{N}). \tag{C.41}$$

This is the only way to factorize into disconnected correlators, because O_i and O_j contain $a_2^\dagger$, while $E^P_{n,m}$'s do not. The two point function $\langle E^{P'\dagger}_{n'm'}E^P_{n,m}\rangle$ vanishes, unless $m, m' = 0$, which is the case that we discussed in the main text. Moreover, the sub-leading term can be $O(\frac{1}{N})$ only if $m' = n' = 0$, hence the only non-trivial four-point function contribution is when $m = n$. In this case, we define $Z^P_n = \frac{:\mathrm{Tr}(P\{a^{\dagger n}a^n\}):}{N^n}$ and find that,

$$\langle\tilde{j}|Z^P_n|\tilde{i}\rangle = \frac{c^P_n}{N} + O(\frac{1}{N^3}), \tag{C.42}$$

for some constant c^P_n, which is non-zero only when $n = 2$. This is consistent with the aKL condition (Eq. (4.18)).

So far, we have discussed the order one and $\frac{1}{N}$ term in Eq. (C.42). All the other error operators can only produce order $\frac{1}{N^2}$ terms when acting on the logical states. This completes the proof of aKL condition.

As a special example, consider the decay mode, $E_{0,2}$, which lower the energy when acting

on the logical states. It also satisfies the aKL condition,

$$\begin{aligned}\langle\tilde{1}|E_{0,2}^{\dagger}E_{0,2}|\tilde{1}\rangle-\langle\tilde{2}|E_{0,2}^{\dagger}E_{0,2}|\tilde{2}\rangle&=\frac{8}{N^2}+O(\frac{1}{N^4})\\ \langle\tilde{2}|E_{0,2}^{\dagger}E_{0,2}|\tilde{1}\rangle&=\frac{4\sqrt{2}}{N^3}+O(\frac{1}{N^5}).\end{aligned}\tag{C.43}$$

So the decay mode belongs to the second class of errors classified in Appendix C.1, and lead to a spontaneous decay of quantum information at zero temperature with a rate proportional to $\frac{1}{N^2}$.

C.2.2 Local model

In this section, we prove the aKL condition for the single-trace errors of the form

$$E_{\{n_i\}}=\frac{:\mathrm{Tr}(P\{a_1^{\dagger n_1}a_2^{\dagger n_2}a_1^{n_3}a_2^{n_4}\}):}{N^{\frac{\sum_{k=1}^{4}n_k}{2}}}\tag{C.44}$$

with logical states defined as

$$\begin{aligned}|\tilde{\uparrow}\rangle&=\frac{\mathrm{Tr}(a_1^{\dagger})}{\sqrt{N}}|0\rangle_{12}\\ |\tilde{\downarrow}\rangle&=\frac{\mathrm{Tr}(a_2^{\dagger})}{\sqrt{N}}|0\rangle_{12}.\end{aligned}\tag{C.45}$$

In the main text, we derived a general formula for the case when $n_3=n_4=0$. Moreover, since the logical states are annihilated by more than two a_1 or a_2, and the error operators are normal ordered, we are left to discuss the case when $n_3+n_4=1$. Without loss of generality, we

will only consider the case with $n_3 = 1,\ n_4 = 0$. Then the relevant overlaps are,

$$\begin{aligned}
&\langle\tilde{\uparrow}|E^{\dagger}_{(n-1,m,0,0)}E_{(n,m,1,0)}|\tilde{\uparrow}\rangle = \frac{n}{N^2} + O(\frac{1}{N^4}) \\
&\langle\tilde{\uparrow}|E^{\dagger}_{(n,0,1,0)}E_{(n,0,1,0)}|\tilde{\uparrow}\rangle = \frac{n}{N^2} + O(\frac{1}{N^4}) \\
&\langle\tilde{\downarrow}|E^{\dagger}_{(n,m,0,0)}E_{(n,m,1,0)}|\tilde{\downarrow}\rangle = \langle\tilde{\downarrow}|E^{\dagger}_{(n,0,1,0)}E_{(n,0,1,0)}|\tilde{\downarrow}\rangle = 0 \\
&\langle\tilde{\downarrow}|E^{\dagger}_{(n,m-1,0,0)}E_{(n,m,1,0)}|\tilde{\uparrow}\rangle = \frac{m}{N^2} + O(\frac{1}{N^4}).
\end{aligned} \tag{C.46}$$

Exceptions of these formulae consist of special cases when $n = 1,\ m = 0$ and $n = 0, m = 1$, where one can derive that,

$$\begin{aligned}
&\langle\tilde{\uparrow}|\frac{\mathrm{Tr}(a_1^{\dagger}a_1)}{N}|\tilde{\uparrow}\rangle = \frac{1}{N},\ \ \langle\tilde{\downarrow}|\frac{\mathrm{Tr}(a_1^{\dagger}a_1)}{N}|\tilde{\downarrow}\rangle = 0 \\
&\langle\tilde{\downarrow}|\frac{\mathrm{Tr}(a_2^{\dagger}a_1)}{N}|\tilde{\uparrow}\rangle = \frac{1}{N}.
\end{aligned} \tag{C.47}$$

These are $O(\frac{1}{N})$ overlap, which are consistnet with Eq. (4.18). So we complete the proof of aKL (4.18) for general single-trace errors in this local model.

C.2.3 Global symmetry

In this section, we prove the aKL condition for the model in Section 4.5. The logical space is spanned by the two states of unit norm

$$\begin{aligned}
|1\rangle &= \frac{\mathrm{Tr}(a^{\dagger L})^2}{N^L\xi(L,L)} \\
|2\rangle &= \frac{\mathrm{Tr}(a^{\dagger L+1})\,\mathrm{Tr}(a^{\dagger L-1})}{N^L\xi(L+1,L-1)},
\end{aligned} \tag{C.48}$$

where the normalization constant are $\xi(L,L) = \sqrt{2}L(1+O(\frac{1}{N^2}))$ and $\xi(L+1,L-1) = \sqrt{L^2-1}(1+O(\frac{1}{N^2}))$. Note that these states are not orthogonal but have overlap

$$\langle 1|2\rangle = \frac{L^2\sqrt{L^2-1}}{\sqrt{2}N^2}. \tag{C.49}$$

To check the aKL condition, we insert the error operators $E_n = \frac{\mathrm{Tr}(a^{\dagger n})}{N^{\frac{n}{2}}\xi(n)}$ with $\xi(n)$ being the normalization constant, and derive the following equations

$$\begin{aligned}
\langle 1|E_m^\dagger E_n|1\rangle - \langle 2|E_m^\dagger E_n|2\rangle &= \delta_{mn}[\frac{2n}{N^2} + O(\frac{1}{N^4})] \\
\langle 1|E_m^\dagger E_n|2\rangle &= \delta_{mn}[\frac{L^2\sqrt{L^2-1}}{\sqrt{2}N^2} + O(\frac{1}{N^4})].
\end{aligned} \tag{C.50}$$

Note that the leading term in the second equation is a consequence of the non-orthogonality between our definition of $|1\rangle$ and $|2\rangle$; it can be easily removed via a change of basis (c.f. equation 4.65). The above equation also holds for $E_n = \frac{\mathrm{Tr}(a^n)}{N^{\frac{n}{2}}\xi(n)}$.

For more general operators $E_{(n,m)} := \frac{\mathrm{Tr}(a^{\dagger n}a^m)}{N^{\frac{m+n}{2}}}$, with $n \neq m$, one can show that

$$\begin{aligned}
\langle 1|E_{n',m'}^\dagger E_{n,m}|1\rangle - \langle 2|E_{n',m'}^\dagger E_{n,m}|2\rangle &= \delta_{n'-m',n-m}[\frac{2}{N^2} + O(\frac{1}{N^4})] \\
\langle 1|E_{n',m'}^\dagger E_{n,m}|2\rangle &= \delta_{n'-m',n-m}[\frac{L^2\sqrt{L^2-1}}{\sqrt{2}N^2} + O(\frac{1}{N^4})],
\end{aligned} \tag{C.51}$$

which indicates the aKL condition holds.

For the special case of $n = m$, the operator also incurs no phase error, because

$$\langle 1|\frac{\mathrm{Tr}(a^{\dagger n}a^n)}{N^n}|1\rangle = \langle 2|\frac{\mathrm{Tr}(a^{\dagger n}a^n)}{N^n}|2\rangle = \frac{2L}{N}. \tag{C.52}$$

We thereby conclude that the aKL conditions hold for all the single trace operators.

C.2.4 Spin model

The approximate Knill-Laflamme condition for the spin model can be calculated using the spin algebra. Recall that we can construct two states that span the code subspace in a way analogous to our definition in the oscillator model,

$$\begin{aligned} |1\rangle &= \frac{\mathrm{Tr}(S^{+L})^2}{N^L \eta(L,L)} \\ |2\rangle &= \frac{\mathrm{Tr}(S^{+L-1})\,\mathrm{Tr}(S^{+L+1})}{N^L \eta(L+1,L-1)}, \end{aligned} \tag{C.53}$$

where $\eta(L, L')$ is the normalization constant. They have the same leading order behavior as $\xi(L, L')$ in the harmonic oscillator model, but have different forms in sub-leading terms. The overlap of these two states is

$$\langle 1|2\rangle = \frac{f(L)L\sqrt{L^2-1}}{\sqrt{2}N^2}, \tag{C.54}$$

where $f(L)$ is some complicated function of L. Again, we insert error operators of the form $E_n = \frac{\mathrm{Tr}(S^{\pm n})}{N^{\frac{n}{2}}\eta(n)}$ and $E_{n,m} = \frac{\mathrm{Tr}(S^{+n}S^{-m})}{N^{\frac{m+n}{2}}}$ into the correlator, and derive the aKL equations for the spin model,

$$\begin{aligned} &\langle 1|E_m^\dagger E_n|1\rangle - \langle 2|E_m^\dagger E_n|2\rangle = \delta_{mn}[\frac{2n}{N^2} + O(\frac{1}{N^4})] \\ &\langle 1|E_{n',m'}^\dagger E_{n,m}|1\rangle - \langle 2|E_{n',m'}^\dagger E_{n,m}|2\rangle = \delta_{n'-m',n-m}[\frac{2}{N^2} + O(\frac{1}{N^4})]. \end{aligned} \tag{C.55}$$

Again, the bit flip error only appears at $O(\frac{1}{N^4})$

$$\langle 1|E_m^\dagger E_n|2\rangle = \delta_{mn}[\frac{f(L)L\sqrt{L^2-1}}{\sqrt{2}N^2} + O(\frac{1}{N^4})], \tag{C.56}$$

where we recall the first term can be removed by choosing an orthonormal basis. This completes our proof for the aKL condition.

C.3 Master equation in Lindblad form

Suppose the coupling between system and thermal reservoir is

$$\begin{aligned} H =& H_S + H_B + V_I \\ V_I =& \sum_a E_a \otimes b_a + h.c., \end{aligned} \tag{C.57}$$

where H_S and H_B are the system and bath Hamiltonian respectively, and b_a's are the bath modes.

In the interaction picture, time evolution is described by

$$\begin{aligned} \dot{\rho}(t) =& -i[V_I(t), \rho(t)] \\ =& -i[V_I(t), \rho_0] - [V_I(t), \int_0^t dt'[V_I(t'), \rho(t')]]. \end{aligned} \tag{C.58}$$

The essential simplification is enabled by the Born-Markov approximation, which allows one to approximate the full density matrix as $\rho(t) \sim \rho_S(t) \otimes \rho_B$ at all times. After tracing out the thermal state, we arrive at,

$$\dot{\rho}_{IS}(t) = \int_0^t dt' \sum_{ab} [E_b(t')\rho_{IS}(t)E_a^\dagger(t) - E_a^\dagger(t)E_b(t')\rho_{IS}(t)] \operatorname{Tr}(\rho_B b_a^\dagger(t)b_b(t')) + h.c.. \tag{C.59}$$

For sufficiently long time t, we can treat the initial time as $-\infty$. We also assume that the bath modes are uncorrelated. Then we define

$$\int_{-\infty}^{t} dt' \operatorname{Tr}(\rho_B b_a^\dagger(t) b_b(t')) e^{i\omega(t-t')} := \frac{\gamma(\omega)}{2}\delta_{ab}. \tag{C.60}$$

For operators $E_a(t)$ with the decomposition,

$$E_a(t) = \sum_k E_a^{(k)} e^{-i\epsilon_a^{(k)} t}, \tag{C.61}$$

Eq (C.59) simplifies as,

$$\dot{\rho}_{IS}(t) = \sum_{a,k} \frac{\gamma(\epsilon_a^{(k)})}{2} [E_a^{(k)} \rho_{IS}(t) E_a^\dagger(t) - E_a^\dagger(t) E_a^{(k)} \rho_{IS}(t)] e^{-i\epsilon_a^{(k)} t} + h.c.. \tag{C.62}$$

For example, consider the error operator $E_{ijkl} = a_j^{\dagger i} a_l^{\dagger k}$ in Section 4.5. It can be decomposed as,

$$\begin{aligned} E_{ijkl}(t) =& \widetilde{a_j^{\dagger i} a_l^{\dagger k}} e^{-2i\mathcal{J}t} + [\frac{\widetilde{(a^{\dagger 2})_l^i}}{N}\delta_j^k + \frac{\widetilde{(a^{\dagger 2})_j^k}}{N}\delta_l^i + \frac{\operatorname{Tr}(a^\dagger)}{N}\tilde{a}_j^{\dagger i}\delta_l^k + \frac{\operatorname{Tr}(a^\dagger)}{N}\tilde{a}_l^{\dagger k}\delta_j^i] e^{-i\mathcal{J}t} \\ &+ \frac{\operatorname{Tr}(a^{\dagger 2})}{N^2}\delta_l^i\delta_j^k + \frac{\operatorname{Tr}(a^\dagger)^2}{N^2}\delta_j^i\delta_l^k, \end{aligned} \tag{C.63}$$

where the operator under the tilde vanishes when contracting with the kronecker delta, e.g. $a_j^{\dagger i}\delta_i^j = 0$. Consequently, the tensor coefficients are almost orthogonal to each other, *i.e.*,

$$\sum_{ijkl} E_{ijkl}^{\dagger(m)} E_{ijkl}^{(n)} \propto \delta^{mn} + O(\frac{1}{N}), \tag{C.64}$$

where the $O(\frac{1}{N})$ term denotes operators that has $O(\frac{1}{N})$ expectation value with respect to any low

energy state.

More generally, a tensor product of individual creation and annihilation operators can always be decomposed into different components obtained by index contractions, which are orthogonal to each other up to $O(\frac{1}{N})$, in the sense of Eq. (C.64). As a result, the Lindbladian operator can always be written as a diagonal sum of components that correspond to different contractions,

$$\sum_m \gamma(\epsilon^{(m)}) \sum_a E_a^{(m)} \rho E_a^{\dagger(m)} = \sum_{ma} \gamma(\epsilon^{(m)}) E_a^{(m)} \rho E_a^{\dagger(m)}. \tag{C.65}$$

C.4 Expectation value of the Casimir

In this section, we evaluate the expectation value of the penalty Hamiltonian H_G (in Eq. (4.59)) for a thermal state ρ_T at temperature $T < \frac{\mathcal{J}}{2 \log N}$,

$$\mathrm{Tr}(\rho_T H_G) = \sum_{m=0}^{\infty} d_m m \mathcal{J} e^{-\frac{m(\mathcal{J}+\omega)}{T}}, \tag{C.66}$$

where m is the highest weight of a particular representation, with degeneracy d_m and energy $m\mathcal{J}$. Examples of non-singlet states are the N^2 number of $a_j^{\dagger i}|0\rangle$'s in the adjoint representation with energy $\mathcal{J}$, and the N^4 number of $a_j^{\dagger i} a_l^{\dagger k}|0\rangle$'s in the tensor product representation with energy $2\mathcal{J}$.

In the oscillator model, we expect d_m to scale as $d_m \sim N^{2m}$. This factor cancels with the factor $e^{\frac{-m\mathcal{J}}{T}}$, since $\mathcal{J} > 2T \log N$. Therefore, we estimate the energy expectation value to be

$$\mathrm{Tr}(\rho_T H_G) < \sum_m m \mathcal{J} e^{\frac{-m\omega}{T}}. \tag{C.67}$$

This is an $O(1)$ number times the energy scale $\mathcal{J}$. So we conclude that, for a thermal state

with temperature $T < \frac{\mathcal{J}}{2 \log N}$, the energy expectation value of H_G per oscillator is $O(1)$ times $\frac{\mathcal{J}}{N^2}$.

Bibliography

[1] Xie Chen, Zheng-Cheng Gu, and Xiao-Gang Wen. Local unitary transformation, long-range quantum entanglement, wave function renormalization, and topological order. *Phys. Rev. B*, 82:155138, Oct 2010.

[2] Michael Levin and Xiao-Gang Wen. Detecting topological order in a ground state wave function. *Phys. Rev. Lett.*, 96:110405, Mar 2006.

[3] Ground state entanglement and geometric entropy in the kitaev model. *Physics Letters A*, 337(1):22–28, 2005.

[4] Alexei Kitaev and John Preskill. Topological Entanglement Entropy. *Phys. Rev. Lett.*, 96(11):110404, March 2006.

[5] John Preskill. Quantum computing and the entanglement frontier - rapporteur talk at the 25th solvay conference. 03 2012.

[6] Brian Swingle. Entanglement renormalization and holography. *Phys. Rev. D*, 86:065007, Sep 2012.

[7] Ahmed Almheiri and Henry W. Lin. The entanglement wedge of unknown couplings. *JHEP*, 08:062, 2022.

[8] Ahmed Almheiri, Netta Engelhardt, Donald Marolf, and Henry Maxfield. The entropy of bulk quantum fields and the entanglement wedge of an evaporating black hole. *JHEP*, 12:063, 2019.

[9] Nima Lashkari, Michael B. McDermott, and Mark Van Raamsdonk. Gravitational dynamics from entanglement 'thermodynamics'. *JHEP*, 04:195, 2014.

[10] Thomas Faulkner, Monica Guica, Thomas Hartman, Robert Myers, and Mark Raamsdonk. Gravitation from entanglement in holographic cfts. *Journal of High Energy Physics*, 2014, 12 2013.

[11] Ted Jacobson. Entanglement equilibrium and the einstein equation. *Phys. Rev. Lett.*, 116:201101, May 2016.

[12] Adam R. Brown and Leonard Susskind. Second law of quantum complexity. *Phys. Rev. D*, 97:086015, Apr 2018.

[13] Winton Brown and Omar Fawzi. Scrambling speed of random quantum circuits. 10 2012.

[14] Brian Swingle. Unscrambling the physics of out-of-time-order correlators. *Nature Physics*, 14, 10 2018.

[15] Pasquale Calabrese and John Cardy. Evolution of entanglement entropy in one-dimensional systems. *Journal of Statistical Mechanics: Theory and Experiment*, 2005(04):P04010, apr 2005.

[16] Hong Liu and S. Josephine Suh. Entanglement growth during thermalization in holographic systems. *Phys. Rev. D*, 89:066012, Mar 2014.

[17] Cheryne Jonay, David A Huse, and Adam Nahum. Coarse-grained dynamics of operator and state entanglement.

[18] Pavan Hosur, Xiao-Liang Qi, Daniel A. Roberts, and Beni Yoshida. Chaos in quantum channels. *JHEP*, 2016(2):4, feb 2016.

[19] Patrick Hayden and John Preskill. Black holes as mirrors: quantum information in random subsystems. *JHEP*, 2007(9):120, sep 2007.

[20] Yasuhiro Sekino and Leonard Susskind. Fast scramblers. *JHEP*, 2008(10):065, oct 2008.

[21] Nima Lashkari, Douglas Stanford, Matthew Hastings, Tobias Osborne, and Patrick Hayden. Towards the fast scrambling conjecture. *JHEP*, 2013(4):22, apr 2013.

[22] Thomas Hartman and Nima Afkhami-Jeddi. Speed limits for entanglement. 12 2015.

[23] Josiah Couch, Stefan Eccles, Phuc Nguyen, Brian Swingle, and Shenglong Xu. Speed of quantum information spreading in chaotic systems. *Phys. Rev. B*, 102:045114, Jul 2020.

[24] Marcos Rigol, Vanja Dunjko, and Maxim Olshanii. Thermalization and its mechanism for generic isolated quantum systems. *Nature*, 452(7189):854–858, apr 2008.

[25] Marcos Rigol, Vanja Dunjko, Vladimir Yurovsky, and Maxim Olshanii. Relaxation in a completely integrable many-body quantum system: An ab initio study of the dynamics of the highly excited states of 1d lattice hard-core bosons. *Phys. Rev. Lett.*, 98:050405, Feb 2007.

[26] Luca D'Alessio, Yariv Kafri, Anatoli Polkovnikov, and Marcos Rigol. From quantum chaos and eigenstate thermalization to statistical mechanics and thermodynamics. *Advances in Physics*, 65(3):239–362, 2016.

[27] Maksym Serbyn, Zlatko Papic, and Dmitry Abanin. Local conservation laws and the structure of the many-body localized states. *Physical review letters*, 111:127201, 09 2013.

[28] Rahul Nandkishore and David A. Huse. Many-body localization and thermalization in quantum statistical mechanics. *Annual Review of Condensed Matter Physics*, 6(1):15–38, 2015.

[29] S W Hawking. Breakdown of predictability in gravitational collapse. *Phys. Rev., D; (United States)*.

[30] Ahmed Almheiri, Donald Marolf, Joseph Polchinski, Douglas Stanford, and James Sully. An Apologia for Firewalls. *JHEP*, 09:018, 2013.

[31] Ahmed Almheiri, Donald Marolf, Joseph Polchinski, and James Sully. Black Holes: Complementarity or Firewalls? *JHEP*, 02:062, 2013.

[32] Patrick Hayden and Geoffrey Penington. Learning the alpha-bits of black holes. 07 2018.

[33] Jordan Cotler, Nicholas Hunter-Jones, Junyu Liu, and Beni Yoshida. Chaos, Complexity, and Random Matrices. *JHEP*, 11:048, 2017.

[34] K. A. Landsman, C. Figgatt, T. Schuster, N. M. Linke, B. Yoshida, N. Y. Yao, and C. Monroe. Verified Quantum Information Scrambling. *Nature*, 567(7746):61–65, 2019.

[35] AI Larkin and Yu N Ovchinnikov. Quasiclassical method in the theory of superconductivity. *Sov Phys JETP*, 28(6):1200–1205, 1969.

[36] Stephen H. Shenker and Douglas Stanford. Black holes and the butterfly effect. *JHEP*, 2014(3):67, mar 2014.

[37] Juan Maldacena, Stephen H. Shenker, and Douglas Stanford. A bound on chaos. *Journal of High Energy Physics*, 2016(8):106, Aug 2016.

[38] Martin Gärttner, Justin G. Bohnet, Arghavan Safavi-Naini, Michael L. Wall, John J. Bollinger, and Ana Maria Rey. Measuring out-of-time-order correlations and multiple quantum spectra in a trapped-ion quantum magnet. *Nat. Phys.*, 13(8):781–786, aug 2017.

[39] Brian Swingle, Gregory Bentsen, Monika Schleier-Smith, and Patrick Hayden. Measuring the scrambling of quantum information. *Phys. Rev. A*, 94(4):040302, oct 2016.

[40] Elliott H. Lieb and Derek W. Robinson. The Finite Group Velocity of Quantum Spin Systems. *Commun. math. Phys*, 28(3):251–257, 1972.

[41] Daniel A. Roberts and Brian Swingle. Lieb-robinson bound and the butterfly effect in quantum field theories. *Phys. Rev. Lett.*, 117:091602, Aug 2016.

[42] Alexei Kitaev. A simple model of quantum holography, Part 1 and Part 2 (talks at KITP, Santa Barbara).

[43] Daniel Gottesman. An introduction to quantum error correction and fault-tolerant quantum computation. 05 2009.

[44] Soonwon Choi, Yimu Bao, Xiao-Liang Qi, and Ehud Altman. Quantum error correction in scrambling dynamics and measurement-induced phase transition. *Physical Review Letters*, 125, 07 2020.

[45] Emanuel Knill, Raymond Laflamme, and Lorenza Viola. Theory of Quantum Error Correction for General Noise. *Phys. Rev. Lett.*, 84(11):2525–2528, March 2000.

[46] Daniel Gottesman. Class of quantum error-correcting codes saturating the quantum hamming bound. *Phys. Rev. A*, 54:1862–1868, Sep 1996.

[47] Victor V. Albert. Bosonic coding: introduction and use cases. 11 2022.

[48] Daniel Gottesman, Alexei Kitaev, and John Preskill. Encoding a qubit in an oscillator. *Physical Review A*, 64(1):012310, July 2001.

[49] Zaki Leghtas, Gerhard Kirchmair, Brian Vlastakis, Robert J. Schoelkopf, Michel H. Devoret, and Mazyar Mirrahimi. Hardware-efficient autonomous quantum memory protection. *Phys. Rev. Lett.*, 111:120501, Sep 2013.

[50] Marios H. Michael, Matti Silveri, R. T. Brierley, Victor V. Albert, Juha Salmilehto, Liang Jiang, and S. M. Girvin. New class of quantum error-correcting codes for a bosonic mode. *Phys. Rev. X*, 6:031006, Jul 2016.

[51] A.Yu. Kitaev. Fault-tolerant quantum computation by anyons. *Annals of Physics*, 303(1):2–30, 2003.

[52] Sergey Bravyi and Barbara Terhal. A no-go theorem for a two-dimensional self-correcting quantum memory based on stabilizer codes. *New Journal of Physics*, 11(4):043029, apr 2009.

[53] Olivier Landon-Cardinal and David Poulin. Local topological order inhibits thermal stability in 2d. *Phys. Rev. Lett.*, 110:090502, Feb 2013.

[54] Beni Yoshida. Feasibility of self-correcting quantum memory and thermal stability of topological order. *Annals of Physics*, 326(10):2566–2633, 2011.

[55] Jeongwan Haah. Commuting pauli hamiltonians as maps between free modules. *Communications in Mathematical Physics*, 324, 04 2012.

[56] Jeongwan Haah. Local stabilizer codes in three dimensions without string logical operators. *Phys. Rev. A*, 83:042330, Apr 2011.

[57] Eric Dennis, Alexei Kitaev, Andrew Landahl, and John Preskill. Topological quantum memory. *Journal of Mathematical Physics*, 43(9):4452–4505, September 2002.

[58] R. Alicki, M. Horodecki, P. Horodecki, and R. Horodecki. On thermal stability of topological qubit in Kitaev's 4D model. *arXiv e-prints*, page arXiv:0811.0033, November 2008.

[59] Benjamin J. Brown, Daniel Loss, Jiannis K. Pachos, Chris N. Self, and James R. Wootton. Quantum memories at finite temperature. *Reviews of Modern Physics*, 88(4):045005, October 2016.

[60] James M. Bardeen, B. Carter, and S. W. Hawking. The Four laws of black hole mechanics. *Commun. Math. Phys.*, 31:161–170, 1973.

[61] Jacob D. Bekenstein. Black holes and entropy. *Phys. Rev. D*, 7:2333–2346, Apr 1973.

[62] Juan Martin Maldacena. The Large N limit of superconformal field theories and supergravity. *Adv. Theor. Math. Phys.*, 2:231–252, 1998.

[63] Edward Witten. Anti de sitter space and holography. *Advances in Theoretical and Mathematical Physics*, 2(2):253–290, March 1998.

[64] Douglas Stanford Juan Maldacena, Stephen H. Shenker. A bound on chaos. *JHEP08(2016)106*. https://arxiv.org/abs/1503.01409.

[65] Subir Sachdev. Bekenstein-Hawking Entropy and Strange Metals. *Phys. Rev. X*, 5(4):041025, 2015.

[66] Juan Maldacena and Douglas Stanford. Remarks on the Sachdev-Ye-Kitaev model. *Phys. Rev. D*, 94(10):106002, 2016.

[67] Ahmed Almheiri and Joseph Polchinski. Models of AdS_2 backreaction and holography. *JHEP*, 11:014, 2015.

[68] Claudio Teitelboim. Gravitation and hamiltonian structure in two spacetime dimensions. *Physics Letters B*, 126(1):41–45, 1983.

[69] Juan Maldacena, Douglas Stanford, and Zhenbin Yang. Conformal symmetry and its breaking in two-dimensional nearly anti-de Sitter space. *Progress of Theoretical and Experimental Physics*, 2016(12), 11 2016. 12C104.

[70] Kristan Jensen. Chaos in ads_2 holography. *Phys. Rev. Lett.*, 117:111601, Sep 2016.

[71] Adam Nahum, Sagar Vijay, and Jeongwan Haah. Operator Spreading in Random Unitary Circuits. *Phys. Rev. X*, 8(2):021014, apr 2018.

[72] Curt von Keyserlingk, Tibor Rakovszky, Frank Pollmann, and Shivaji Sondhi. Operator hydrodynamics, OTOCs, and entanglement growth in systems without conservation laws. *Phys. Rev. X*, 8:021013, 2018.

[73] Shenglong Xu and Brian Swingle. Accessing scrambling using matrix product operators.

[74] Subir Sachdev and Jinwu Ye. Gapless spin-fluid ground state in a random quantum Heisenberg magnet. *Phys. Rev. Lett.*, 70(21):3339–3342, may 1993.

[75] Yingfei Gu, Xiao-Liang Qi, and Douglas Stanford. Local criticality, diffusion and chaos in generalized Sachdev-Ye-Kitaev models. *JHEP*, 2017(5):125, may 2017.

[76] David J. Luitz and Yevgeny Bar Lev. Information propagation in isolated quantum systems. *Phys. Rev. B*, 96(2):020406, jul 2017.

[77] A Bohrdt, C B Mendl, M Endres, and M Knap. Scrambling and thermalization in a diffusive quantum many-body system. *New J. Phys.*, 19(6):063001, dec 2016.

[78] Markus Heyl, Frank Pollmann, and Balázs Dóra. Detecting equilibrium and dynamical quantum phase transitions via out-of-time-ordered correlators. *Phys. Rev. Lett.*, 121:016801, 2018.

[79] Cheng-Ju Lin and Olexei I. Motrunich. Out-of-time-ordered correlators in a quantum Ising chain. *Phys. Rev. B*, 97(14):144304, apr 2018.

[80] Adam Nahum, Jonathan Ruhman, Sagar Vijay, and Jeongwan Haah. Quantum Entanglement Growth under Random Unitary Dynamics. *Phys. Rev. X*, 7(3):031016, jul 2017.

[81] Tibor Rakovszky, Frank Pollmann, and C. W. von Keyserlingk. Diffusive hydrodynamics of out-of-time-ordered correlators with charge conservation. 2017.

[82] Vedika Khemani, Ashvin Vishwanath, and David A Huse. Operator spreading and the emergence of dissipation in unitary dynamics with conservation laws.

[83] Vedika Khemani, David A Huse, and Adam Nahum. Velocity-dependent Lyapunov exponents in many-body quantum, semi-classical, and classical chaos.

[84] Stephen H. Shenker and Douglas Stanford. Stringy effects in scrambling. *JHEP*, 2015(5):132, may 2015.

[85] Igor L Aleiner, Lara Faoro, and Lev B Ioffe. Microscopic model of quantum butterfly effect: Out-of-time-order correlators and traveling combustion waves. *Ann. Phys. (N. Y).*, 375:378–406, 2016.

[86] Brian Swingle and Debanjan Chowdhury. Slow scrambling in disordered quantum systems. *Phys. Rev. B*, 95(6):060201, 2017.

[87] Sašo Grozdanov, Koenraad Schalm, and Vincenzo Scopelliti. Kinetic theory for classical and quantum many-body chaos.

[88] Aavishkar A Patel, Debanjan Chowdhury, Subir Sachdev, and Brian Swingle. Quantum Butterfly Effect in Weakly Interacting Diffusive Metals. *Phys. Rev. X*, 7(3):031047, sep 2017.

[89] Brian Swingle and Nicole Yunger Halpern. Resilience of scrambling measurements. *Phys. Rev. A*, 97:062113, Jun 2018.

[90] Justin Dressel, José Raúl González Alonso, Mordecai Waegell, and Nicole Yunger Halpern. Strengthening weak measurements of qubit out-of-time-order correlators. *Phys. Rev. A*, 98:012132, Jul 2018.

[91] G. Menezes and J. Marino. Slow scrambling in sonic black holes. *EPL (Europhysics Letters)*, 121:60002, March 2018.

[92] T. Scaffidi and E. Altman. Semiclassical Theory of Many-Body Quantum Chaos and its Bound. *ArXiv e-prints*, November 2017.

[93] Ken Xuan Wei, Chandrasekhar Ramanathan, and Paola Cappellaro. Exploring localization in nuclear spin chains. *Phys. Rev. Lett.*, 120:070501, Feb 2018.

[94] Jun Li, Ruihua Fan, Hengyan Wang, Bingtian Ye, Bei Zeng, Hui Zhai, Xinhua Peng, and Jiangfeng Du. Measuring out-of-time-order correlators on a nuclear magnetic resonance quantum simulator. *Phys. Rev. X*, 7(3):031011, jul 2017.

[95] Eric J. Meier, Jackson Ang'ong'a, Fangzhao Alex An, and Bryce Gadway. Exploring quantum signatures of chaos on a Floquet synthetic lattice. *arXiv e-prints*, page arXiv:1705.06714, May 2017.

[96] Kevin A. Landsman, Caroline Figgatt, Thomas Schuster, Norbert M. Linke, Beni Yoshida, Norman Y. Yao, and Christopher Monroe. Verified Quantum Information Scrambling. *arXiv e-prints*, page arXiv:1806.02807, June 2018.

[97] Ken Xuan Wei, Pai Peng, Oles Shtanko, Iman Marvian, Seth Lloyd, Chandrasekhar Ramanathan, and Paola Cappellaro. Emergent prethermalization signatures in out-of-time ordered correlations. *arXiv e-prints*, page arXiv:1812.04776, December 2018.

[98] N. Read Jinwu Ye, Subir Sachdev. A solvable spin-glass of quantum rotors. *Phys. Rev. lett*, 70:4011, 1993. `https://arxiv.org/abs/cond-mat/9212027`.

[99] I. Danshita, M. Hanada, and M. Tezuka. Creating and probing the Sachdev-Ye-Kitaev model with ultracold gases: Towards experimental studies of quantum gravity. *Progress of Theoretical and Experimental Physics*, 2017(8):083I01, August 2017.

[100] A. Chen, R. Ilan, F. de Juan, D. I. Pikulin, and M. Franz. Quantum Holography in a Graphene Flake with an Irregular Boundary. *Physical Review Letters*, 121(3):036403, July 2018.

[101] H. Gharibyan, M. Hanada, B. Swingle, and M. Tezuka. Quantum Lyapunov Spectrum. *ArXiv e-prints*, September 2018.

[102] Brian Swingle Debanjan Chowdhury. Onset of many-body chaos in the o(n) model. *Phys. Rev. D*, 96, 065005, 2017. `https://arxiv.org/abs/1703.02545`.

[103] A Kitaev. A simple model of quantum holography. In *KITP Progr. Entanglement Strongly-Correlated Quantum Matter*, 2015.

[104] Andrew Hallam, James Morley, and Andrew G. Green. The Lyapunov spectra of quantum thermalisation. *Nature Commun.*, 10(1):2708, 2019.

[105] Shenglong Xu and Brian Swingle. Locality, Quantum Fluctuations, and Scrambling.

[106] Daniel A. Roberts and Douglas Stanford. Diagnosing Chaos Using Four-Point Functions in Two-Dimensional Conformal Field Theory. *Phys. Rev. Lett.*, 115(3):131603, sep 2015.

[107] Stephen H. Shenker and Douglas Stanford. Multiple shocks. *Journal of High Energy Physics*, 2014(12):46, Dec 2014.

[108] Vedika Khemani, Ashvin Vishwanath, and David Huse. Operator spreading and the emergence of dissipative hydrodynamics under unitary evolution with conservation laws. *Physical Review X*, 8, 09 2018.

[109] Andrew Lucas. Constraints on hydrodynamics from many-body quantum chaos. 10 2017.

[110] Mike Blake. Universal charge diffusion and the butterfly effect in holographic theories. *Physical Review Letters*, 117(9), Aug 2016.

[111] Mike Blake and Aristomenis Donos. Diffusion and chaos from near ads2 horizons. *Journal of High Energy Physics*, 2017(2), Feb 2017.

[112] Sašo Grozdanov, Koenraad Schalm, and Vincenzo Scopelliti. Black hole scrambling from hydrodynamics. *Physical Review Letters*, 120(23), Jun 2018.

[113] Mike Blake, Hyunseok Lee, and Hong Liu. A quantum hydrodynamical description for scrambling and many-body chaos. *Journal of High Energy Physics*, 2018(10), Oct 2018.

[114] Mike Blake, Richard A. Davison, Sašo Grozdanov, and Hong Liu. Many-body chaos and energy dynamics in holography. *Journal of High Energy Physics*, 2018(10), Oct 2018.

[115] J. Marino and A. M. Rey. Cavity-qed simulator of slow and fast scrambling. *Physical Review A*, 99(5), May 2019.

[116] Sašo Grozdanov, Koenraad Schalm, and Vincenzo Scopelliti. Kinetic theory for classical and quantum many-body chaos. *Physical Review E*, 99(1), Jan 2019.

[117] Xiao Chen, Yingfei Gu, and Andrew Lucas. Many-body quantum dynamics slows down at low density. *SciPost Physics*, 9(5), Nov 2020.

[118] David M. Ramirez. Chaos and pole skipping in cft_2, 2020.

[119] Navid Abbasi and Javad Tabatabaei. Quantum chaos, pole-skipping and hydrodynamics in a holographic system with chiral anomaly. *Journal of High Energy Physics*, 2020(3), Mar 2020.

[120] Joao Penedones. *High Energy Scattering in the AdS/CFT Correspondence*. PhD thesis, Porto U., 2007.

[121] Tevian Dray and Gerard 't Hooft. The Effect of Spherical Shells of Matter on the Schwarzschild Black Hole. *Commun. Math. Phys.*, 99:613–625, 1985.

[122] Tevian Dray and Gerard 't Hooft. The Gravitational Shock Wave of a Massless Particle. *Nucl. Phys.*, B253:173–188, 1985.

[123] Andrei Starinets. Quasinormal spectrum and the black hole membrane paradigm. *Physics Letters B*, 670(4):442 – 445, 2009.

[124] Christopher P Herzog and Dam Thanh Son. Schwinger-keldysh propagators from AdS/CFT correspondence. *Journal of High Energy Physics*, 2003(03):046–046, mar 2003.

[125] Dam T. Son and Andrei O. Starinets. Minkowski space correlators in AdS / CFT correspondence: Recipe and applications. *JHEP*, 09:042, 2002.

[126] Christopher Herzog. The hydrodynamics of m-theory. *Journal of High Energy Physics*, 2002, 10 2002.

[127] Christopher Herzog. Sound of m theory. *Phys. Rev. D*, 68, 07 2003.

[128] Dam T. Son and Andrei O. Starinets. Viscosity, Black Holes, and Quantum Field Theory. *Ann. Rev. Nucl. Part. Sci.*, 57:95–118, 2007.

[129] A.Y. Kitaev. *Proceedings of the 3rd International Conference of Quantum Communication and Measurement, Ed. O. Hirota, A. S. Holevo, and C. M. Caves*. Plenum, New York, 1997.

[130] R. Alicki, M. Fannes, and M. Horodecki. On thermalization in Kitaev's 2D model. *Journal of Physics A Mathematical General*, 42(6):065303, February 2009.

[131] Alexei Kitaev. Anyons in an exactly solved model and beyond. *Annals of Physics*, 321(1):2–111, January 2006.

[132] Ahmed Almheiri, Xi Dong, and Daniel Harlow. Bulk Locality and Quantum Error Correction in AdS/CFT. *JHEP*, 04:163, 2015.

[133] S. W. Hawking and Don N. Page. Thermodynamics of black holes in anti-de Sitter space. *Communications in Mathematical Physics*, 87(4):577 – 588, 1982.

[134] Edward Witten. Anti-de Sitter space, thermal phase transition, and confinement in gauge theories. *Adv. Theor. Math. Phys.*, 2:505–532, 1998.

[135] Ning Bao, ChunJun Cao, and Guanyu Zhu. Deconfinement and Error Thresholds in Holography. *arXiv e-prints*, page arXiv:2202.04710, February 2022.

[136] Fernando Pastawski, Beni Yoshida, Daniel Harlow, and John Preskill. Holographic quantum error-correcting codes: Toy models for the bulk/boundary correspondence. *JHEP*, 06:149, 2015.

[137] Gong Cheng, ChunJun Cao, and Brian Swingle. In preparation.

[138] Cédric Bény and Ognyan Oreshkov. General Conditions for Approximate Quantum Error Correction and Near-Optimal Recovery Channels. *Phys. Rev. Lett.*, 104(12):120501, March 2010.

[139] Eric Mintun, Joseph Polchinski, and Vladimir Rosenhaus. Bulk-Boundary Duality, Gauge Invariance, and Quantum Error Corrections. *Phys. Rev. Lett.*, 115(15):151601, 2015.

[140] Alexey Milekhin. Quantum error correction and large N. *SciPost Physics*, 11(5):094, November 2021.

[141] Dave Bacon. Operator quantum error-correcting subsystems for self-correcting quantum memories. *Phys. Rev. A*, 73:012340, Jan 2006.

[142] Olivier Landon-Cardinal, Beni Yoshida, David Poulin, and John Preskill. Perturbative instability of quantum memory based on effective long-range interactions. *Phys. Rev. A*, 91:032303, Mar 2015.

[143] Courtney G. Brell. A proposal for self-correcting stabilizer quantum memories in 3 dimensions (or slightly less). *New Journal of Physics*, 18(1):013050, January 2016.

[144] Keiichiro Furuya, Nima Lashkari, and Mudassir Moosa. Renormalization group and approximate error correction. 12 2021.

[145] Robert J. Harris, Nathan A. McMahon, Gavin K. Brennen, and Thomas M. Stace. Calderbank-Shor-Steane holographic quantum error-correcting codes. *Phys. Rev. A*, 98(5):052301, 2018.

[146] ChunJun Cao and Brad Lackey. Approximate Bacon-Shor Code and Holography. *JHEP*, 05:127, 2021.

[147] Kfir Dolev, Vladimir Calvera, Samuel S. Cree, and Dominic J. Williamson. Gauging the bulk: generalized gauging maps and holographic codes. *JHEP*, 05:158, 2022.

[148] Ofer Aharony, Joseph Marsano, Shiraz Minwalla, Kyriakos Papadodimas, and Mark Van Raamsdonk. The Hagedorn - deconfinement phase transition in weakly coupled large N gauge theories. *Adv. Theor. Math. Phys.*, 8:603–696, 2004.

[149] Nissan Itzhaki and John McGreevy. The Large N harmonic oscillator as a string theory. *Phys. Rev. D*, 71:025003, 2005.

[150] David Berenstein. A toy model for the AdS/CFT correspondence. *Journal of High Energy Physics*, 2004(07):018–018, jul 2004.

[151] Igor R. Klebanov. String theory in two-dimensions. In *Spring School on String Theory and Quantum Gravity (to be followed by Workshop)*, 7 1991.

[152] Clifford V. Johnson. Consistency Conditions for Non-Perturbative Completions of JT Gravity. 12 2021.

[153] Stefano Chesi, Beat Röthlisberger, and Daniel Loss. Self-correcting quantum memory in a thermal environment. *Phys. Rev. A*, 82:022305, Aug 2010.

[154] Giuseppe Policastro, Dam T Son, and Andrei O Starinets. From AdS/CFT correspondence to hydrodynamics. II. sound waves. *Journal of High Energy Physics*, 2002(12):054–054, dec 2002.

[155] Simon Caron-Huot and Omid Saremi. Hydrodynamic Long-Time tails From Anti de Sitter Space. *JHEP*, 11:013, 2010.

[156] Xinyi Chen-Lin, Luca V. Delacrétaz, and Sean A. Hartnoll. Theory of diffusive fluctuations. *Phys. Rev. Lett.*, 122(9):091602, 2019.